ISSN 1520-5045

Industrial & Engineering Chemistry Research

Volume No. 64

Issue No. 3

Sept - Dec 2025

ENRICHED PUBLICATIONS

ENRICHED PUBLICATIONS PVT.LTD

JE - 18,Gupta Colony, Khirki Extn,
Malviya Nagar, New Delhi - 110017.
E- Mail: info@enrichedpublication.com
Phone :- +91-8877340707

ISSN 1520-5045

Industrial & Engineering Chemistry Research

Managing Editor
Mr. Amit Prasad

ISSN 1520-5045

Industrial & Engineering Chemistry Research

(Volume No. 64, Issue No. 3, Sept - Dec 2025)

Contents

ISSN 1520-5045

A Visible Light-Responsive Mixed-Valence Bimetallic Eu−Zr MOFBased Nanoarchitecture toward Efficacious H2O2 and H2 Production

Srabani Dash,# Suraj Prakash Tripathy,# Satyabrata Subudhi, and Kulamani Parida

ABSTRACT

A mixed-valence bimetallic Eu/Zr MOF has been fabricated via a one-step solvothermal method by incorporating Eu^{3+} ions into the Zr-MOF,thereby making a single-component photocatalyst that can be utilized towardrobust photon utilization from the visible light spectrum for the photocatalyticproduction of green energy like H_2 and H_2O_2. The one-step synthesized bimetallicEu/Zr-MOF exhibits more visible light captivation properties along withimproved charge carrier separation, confined band gap, and excellent ligand-tometal charge transfer (LMCT) because of the existence of an interconvertibleEu^{3+}/Eu^{2+} ion pair compared with the pristine MOF counterparts. The addition ofEu ions directed to an upsurge in the electron density around Zr^{4+} ion, as seenfrom XPS analysis. Moreover, the introduction of Eu^{3+} enhanced the excitonsegregation, as seen from PL and EIS analyses, thereby leading to superiorcatalytic performances. An increased photocatalytic H_2 generation efficacy of331.26 μmol h^{-1} (ACE = 2.42%) was demonstrated by the synthesized EZUNH-2 MOF, which is approximately three times greaterthan pristine MOFs. As a result, the bimetallic EZUNH-2 MOF can be easily utilized as a robust photocatalyst that has increasedinclinations to produce H_2O_2 at 35.2 μmol h^{-1}, around 4 times more than that of the parent material. Consequently, the one-potsynthesized bimetallic MOF paves a suitable mechanistic pathway for paramount performance toward photocatalytic H_2O_2 and H_2production.

1. INTRODUCTION

The usage of hydrogen peroxide (H_2O_2) as an environmentally friendly oxidant in industries like chemical synthesis, food andpaper manufacturing, medical decontamination, and wastewater purification has recently attracted a lot of attention fromresearchers on the front lines.[1,2] The water solubility andreleasing H_2O as a byproduct are the major factors to makeH_2O_2 as an energy carrier for future generations.[3−5] Severaltechniques have been invented to produce H_2O_2, including theanthraquinone process, alcohol oxidation, direct synthesis fromthe mixture of oxygen and hydrogen gases, and electrochemicalsynthesis. But some of the drawbacks of the synthesis methodslisted above include the need for a lot of energy and solvents,as well as the increased risk of explosion brought on by thecombination of H_2 and O_2 gases. An effective and low-energygreen method for producing H_2O_2 is therefore highlydesired.[6,7] In recent years, the photocatalytic H_2O_2 productionhas received massive attention because of the use ofphotocatalysts to accomplish the reaction with O_2-saturatedH_2O, alcohol, and light energy.[8−10] In addition, water splittingvia a photon-assisted hydrogen evolution reaction has beenperformed to assess the semiconducting materials' photocatalytic energy production capabilities. Following theinnovation of Fujishima and Honda in hydrogen productionfrom H_2O utilizing TiO_2 semiconductor under light irradiation, which aimed to lower the world's energy demand, the production of H_2 from photocatalytic water splitting reaction has developed into an active study area. Moreover, toovercome the current energy crisis, hydrogen (H2) has drawn a lot of interest as a clean, sustainable energy substitutefor nonrenewable energy sources. As a result, owing to its lowcost and simple procedure, the photocatalytic hydrogengeneration via water splitting has been considered a promisingmethod.11−13 Some bimetallic MOFs like Ce−Co MOF, Ni−Ti MOF, and Ce−Zr MOF show excellent hydrogen evolutionefficiency as photocatalysts.14−16

The current situation of an expanding world population,accompanied by the quick industrial development andimpending fossil fuel depletion, has prompted efforts to findan environmentally favorable and affordable substitute forrenewable energy as well as sustainable catalysis. In order toovercome such issues, the development of a suitable photocatalyst with a tunable band structure, excellent photostability,and greater exciton separation ability is a major challenge.

Scheme 1. Facile One-Step Synthesis Method of (Eu/Zr) Bimetallic MOF

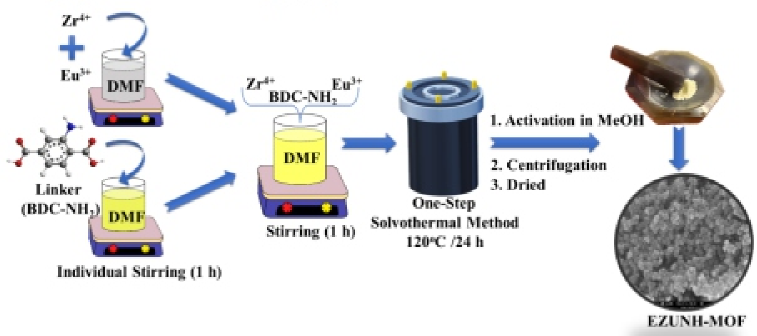

Since many years, different scientific groups have been enduring multiple semiconducting photocatalysts to get oversuch problems.17−19 Yet, in recent times, organic−inorganichybrids, also known as metal-organic frameworks (MOFs),have become extremely well-liked because of their exceptionalbenefits, which include high specific surface area, flexiblefunctionalization, high porosity, and tailored compositionslinked to an infinite variety of organic linkers and metalclusters, resulting in a broad range of potential MOFnanostructures. However, pristine MOFs have some limitations like faster recombination of charge carriers, lack of asuitable band gap, and low light absorption tendency, whichmakes them inadequate photocatalysts. Hence, to conquerthese, some modifications have been involved, such asfunctional group introduction, guest molecule introduction,and making heterojunction with other photocatalysts.17,18,20However, composite materials have some limitations, likereduction of surface area, undesirable active site coverage,deficient interaction among photocatalysts, lower chargecarrier separation, etc. In recent years, scientists have beenobserving paths to surmount these difficulties in making composite photocatalysts, which have created an extensive need for the production of single-component MOF-basedphotocatalysts.21,22 Nowadays, single-component MOF-basedphotocatalysts are in high demand, so researchers are exploringa variety of strategies to produce these type of photocatalysts,with tailored functionalities and tuned band structures for awide range of applications.12,23−25Generally, to overcome the above-mentioned issues, variousmixed-metal MOFs such as UiO-66-NH2 (Zr/Hf), UiO-66-NH2 (Pt/Sn), UiO-66 (Ti/Zr), MOF-NH2 (Fe/Ti), UiO-66-NH2 (Ce/Zr), etc. were reported.15,26−28 Moreover, thelanthanide-based metal−organic frameworks (Ln-MOFs),especially Eu3+, are interesting due to their adaptablecoordination geometry and distinctive luminescent andoptical-electrical properties. In current years, the applicationof Ln-MOFs as photocatalysts has gained significant interestdue to their unique physicochemical as well as surfacefunctionalization properties.29,30 They also show easilyinterconvertible oxidation states of the Europium ion (Eu3+/Eu2+), so the Eu ion insertion presents as a superior alternativeover other metals for MOF fabrication. Yet the pristine EuMOF is not stable enough or has insufficient excitonsegregation capabilities; therefore, to achieve optimal photocatalytic activity and stability, it is crucial to optimallyintroduce these redox mixed valence Eu^{3+}/Eu^{2+} ions intowater-stable frameworks, such as visible-light-responsive functionalized UiO-66 series Zr-based MOFs. The presence of easily interconvertible Eu^{2+} and Eu^{3+} oxidation states in anaqueous stable framework such as visible light-active UiO-66series Zr-based MOFs promotes superior photocatalyticactivity and stability.32 Since the incorporated metal ionsdetermine their properties, bimetallic MOFs are expected tohave new functionalities in addition to their structuralcomplexity. A second hetero metal node can be added to thesame framework to create synergistic effects that improve itsinherent qualities.32,33 The integration of Eu^{3+} into the UiO66-NH_2 framework not only builds a stable and porousstructure but also regulates the energy levels of the MOFs. Wehave chosen the Eu^{3+} ion as the constituent metal due to itslow reduction potential (E_{red} (Eu^{3+} /Eu^{2+}) = −0.35 V vs NHE)and the ability of the resulting Eu^{2+} ion to be reconverted easilyto its initial state.34 Furthermore, it is very difficult to find aphotocatalyst that meets the thermodynamic requirements forphotocatalytic water oxidation (At pH = 7, O_2/•O_2^-/H_2O_2 =−0.33 V and +0.69 V, OH^-/OH• = 1.99 V). The key findings for a one-pot synthesized bimetallic Eu/Zr MOF-basednanoarchitecture toward visible light-supported H_2O_2 production and H_2 evolution have been presented in the currentinvestigation. After extensive research on the neat Zr-MOF and its bimetallic MOF, such as (Eu/Zr) UiO-66-NH_2 [EZUNH],the composite showed improved exciton segregation androbust LMCT, accompanied by the mixed valency states ofEu^{3+} and Eu^{2+}, which endorse its excellent photocatalyticoutput. Moreover, due to the strong bond of Zr−O, thepristine MOF with Zr as the metal center has high stabilitytoward acid−base, aqueous, and thermal changes, and a similarimpact can be inherited in the EZUNH MOF.35 The currentwork represents the one-pot synthesized EZUNH bimetallicMOF-based nanomaterials toward photocatalytic H_2O_2 and H_2production. Among the prepared bimetallic MOFs, theEZUNH-2 exhibits boosted photocatalytic H_2 production upto 331.26 μmol h^{-1} and H_2O_2 production up to 35.2 μmol h^{-1},which is around 3-fold and 4-fold higher than that of the pristine MOF.

2. MATERIALS AND METHODS

2.1. Chemicals Used. Several chemicals, for example,zirconium chloride ($ZrCl_4$, 99.99%), 2-aminoterephthalic acid(BDC-NH_2, 99%), europium(III) chloride hexahydrate($EuCl_3.6H_2O$, 99.99%) Nafion-117 (~5% in lower aliphaticalcohol/water mixture), and potassium bromide (KBr, 99.5%)were bought from Sigma-Aldrich. In addition, sodium sulfate(Na_2SO_4, 99%), methanol (MeOH, 99%), isopropanol (99%),

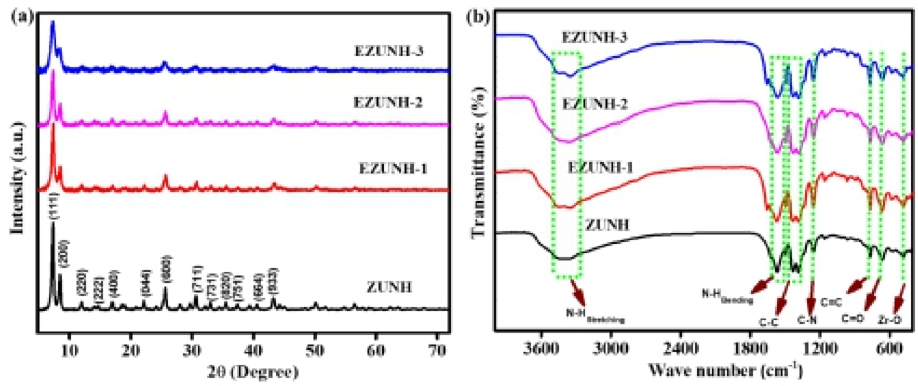

Figure 1. (a) XRD pattern and (b) FTIR spectra of ZUNH and EZUNH-1, 2, and 3 MOFs.

and N,N-dimethylformamide (DMF, 99.8%) were purchased from Merck. All the chemicals involved were used in several reactions.

2.2. Fabrication of Photocatalyst. 2.2.1. Pristine MOFs.The UiO-66-NH2 MOF was prepared by following asolvothermal approach by procuring an equimolar ratio ofmetal salts ($ZrCl_4$, 2 mmol) and linkers (ATA, 2 mmol), asdescribed earlier.36,37 First, with DMF (40 mL), the metal saltand linker were added individually with continued stirring for 1h. Then, both solutions were mixed together and further stirredfor 1 h. Afterward, the mixture solution was transferred into aTeflon-lined stainless steel vessel and kept for solvothermaltreatment (120 °C for 24 h). After the reaction time was over,the reactor vessel was allowed to cool down to roomtemperature. Subsequently, the pore activation of the productwas done by a solvent exchange method using methanol for 24h. The products were then collected through centrifugationand dried overnight at 80 °C. Last, the obtained yellow-coloredsample was named ZUNH.
2.2.2. Bimetallic Eu/Zr-UiO-66-NH2 MOF. The Eu/Zr bimetallic MOF was fabricated in an analogous way to theparent ZUNH MOF through a one-step solvothermal method(120 °C for 24 h), as illustrated in Scheme 1. Herein, thisprocess differs from the ZUNH fabrication method by usingmixed metallic salts with variable molar concentrations as Eu0.2 mmol/Zr-1.8 mmol, Eu-0.4 mmol/Zr-1.6 mmol, and Eu0.6 mmol/Zr-1.4 mmol, which were termed as EZUNH-1,EZUNH-2, and EZUNH-3, respectively. Then, to each ofthese salt mixtures, DMF (40 mL) was added. Further, themetal salts and linker were added individually with continuousstirring for 1 h. Then, after both solutions were mixed together,they were further subjected to stirring for 1 h. Afterward, themixture solution was transferred into a Teflon-lined stainlesssteel vessel and kept for solvothermal treatment (120 °C for 24h). After the reaction time was over, the reactor vessel wasallowed to cool down to room temperature. Subsequently, thepore activation of the product was done by a solvent exchangemethod using methanol for 24 h. The detailed characterizationmethods involved and other experimental processes followed in this work are reported in the Supporting Information(Experimental Techniques).

2.2.3. Photocatalytic H_2O_2 and H_2 Production. Thesynthesized samples were subjected to analysis of the photocatalytic activity toward H_2O_2 production under an O_2-saturated atmosphere with 2 h of visible light illumination ($\lambda \geq 420$ nm). A suspension solution was prepared by adding 19 mL of deionized water (DI) and 1 mL of isopropanol (IPA) with 20 mg of photocatalyst, and then, the suspension underwent anultrasonication process for about 10 min for proper dispersionof the contents. Subsequently, the solution was kept under O2purging for 30 min in the presence of light to attain an O2saturated atmosphere. After the reaction time, a clear solutionwas obtained by centrifugation of the suspension solution.Thereafter, to 1 mL of the resulting solution, 2 mL of 0.1 M KIsolution and 0.05 mL of 0.01 M ammonium molybdatesolution were added to change the colorless sample into alight-yellow color. Finally, the concentration of the producedphotocatalytic H_2O_2 was evaluated through a Uv−visiblespectrophotometer
Furthermore, the prepared nanomaterials were toward the photocatalytic evolution of hydrogen gas. In this process, a closed quartz batch-type reactor (100 mL) was usedto acquire the photocatalytic H_2 production efficacy of thefabricated photocatalysts, such as pure ZUNH and bimetallicEZUNH MOFs. Here, 20 mg of the as-synthesized photocatalysts was taken in the photoreactor with 20 mL of 10% V/V MeOH-water mixture, and the visible light source (Xenonarc lamp, 300 W, $\lambda \geq 420$ nm) was irradiated for 1 h. Thesubstances in the reactor were continuously stirred to promotea uniform distribution and avoid particle aggregation duringthe reaction time. Formerly. by utilizing the Xe lamp, suspension mixture was thoroughly bubbled for 30 min under N_2 gas to eradicate the dissolved gases present. The gaseous mixtures that emerged were agitated via direct water displacement and investigated using gas

chromatography/GC (GC-7890B, Agilent Technologies) tailored with 5 Åmolecular sieves and a thermal conductivity detector (TCD).Photocatalytic experiments were performed in triplicate tominimize experimental errors.

3. RESULTS AND DISCUSSION

3.1. Physicochemical Characterizations. Figure 1a illustrates a PXRD (powder X-ray diffraction) pattern analysis,which was executed to construe the formation and crystallographic nature of all the synthesized photocatalysts. Typically,the diffraction pattern of the pristine MOF ZUNH suggestshigh crystallinity. Remarkably, the EZUNH MOFs show thecharacteristic XRD pattern, suggesting the conservancy ofcrystallographic peaks of the pristine grid framework upon theinsertion of Eu ions. The Zr4+ and Eu3+ competitivelycoordinate with the ligand to produce a disrupted and slightly reduced crystallinity in bimetallic EZUNH MOFs.

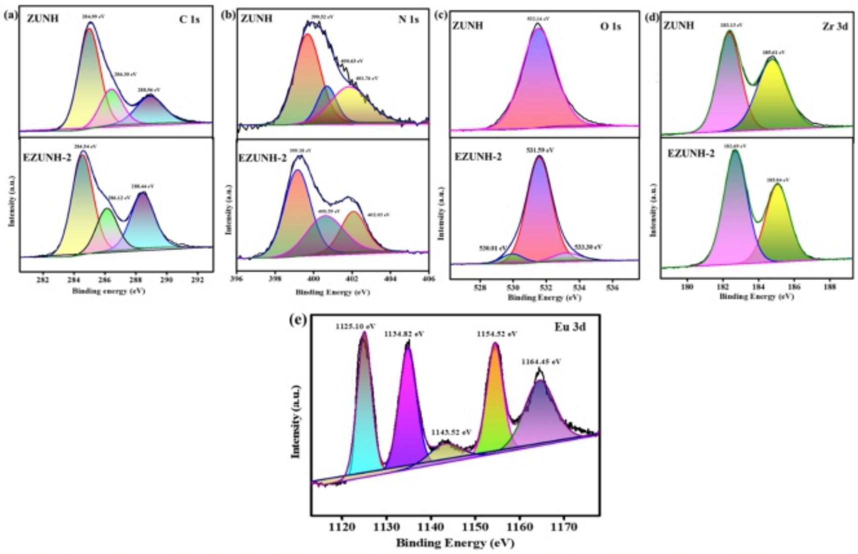

Figure 2. XPS spectra of (a) C 1s, (b) N 1s, (c) O 1s, (d) Zr 3d, and (e) Eu 3d of ZUNH and bimetallic EZUNH-2 MOF.

Consequently, the diffraction at 7.35° and 8.41°, corresponding to the (111) and (200) planes, respectively, gradually decreases as the amount of Eu3+ ions increases. Additionally,the diffraction peaks shown in Figure 1a exhibit a reduction inthe intensity of peak, accompanied by broadening of peakswith respect to the parent ZUNH, especially for the twonoticeable Zr-cluster peaks, signifying the Eu ions' insertioninto the lattice of MOF and eventually instigating the slightreduction in Zr-Oxy clusters.15,38Additionally, the FT-IR (Fourier transform infrared) studywas performed to detect various functional groups by means oftheir modes of vibration existing in the pristine ZUNH andbimetallic EZUNH MOF, as illustrated in Figure 1b. Theobserved peaks at 3475 and 3340 cm−1 represent the -Nh2groups of both ZUNH and EZUNH, which are accompaniedby asymmetrical and symmetrical vibrational stretching modes,respectively. In the frequency region, the 1640 and 1245 cm−1bands determine the vibrational bending of N−H andstretching of the C−N bond of the aromatic -NH2 groupsexisting in the ATA linkers, respectively. Furthermore, thesmall vibrational band at 1511 cm−1 represents the C�Cmoiety of the benzene ring, whereas, the vibrational peaks observed around 485, 763, 662 cm−1 are accompanied bymetal-(OC) asymmetric stretching, C�C stretching of thearomatic ring, and car boxylate O�C�O bending, respectively.12,39 Typically, from the FT-IR analysis results of bimetallic EZUNH-1, 2, and 3 MOFs, it has been observedthat the nature is quite similar to pristine ZUNH. Hence, theanalysis outcome suggests an equivalent chemical bondingatmosphere and indistinguishable functional groups in the frameworks along with it signify no

noticeable difference in the peak positions. The FT-IR results support the earlier reported results.32,40 Textural properties of the synthesized MOFs were persistent through the (BET) surface area technique with the support ofthe N2 adsorption/desorption isotherm method. Figure S1depicts the bimetallic EZUNH-2 MOF's BET adsorption/desorption curve, which is similar to the Type-IV isotherm thatindicates the microporous and mesoporous nature of theframework. Herein, the insertion of Eu ions into the frameworkof ZUNH assisted in the diminution of the BET surface area,i.e., 533.5 m2 g−1 as given in Figure S1. However, thephotocatalytic yield does not distress with the reduction insurface area due to the synergistic effect of bimetallic ions.Regardless, the insertion of Eu ions does not affect the rigidityof the framework structure, which shows that the isothermpattern of the bimetallic MOF persisted similarly to that of theparent ZUNH MOF.18
Chemical states and surface elemental compositions of the prepared photocatalysts were investigated through X-rayphotoelectron spectroscopy (XPS). Herein, for EZUNH-2bimetallic MOF, the XPS survey spectra have been depicted inFigure S2, which validates the presence of Eu, Zr, C, N, and O,as confirmed by the EDAX and elemental mapping analysis.Moreover, from the XPS analysis of the fabricated bimetallicEZUNH-2 MOF, the presence of each element's spectra wascompiled and deconvoluted, as illustrated in Figure 2b−f.From the deconvoluted spectra, the C 1s present in EZUNH-2exhibits peaks at 284.54, 285.12, and 288.44 eV, whichresemble the carbon atoms of the BDC-NH2 linker thatcorrespond to C�C, C−NH2, and O�C−O, respectively.13Also, for N 1s, the deconvoluted XPS peaks observed at

Table 1. Summarization of XPS Binding Energy Peak Values for the Prepared Photocatalysts

Element	Binding Energy in eV					Ref.
Carbon/C 1s						
ZUNH	284.99		286.30	288.96		41,42
20% EZUNH	284.54		286.12	288.44		
Speculation:	C=C of linker		C-NH_2 of linker	(O=C—O) of linker		
Difference:	−0.45		−0.18	−0.52		
			Nitrogen/N 1s			
ZUNH	399.52		400.63	401.76		13
20% EZUNH	399.18		400.59	402.03		
Speculation:	-NH_2 of linker		-NH_3^+ of linker	=NH_2^+ of linker		
Difference:	−0.34		−0.04	+0.27		
			Oxygen/O 1s			
ZUNH	--		532.14	--		43
20% EZUNH	530.01		531.59	533.30		
Speculation:	Mn−O bond		Zr−O bond	Adsorbed H_2O		
Difference:	+0.69		−0.55	--		
			Zirconium/Zr 3d			
ZUNH	183.13		185.61			18,44
20% EZUNH	182.69		185.04			
Speculation:	$Zr^{4+}(3d_{5/2})$		$Zr^{4+}(3d_{3/2})$			
Difference:	−0.44		−0.57			
			Europium/Eu 3d			
ZUNH	--			--		23,45,46
20% EZUNH	1125.10	1134.82	1143.52	1154.52	1164.45	
Speculation:	Eu ($3d_{5/2}$)	Sat. Peak		Eu ($3d_{3/2}$)		
Difference:	--			--		

399.18, 400.15, and 402.03 eV relate to the -NH2 functionalized groups of linkers such as −NH2 and −NH3 +,respectively, which is almost analogous to the previouslyanalyzed N 1s spectra for pristine ZUNH MOF. Besides, thedeconvoluted O 1s XPS spectra found at 530.01, 531.59, and533.30 eV signify lattice O, metal-O, and surface-adsorbedH2O molecule, respectively, for the prepared bimetallicEZUNH-2 MOF. Additionally, the deconvoluted peaks forZr found at 182.69 and 185.04 eV represent the two spin statesof Zr, such as 3d5/2 and Zr 3d3/2 in the EZUNH-2 sample. Thedownshifting of Zr spin states binding energy demonstrates that the electron density of Zr4+ increases due to the transfer ofelectrons from lower oxidation species (Eu3+) in the bimetallicEZUNH-2 MOF. In the deconvoluted peaks, the XPS of the Eu peak comprises dual sets corresponding to the states Eu 3d5/2 and Eu 3d3/2. Herein, the deconvoluted peaks of Eu correspond to the 3+ oxidation state of Eu 3d5/2 and Eu 3d3/2,respectively; also, the presence of the 2+ oxidation state of Euions has been confirmed from the plotted data. From thedeconvoluted plot of Eu, the existence of both the 3+ and 2+oxidation states in the MOF has been clearly perceived,suggesting the formation of mixed valency MOF. Moreover,the XPS analysis outcome confirms the formation of a singlecomponent bimetallic EZUNH MOF along with it unveils therole of Eu3+/Eu2+ redox pair. The deconvoluted peak values ofXPS confirm the pristine ZUNH and bimetallic EZUNH-2, along with their corresponding chemical environments, arepresented in Table 1 for lucid comprehension. Additionally,the ICP-OES analysis result confirms the existence of Eu:Zr inthe bimetallic MOFs with different molar ratios, such asEZUNH-1 (0.08:0.84), EZUNH-2 (0.17:0.76), and EZUNH-3(0.26:0.67), respectively

3.2. Morphological Studies. To study the surface morphology and elemental composition of the pristineZUNH and one-pot synthesized mixed-metallic EZUNH-2MOF, the FESEM (field-emission scanning electron microscopy) and HRTEM (high-resolution transmission electronmicroscopy) analyses were carried out. The FESEM image(Figure 3a) reveals the morphology of EZUNH-2, which isquite similar to that of the pristine MOF, as shown in FigureS3a. Additionally, the analogous morphological features of themixed-metallic MOF substantially corroborate the PXRDresults, indicating a framework structure similar to that ofpristine MOFs. From the HRTEM images given in Figure 3b,the octahedral morphology of EZUNH-2 was distinctlyperceived at 20 nm scales as depicted. Also, it is significantlyobserved that the morphology of the bimetallic MOF is wellsupported by the pristine MOF (Figure S3b). Herein, theaddition of Eu into the Zr-framework significantly does notaffect the crystal structure, which specifies the similarmorphology of the synthesized bimetallic MOF. The parentZUNH MOF has high sensitivity toward the electron beams;also, the bimetallic framework exhibits a similar property.However, it is difficult to find high-quality HRTEM images aswell as a well-defined SAED pattern. The SAED analysispattern given in Figure 3c corresponds with the neat ZUNHMOF, as reported formerly by us.17 Furthermore, the elementalcolor mapping (Figure 3e−j) and EDS (Figure 3d) outcomesoffer extra sustenance to the existence of C, O, N, Eu, and Zrelements in the EZUNH-2 bimetallic framework, which is alsoconfirmed by XPS analysis.

3.3. Optical Characterization. The optical properties of the prepared photocatalysts were analyzed through Uv−visiblediffuse reflectance spectra (UV-DRS) and are shown in Figure4a. The two intense bands obtained at 265 and 365 nm were

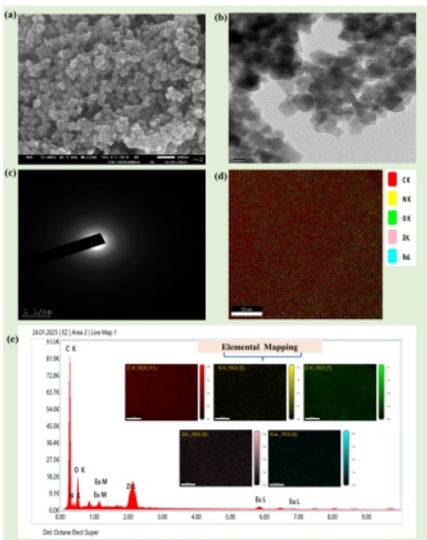

Figure 3. (a) FESEM image of bimetallic EZUNH-2 MOF, (b) HRTEM image of bimetallic EZUNH-2 MOF, (c) SAED pattern of bimetallic EZUNH-2 MOF, (d) Element mapping overlay image of bimetallic EZUNH-2 MOF, and (e) EADX (inset: individual elemental color mapping results) of bimetallic EZUNH-2 MOF.

associated with ZUNH, which are attributed to the lone pair electron n-π* transitions present in the -NH2 group of theATA linker and the π−π* transitions overlapping the ATAlinker accompanied by Zr−O cluster absorption bands,respectively.15,47 Additionally, the similar bands in thebimetallic EZUNH MOFs imply the suitable introduction of Eu ions into the ZUNH framework structure. The optical band gaps of the materials were evaluated by following the Kubelka−Munk equation, as given below in eq 1.

$$\alpha h\nu = A(h\nu - E_g)^{n/2} \qquad (1)$$

Herein, α indicates proportionality constant, h represents Planck's constant, ν specifies the frequency of incident light, Asignifies the light absorption coefficient, and Eg represents the

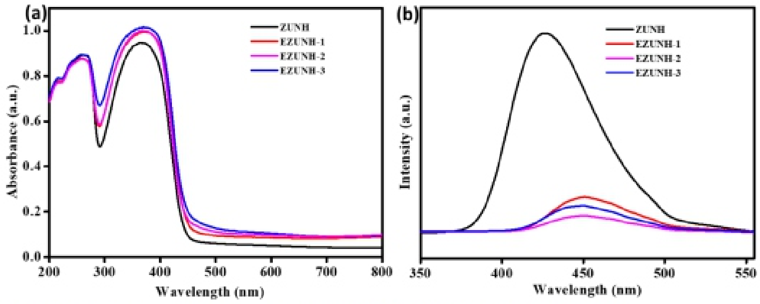

Figure 4. (a) UV−visible DRS spectra and (b) PL spectra of pristine ZUNH and bimetallic EZUNH MOFs.

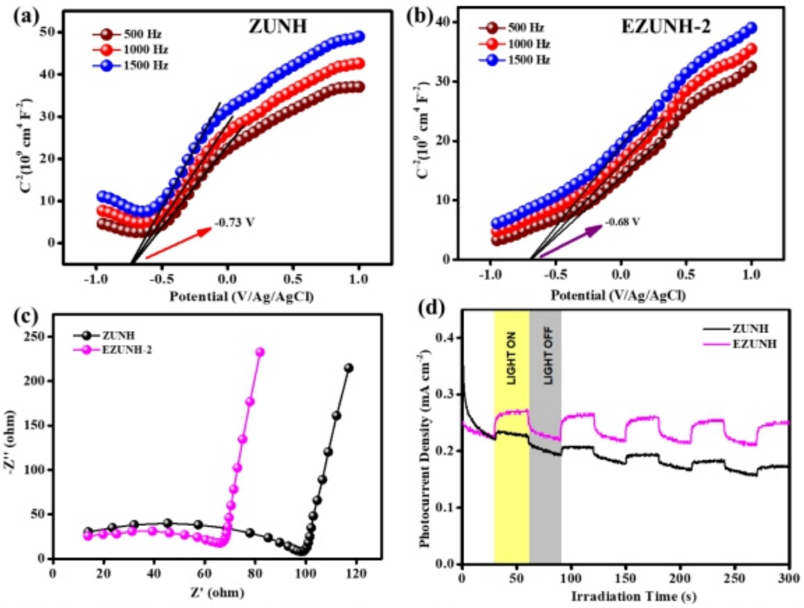

Figure 5. (a−b) Mott−Schottky plot, (c) EIS analysis plot, and (d) transient photocurrent representation of ZUNH and EZUNH-2 MOFs.

optical band gap, respectively. Additionally, the parameter "n"describes the probable reduction of electronic transitions withn = 1, 3, 4, and 6, which correspond to allowed directtransition, forbidden direct transition, allowed indirecttransition, and forbidden indirect transition, respectively.Herein, the fabricated mixed metallic MOF and pristineMOF exhibited allowed indirect transition (n = 4).16 Theoptical band gap of ZUNH was calculated as 2.67 eV. Also, thecalculated band gap energy for the synthesized EZUNHbimetallic MOFs were 2.63, 2.59, and 2.52 eV for EZUNH-1,EZUNH-2, and EZUNH-3 by varying Eu percentage,respectively. The Tauc plots of the prepared photocatalystsare given in Figure S4. It is fairly evident that the addition ofEu ions in their mixed valency states (Eu2+ and Eu3+) accelerates the process of excellent ligand-to-metal charge transfer (LMCT) and that the enhancement of their light absorption tendency is a result of the reduction of the optical band gap, which

in turn improves photocatalytic performance.38
The photoluminescence (PL) analysis was carried out to reveal the migration and separation efficacy of photogeneratedexcitons. Usually, the lower intensity of PL peaks indicatessuperior separation of exciton pairs, which results in higherphotocatalytic activity. From the resulting PL spectra plot,EZUNH-2 shows substantially weaker fluorescence emissionintensity compared to the pristine ZUNH and the other metal-doped composites such as EZUNH-1 and EZUNH-3,which explains the lowering in the recombination rate of photogenerated excitons, as illustrated in Figure 4b. Also, the Zr4+ has been substituted by some Eu3+ content, which exhibitsa superior electron trapping tendency with a slight red shift ofthe emission peak observed that is associated with thenarrowing effect of Eu doping.48,49 Moreover, the timeresolved photoluminescence (TRPL) study of the neat ZUNH and bimetallic EZUNH-2 MOF was used to investigatethe exciton lifetime. This analysis is illustrated in Figure S5 andTable S1, which are adapted to a biexponential modelequation, as stated in eq 2.

$$R(t) = A_1 \exp\{-t/\tau_1\} + A_2 \exp\{-t/\tau_2\} \quad (2)$$

where A stands for amplitude, τ is the exciton life span of each individual component, and R is the normalized emissionintensity. Here, the extended lifetime τ2 and short lifespan τ1reflect the nonradiative relaxation mechanism of light excitonsand radiative recombination, respectively. Herein, the averagelifetime (τavg) can be evaluated to explicate the whole TRPLcharacteristics of both exponential decays by using eq 3.

$$\tau_{avg} = \frac{A_1\tau_1^2 + A_2\tau_2^2}{A_1\tau_1 + A_2\tau_2} \quad (3)$$

For ZUNH and EZUNH-2 MOFs, the excited state lifetimes have averages of 0.504 and 0.533 ns, respectively. This resultincreases the photocatalytic efficiency and supports the PLexperimental results by explaining EZUNH-2 longerexciton than due charge antirecombination.37,50
Electrochemical The Mott−Schottky (MS) study was performed to investigate the band position and charge transfer path in the mixed metallic MOF,as illustrated in Figure 5a,b. The obtained flat band potential(Efb) from the MS plot is a fundamental parameter to obtainthe band edge potentials and paths followed by thephotogenerated e−/h+ in a semiconductor photocatalyst.Here, the flat band potentials of ZUNH and EZUNH-2 are−0.73 and −0.68 eV, respectively, in contrast to the Ag/AgClelectrode, which was evaluated by extrapolating the C2− = 0curve. Subsequently, the CB of ZUNH and EZUNH-2 werefound by following eq 4.

$$E_{(NHE,pH=7)} = E_{Ag/AgCl} - 0.059 \times (7\text{-pH of the electrolyte}) + 0.198 \quad (4)$$

In MS analysis, the pristine ZUNH and bimetallic EZUNH2 show a positive slope, which endorses the n-type behavior of both the prepared MOFs. Furthermore, it is relatively evidentthat the n-type characteristic of the neat ZUNH was inheritedin the bimetallic MOF. Moreover, the slope of the MS graphwas inversely proportional to the charge carrier density. So, thereduction in the slope of EZUNH-2 was supported by highercarrier density, which was calculated using the eq 5.

$$\frac{1}{C^2} = \frac{2}{q \in \epsilon_0 N_d}\left(E - E_{fb} - \frac{K_b T}{q}\right)(\text{n-type}) \quad (5)$$

where kb represents the Boltzmann's constant, E signifies the applied potential, T is the absolute temperature, C shows thespace charge capacitance, Nd is the donor density, Na exhibitsacceptor density, and q represents the electronic charge. $\epsilon 0$ isthe permittivity in vacuum, and ϵ is the dielectric constant ofthe photocatalyst. A positive shift of 0.05 eV was observed inthe flat band potential of EZUNH-2 with respect to pristine ZUNH, signifying the enhanced charge carrier density in the mixed metallic MOF (containing the Eu redox couple). Hence,this higher carrier density promotes the boosted photocatalyticresult in the bimetallic EZUNH-2 MOF. Moreover, from theEfb values, the band structure of parent ZUNH (VB = 2.03 eV,CB = −0.64 eV) and bimetallic EZUNH-2 (VB = 2.0 eV, CB =−0.59 eV) vs Ag/AgCl was obtained by using eq 5 in the NHEscale. Furthermore, the VB and CB values were changed in theNHE scale and are illustrated in mechanism Scheme 2. It hasbeen evidently observed that the CB is slightly shifted towardVB in EZUNH-2 before a minor variation in the actual VBposition, pointing toward a robust and effective LMCT inEZUNH-2 MOF rather than pure ZUNH.51

Also, from electrochemical impedance spectroscopy (EIS)analysis, the effective separation and migration of chargecarriers in the mixed metallic MOF were discovered. Basically,the smaller lower interfacial charge transfer resistance refers tothe semicircular arc diameter, which exhibited superior transferof charge carriers in the material. Figure 5c exhibits theEZUNH-2 composite that shows a quite reduced semicirculararc diameter compared to the pristine ZUNH MOF thatrecommends the antirecombination of charge carriers, whichindicates improved electrical conductivity of the bimetallicEZUNH-2 MOF.50,52,53 The EIS outcome of the bimetallicEZUNH-2 MOF was well supported by the PL studies. Inaddition, current versus potential measurements (LSV) wereperformed to analyze the photogenerated charge carriertransfer and the mechanism of the photocatalyst. Thisinvestigation was performed for the parent ZUNH and allthe bimetallic EZUNH MOFs at 5 mV s−1 in an appropriatepotential range, as depicted in Figure S6. The pristine ZUNHMOF produces an anodic photocurrent, which represents an ntype feature. Also, the bimetallic EZUNH MOFs exhibitanalogous characteristics, possessing enhanced photocurrentcompared to the pristine MOF

At last, the transient photocurrent investigation was executed for the ZUNH and EZUNH-2 MOFs. Theexperiment was accomplished under alternative cycles in darkand visible light ($\lambda \geq 420$ nm) irradiation environments toexhibit the boosted separation efficiency of exciton pairs.Herein, the analysis result was well established with theproduction of photocurrent, which mainly comprises thediffusion of photogenerated e−s to the back contact, and theconsumption of h+s takes place by the hole scavengers presentin the electrolyte solution. As indicated in Figure 5d, theEZUNH-2 MOF exhibited increased transient current, whichsignifies an enhanced lifetime of the excitons in the bimetallicMOF than in the pristine MOF. This was accredited to theeffective separation of photoexcitons or lower recombinationrate promoted through the Eu ion insertion into the ZUNHframework, and this eventually improves the photocatalyticactivity. Moreover, the transient photocurrent investigationoutcomes validate the PL and EIS results, as reported earlier.

4. PHOTOCATALYTIC PERFORMANCE

The photocatalytic behaviors of the prepared samples were analyzed by executing the hydrogen peroxide (H_2O_2) andhydrogen (H_2) production reactions under visible lightirradiation. Primarily, the H_2O_2 production reaction wasexecuted in an O_2-saturated atmosphere with 2 h of visiblelight ($\lambda \geq 420$ nm) illumination under ambient conditions. Butthere was no H_2O_2 production observed in the absence of acatalyst or light, which explains that the catalysts and light are

ISSN 1520-5045

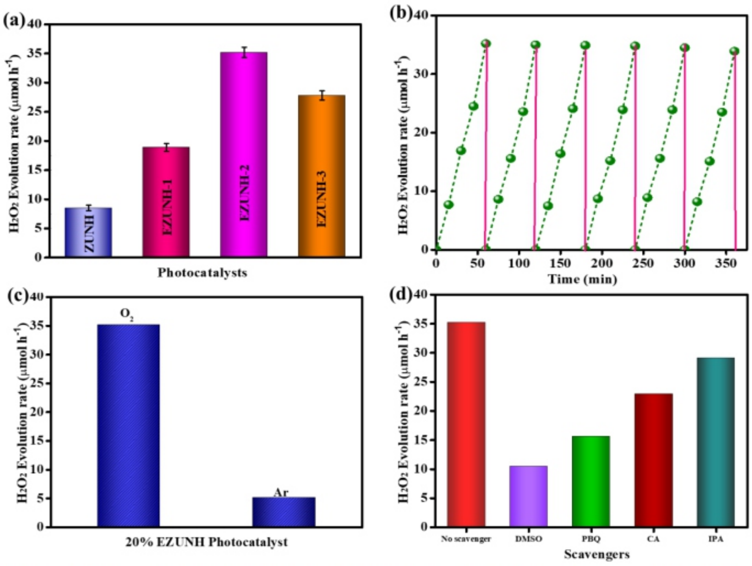

Figure 6. (a) H_2O_2 production rate of pristine ZUNH and bimetallic EZUNH-1, 2, and 3 MOFs (for each photocatalyst, the H_2O_2 production is represented as mean ± SD), (b) reusability test for H_2O_2 production over EZUNH-2 MOF, (c) H_2O_2 production rate in different environments, and (d) scavenger test for H_2O_2 production rate.

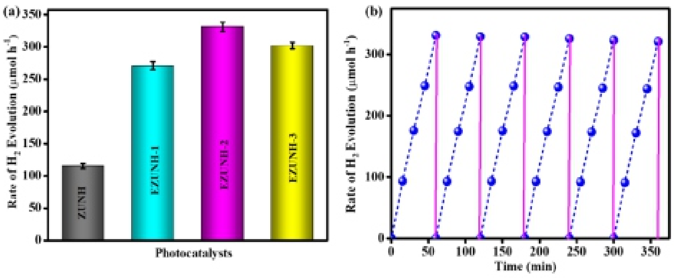

Figure 7. (a) H_2 production rate of pristine ZUNH and bimetallic EZUNH-1, 2, and 3 MOFs (for each photocatalyst, the H_2 production is represented as mean ± SD) and (b) reusability test for H_2 production over EZUNH-2 bimetallic MOF.

he key factors for the reaction to occur. The H2O2 production rate of pristine ZUNH was found to be 8.52 μmol h−1. Herein,among the prepared bimetallic photocatalysts, the EZUNH-2MOF shows maximum H2O2 production rate (35.2 μmol h−1),as shown in Figure 6a. Similarly, a series of experiments wasperformed for H2O2 production of EZUNH-1 and 3 MOFs,where the obtained outcomes were 27.8 and 18.9 μmol h−1respectively. Among all the photocatalytic H2O2 productionresults by the prepared materials, it was observed that thebimetallic MOFs show significantly greater photocatalyticactivity than the pristine ZUNH, which was attributed totheir enhanced light absorption behavior and charge carrierantirecombination capacity due to the presence of Eu ions.

The photocatalytic activity of the synthesized bimetallic MOF (EZUNH-2) was four times greater than that of the pristineZUNH MOF. Furthermore, the reusability experiment of thematerial indicates that the EZUNH-2 MOF exhibits photostability for up to four successive cycles, as depicted in Figure6b. Additionally, the O2 dependency was studied for thephotocatalytic H2O2 production by EZUNH-2 bimetallicMOF, and under Ar and O2 gas purging, two separatereactions were executed, which resulted in a very smallquantity of H2O2 production taking place in the Aratmosphere, as shown in Figure 6c. Thus, it appears that theexistence of an O2 atmosphere is necessary for the photocatalytic generation of H2O2. Moreover, the impact of

Scheme 2. Schematic Illustration of the Mechanistic Path for Photocatalytic H_2O_2 and H_2 Production by the Prepared Bimetallic MOF

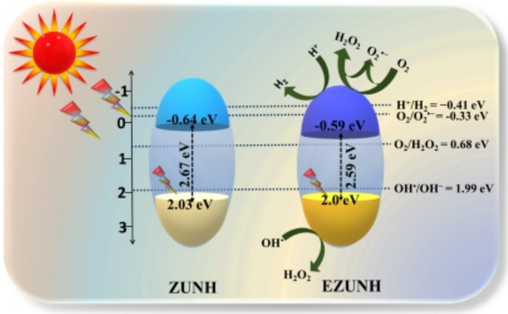

scavengers affecting the production of H2O2 is shown in Figure 6d and is discussed briefly in the Supporting Information. Thecomparison table to show the significance of the preparedbimetallic MOF for H2O2 production is given in Table S4.Alternatively, the photocatalytic H2 evolution efficiency ofthe synthesized materials was also measured with visible lightirradiation. In the absence of light or catalyst, the blankreadings were taken to prove that both the catalyst and lightirradiation are essential for the H2 evolution reaction to takeplace. The pristine MOF ZUNH exhibits less H2 evolution rateof up to 115 μmol h−1, which is due to the fasterrecombination of exciton pairs. However, the bimetallicMOFs show an enhanced H2 production rate because of thesuperior visible light absorption along with greater chargesegregation and transfer. The photocatalytic rate of H2evolution for the prepared bimetallic MOFs EZUNH-1, 2,and 3 was found to be 331.26, 302.01, and 270.81 μmol h−1,respectively, as depicted in Figure 7a. From the resulting plot,the EZUNH-2 exhibits the utmost photocatalytic H2production rate, which is almost 4-fold greater than thepristine ZUNH MOF. The apparent conversion efficiency(ACE) was analyzed to be 2.42%, as shown in Table S3. Thestability of the bimetallic MOF EZUNH-2 was checked byperforming four consecutive cycles of H2 evolution, whichsuggests that there was no substantial change in the rate of H2production, as shown in Figure 7b. Also, the postphotocatalyticXRD has been studied, as given in Figure S5. Table S4 suggeststhe comparative H2 evolution table to show the importance of the prepared EZUNH-2 bimetallic MOF.

5. MECHANISM INSIGHT

Herein, Scheme 2 demonstrates the plausible mechanism of the fabricated mixed metallic EZUNH-2 MOF towardphotocatalytic H2O2 production and H2 evolution undervisible light irradiation, which was expressed thoroughlybased on the aforementioned analytical outcomes. Toinvestigate the fundamental mechanism, characterization analyses like UV−visible DRS, PL, XPS, MS, and EIS weretaken into consideration, from which the experimental resultsindicated a suitable reduction of band edge as well as superiorexciton pair segregation by the insertion of Eu ions into the ZUNH framework toward the H2O2 and H2 production.

Mainly, the reduction in band gap was observed for the EZUNH-2 MOF, which was effectively obtained from Uv−visible DRS and MS investigation outcomes, signifying a robustLMCT and excellent light-harvesting propensity compared tothe pristine counterparts. From the Tauc plot, the obtainedband gap of bimetallic EZUNH-2 MOF was 2.59 eV, which islower than the pristine ZUNH.42 The Eu ion insertion into thepristine MOF lattice reduces the band gap and increases thevisible light captivation capacity. Also, the analysis outcomes ofPL and EIS offer a fascinating observation of improvedantirecombination of photoexcitons in the prepared bimetallicMOFs and promote a longer exciton lifespan than the pristineZUNH. The Eu3+/Eu2+ redox pair shows amended LMCT,which is well supported by the reduction of Zr4+ binding energy in XPS peaks, signifying superior transfer of electrons in the cluster, accelerating the boosted photocatalytic activities.15,53 When the prepared materials were kept for visible light irradiation, the electrons from VB got excited to CB,leaving behind the holes and leading to the production ofhydroxyl radicals. These radicals act as strong oxidants forH_2O_2 production. This process leads to the undesirablerecombination of exciton pairs, which rapidly reduces thephotocatalytic activity. As reported by different groups, theEu^{3+} ions have unfulfilled 4f orbitals, which lead to thereduction of Eu^{3+}. Herein, the Eu^{3+} may accept electrons in theCB to form Eu^{2+}, and these Eu^{2+} ions transport the electrons todissolve O_2 to produce superoxide radicals, inhibiting therecombination of photoexcited charge carriers. This shows thatEu^{3+} acts as an electron scavenger. However, it has beenobserved that the excessive presence of europium ions may act as recombination centers for photogenerated e− and h+ or elsemay block the active sites of the catalyst's surface. Therefore,increasing the dopant concentration causes a sharp decrease inphotoactivity, as seen for EZUNH-3.31,48,54,55 The MS analysisoutcome determines the CB and VB positions of EZUNHMOF as 2.0 and −0.59 eV, respectively. Upon light irradiation,the bimetallic EZUNH-2 got excited to produce the photoexcitons, which occur by the electrons transferred from VB tothe CB, leaving behind holes in the VB, which directed to theprobable efficient reduction and recombination because of the existence of mixed valency metal ions in the framework structure. To investigate the photocatalytic mechanistic insights of H_2O_2 production, the CB potential of EZUNH-2 MOF was found to be −0.59 eV, which is more negative thanthat of the potential of H_2O_2 production at −0.33 eV, which isthe one-electron pathway, and at 0.68 eV, which represents thetwo-electron pathway.56 Thus, the longer lifetime of excitedelectrons endorses O_2 reduction to produce H_2O_2, as shown ineqs 6 and 7.

Single-step two-electron reduction pathway;

$$O_2 + 2H^+ + 2e^- \rightarrow H_2O_2 \tag{6}$$

Two-step single-electron reduction pathway;

$$O_2 \rightarrow {}^{\bullet}O_2^- \rightarrow H_2O_2 \tag{7}$$

Although, the VB of EZUNH-2 consisted of photogenerated h+s, which further get trapped by ethanol (EtOH) as asacrificial agent. Also, the VB potential of EZUNH-2 satisfiesthe formation of hydroxyl radicals (OH•/OH− = 1.99 eV vsNHE). Henceforth, the combination of two OH• radicalsproduces H_2O_2, as depicted in eq 8.

$$OH^{\bullet} + OH^{\bullet} \rightarrow H_2O_2 \tag{8}$$

The efficient H_2O_2 production shown by EZUNH-2 bimetallic MOF is 35.2 μmol h−1. Moreover, the reusabilitytest was performed for stability check of the as-synthesizedmaterial, which endows the stability of the sample up to foursuccessive cycles, as displayed in Figure 6b. Furthermore, toexplicate the mechanistic pathway, scavenger tests were carriedout. As depicted in Figure 6d, there are different scavengingagents like isopropanol (IPA), dimethyl sulfoxide (DMSO),parabenzoquinone (PBQ), and citric acid (CA) were used toexplore the role of OH•, e−, •O2−, and h+, respectively,throughout the photocatalytic H_2O_2 production reaction. Theobserved substantial decrease in the H_2O_2 productionefficiency with PBQ and DMSO addition during the reactiontime can be witnessed in Figure 6d, which demonstrates thate− − and •O2− act as the major active species for O_2 reduction.In addition, IPA and CA play a very certain role towardphotocatalytic H_2O_2 production, which signifies that OH• andh+ are less reactive for the O_2 reduction reaction. Therefore,the analysis results of scavenger tests follow the order e− > • O2− > OH• > h+ toward H_2O_2 production through O2reduction. 9,13 Also, supporting the scavenger tests, the TA(terephthalic acid) and NBT (n itroblue tetrazolium hydrochloride) test results confirm the formation of •O2− and OH• radicals by the bimetallic MOF

EZUNH-2, as shown in Figure S7.57,58

Moreover, the photocatalytic H2 evolution by mixed metal MOFs has been studied by following the mechanistic pathway.With the hole scavenger (10% methanol v/v solution), themanufactured mixed metal composite EZUNH-2 wasemployed for the photoreduction of water to create H2 gas.The H2O molecules can readily be adsorbed on the MOFsurface due to the hydrophilic character of the EZUNH-2framework, which is enhanced by the presence of −NH2moieties. Following this, the protons formed by thedissociation of water molecules uptake the photoexcitedelectrons from the CB of EZUNH-2 and get reduced togenerate H2 gas. The reactions that followed for photocatalyticH2 production were designated as follows:

$$\text{EZUNH}-2 + h\nu \rightarrow \text{EZUNH}-2\ [\text{VB}(h^+)/\text{CB}(e^-)] \quad (9)$$

$$H_2O \rightarrow H^+ + OH^- \quad (10)$$

$$\text{EZUNH}-2\ [\text{CB}(e^-)] + H^+ \rightarrow H_2 \quad (11)$$

$$CH_3OH + h^+ \rightarrow {}^{\bullet}CH_2OH + H^+ \quad (12)$$

$${}^{\bullet}CH_2OH \rightarrow CH_2O + e^- + H^+ \quad (13)$$

$$2H^+ + e^- \rightarrow H_2 \quad (14)$$

6. SUMMARY

Summarily, the synthesized single-component mixed metallic EZUNH MOF has been found to be a robust photocatalysttoward H2O2 and H2 production under light irradiation. Thesuperiority of the current work is followed by (i) The preparedsingle-component photocatalyst is a mixed valency (Eu3+/Eu2+) and bimetallic (Eu/Zr) MOF, i.e., (Eu3+/Eu2+) EZUNH,which is synthesized by a one-step solvothermal method.(ii)The integration of mixed valency (Eu3+/Eu2+) into thebimetallic framework gives superior exciton pair antirecombination, high light absorption efficacy, and enhanced electrochemical properties, resulting in boosted photocatalytic activitycompared to the pristine ZUNH MOF. (iii)The joint effect ofboth the metal nodes and -NH2 functionalized linker inEZUNH MOFs results in a blueshift of the band gap andeffective band edge positions for superior light absorption witha slight reduction in surface area. (iv)The fabricated EZUNH-2bimetallic MOF exhibits the highest photocatalytic H2evolution rate of up to 331.26, along with an ACE value of2.42%, which is almost 3-fold that of the pristine MOF. Also,the photocatalytic H2O2 production rate has been found to be35.2, which is up to 4-fold compared to that of the pristineframework. Herein, e−s are the main active species for H2O2production, as found from the scavenger test experiments.Finally, from the above results, it has been confirmed thatthe bimetallic EZUNH MOF is the first used photocatalysttoward H2 and H2O2 production (μmol h−1) under visible lightirradiation.

■ ASSOCIATED CONTENT

*sı Supporting Information

The Supporting Information is available free of charge at https://pubs.acs.org/doi/10.1021/acs.iecr.4c04234.1. Experimental techniques (1.1. CharacterizationTechniques, 1.2. FTO preparation, 1.3. Scavenger testprocedure, and 1.4. TA and NBT analysis procedure);BET surface of EZUNH-2 (Figure S1); XPS surveyspectrum of EZUNH-2 (Figure S2); (a) FESEM and(b) HRTEM images of pristine ZUNH MOF (FigureS3); Tauc plot for ZUNH, EZUNH-1, EZUNH-2 andEZUNH-3 (Figure S4); TRPL plot of EZUNH-2(Figure S5); LSV plot for pristine ZUNH and bimetallicEZUNH-1,2 and 3 MOFs (Figure S6); TA and NBTanalysis results (Figure S7); postphotocatalytic and 24-haqueous string PXRD (Figure S8); TRPL data of ZUNHand

EZUNH-2 (Table S1); apparent conversionefficiency (ACE) expression and calculation for photocatalytic hydrogen evolution by the prepared photocatalysts (Table S2); comparative table for photocatalytic H2 production by various photocatalysts (Table S3); comparative table for photocatalytic H2O2production by various photocatalysts (Table S4) (PDF)

■ AUTHOR INFORMATION

Corresponding Author

Kulamani Parida − Centre for Nano Science and Nanotechnology, Siksha 'O' Anusnadhan (Deemed to beUniversity), Bhubaneswar, Odisha 751030, India;orcid.org/0000-0001-7807-5561; Phone: +91-674-2351777; Email: paridakulamani@yahoo.com,kulamaniparida@soa.ac.in; Fax: +91-674-2350642

Authors

Srabani Dash − Centre for Nano Science and Nanotechnology,Siksha 'O' Anusnadhan (Deemed to be University),Bhubaneswar, Odisha 751030, India

Suraj Prakash Tripathy − Centre for Nano Science and Nanotechnology, Siksha 'O' Anusnadhan (Deemed to beUniversity), Bhubaneswar, Odisha 751030, India

Satyabrata Subudhi − Centre for Nano Science and Nanotechnology, Siksha 'O' Anusnadhan (Deemed to beUniversity), Bhubaneswar, Odisha 751030, India

Complete contact information is available at:https://pubs.acs.org/10.1021/acs.iecr.4c04234

Author Contributions

#S.D. and S.P.T have equal contributions.

Notes

The authors declare no competing financial interest.

■ ACKNOWLEDGMENTS

The S 'O' A (Deemed to be University) management is very much thankful and acknowledges the encouragement andconstant support in the research work.

■ *REFERENCES*

(1) Ray, A.; Subudhi, S.; Tripathy, S. P.; Acharya, L.; Parida, K.MOF Derived C/N Co-Doped ZnO Modified through Facile In SituCoupling with NixPy toward Photocatalytic H2O2 Production andH2 Evolution Reaction. Adv. Mater. Interfaces 2022, 9 (34), 2201440.

(2) Ma, L.; Gao, Y.; Wei, B.; Huang, L.; Zhang, N.; Weng, Q.;Zhang, L.; Liu, S. F.; Jiang, R. Visible-Light Photocatalytic H 2 O 2Production Boosted by Frustrated Lewis Pairs in Defected PolymericCarbon Nitride Nanosheets. ACS Catal. 2024, 14 (4), 2775−2786.

(3) Guo, Y.; Tong, X.; Yang, N. Photocatalytic and ElectrocatalyticGeneration of Hydrogen Peroxide: Principles, Catalyst Design andPerformance. Nano-Micro Lett. 2023, 15 (1), 77.

(4) Hou, H.; Zeng, X.; Zhang, X. Production of Hydrogen Peroxide by Photocatalytic Processes. Angew. Chem., Int. Ed. 2020, 59, 17356−17376.

(5) Xue, C.; Wang, P.; Che, H.; Liu, W.; Liu, B.; Ao, Y. Simultaneous Organic Pollutant Degradation and Hydrogen Peroxide Productionby Molecular-Engineered Carbon Nitride. Appl. Catal., B 2024, 340,123259.

(6) Xu, J.; Che, H.; Tang, C.; Liu, B.; Ao, Y. Tandem Fields Facilitating Directional Carrier Migration in

Van Der WaalsHeterojunction for Efficient Overall Piezo-Synthesis of H2O2. Adv. Mater. 2024, 36 (32), 2404539.

(7) Che, H.; Gao, X.; Chen, J.; Hou, J.; Ao, Y.; Wang, P. IodideInduced Fragmentation of Polymerized Hydrophilic Carbon Nitride for High-Performance Quasi-Homogeneous Photocatalytic H2O2 Production. Angew. Chem., Int. Ed. 2021, 60 (48), 25546−25550.

(8) Panda, J.; Behera, P.; Subudhi, S.; Tripathy, S. P.; Swain, G.;Dash, S.; Parida, K. MgIn2S4-decorated MOF-derived C/N−CeO2nanorod heterojunctions as efficient photocatalysts towards H2O2production reactions and H2 evolution reactions. Mater. Adv. 2024, 5(11), 4865−4877.

(9) Biswal, L.; Tripathy, S. P.; Dash, S.; Das, S.; Subudhi, S.; Parida,K. Aggrandized photocatalytic H 2 O 2 and H 2 production by a TiO2 /Ti 3 C 2 −TiC/mixed metal Ce−Zr MOF composite: aninterfacial engineered solid-state-mediator-based Z-scheme heterostructure. Mater. Adv. 2024, 5 (10), 4452−4466.

(10) Chen, X.; Kuwahara, Y.; Mori, K.; Louis, C.; Yamashita, H.Introduction of a Secondary Ligand into Titanium-Based MetalOrganic Frameworks for Visible-Light-Driven Photocatalytic Hydrogen Peroxide Production from Dioxygen Reduction. J. Mater. Chem. A2021, 9 (5), 2815−2821.

(11) Subudhi, S.; Swain, G.; Tripathy, S. P.; Parida, K. UiO-66-NH2Metal-Organic Frameworks with Embedded MoS2Nanoflakesfor Visible-Light-Mediated H2and O2Evolution. Inorg. Chem. 2020,59 (14), 9824−9837.

(12) Tripathy, S. P.; Subudhi, S.; Ray, A.; Behera, P.; Panda, J.;Dash, S.; Parida, K. Hydrolytically Stable Mixed Ditopic Linker BasedZirconium Metal Organic Framework as a Robust Photocatalysttowards Tetracycline Hydrochloride Degradation and HydrogenEvolution. J. Colloid Interface Sci. 2023, 629, 705−718.

(13) Dash, S.; Tripathy, S. P.; Subudhi, S.; Acharya, L.; Ray, A.;Behera, P.; Parida, K. Ag/Pd Bimetallic Nanoparticle-Loaded ZrMOF: An Efficacious Visible-Light-Responsive Photocatalyst forH2O2 and H2 Production. Energy Adv. 2024, 3 (5), 1073−1086.

(14) Chang, H.; Li, Y.; Jia, X.; Shen, Q.; Li, Q.; Liu, X.; Xue, J.Construction of an Amino-Rich Ni/Ti Bimetallic MOF Compositewith Expanded Light Absorption and Enhanced Carrier Separation forEfficient Photocatalytic H2 Evolution. Mater. Sci. Semicond. Process.2022, 150, 106914.

(15) Tripathy, S. P.; Subudhi, S.; Ray, A.; Behera, P.; Bhaumik, A.;
Parida, K. Mixed-valence bimetallic Ce/Zr MOF-based nanoarchitecture: a visible-light-active photocatalyst for ciprofloxacin degradation and hydrogen evolution. Langmuir 2022, 38 (5),1766−1780.

(16) Li, T.; Zhang, L.; Li, X.; Wang, X.; Jin, Z. Design and Synthesis of Phosphating Bimetallic CeCo-MOF for Substantially ImprovedPhotocatalytic Hydrogen Evolution. J. Mater. Chem. C 2022, 10 (22),8750−8761.

(17) Prakash Tripathy, S.; Subudhi, S.; Das, S.; Kumar Ghosh, M.;Das, M.; Acharya, R.; Acharya, R.; Parida, K. Hydrolytically StableCitrate Capped Fe3O4@UiO-66-NH2MOF: A Hetero-StructureComposite with Enhanced Activity towards Cr (VI) Adsorptionand Photocatalytic H2 Evolution. J. Colloid Interface Sci. 2022, 606,353−366.

(18) Subudhi, S.; Mansingh, S.; Tripathy, S. P.; Mohanty, A.;Mohapatra, P.; Rath, D.; Parida, K. The Fabrication of Au/PdPlasmonic Alloys on UiO-66-NH2: An Efficient Visible Light-InducedPhotocatalyst towards the Suzuki Miyaura Coupling Reaction underAmbient Conditions. Catal. Sci. Technol. 2019, 9 (23), 6585−6597.

(19) Luo, J.; Zhang, S.; Sun, M.; Yang, L.; Luo, S.; Crittenden, J. C.A Critical Review on Energy Conversion and EnvironmentalRemediation of Photocatalysts with Remodeling Crystal Lattice,Surface, and Interface. ACS Nano 2019, 13, 9811−9840.

(20) Zhou, H. C.; Long, J. R.; Yaghi, O. M. Introduction to MetalOrganic Frameworks. Chem. Rev. 2012,

112 (2), 673−674.
(21) Subudhi, S.; Tripathy, S. P.; Parida, K. Highlights of the Characterization Techniques on Inorganic, Organic (COF) andHybrid (MOF) Photocatalytic Semiconductors. Catal. Sci. Technol.2021, 11 (2), 392−415.
(22) Tripathy, S. P.; Subudhi, S.; Ray, A.; Behera, P.; Parida, K.Metal Organic Framework-Based Janus Nanomaterials: RationalDesign, Strategic Fabrication and Emerging Applications. DaltonTrans. 2022, 51 (14), 5352−5366
(23) Zhang, L.; He, Y.; Wu, Y.; Zhang, J.; Li, S.; Zhang, Z. Highly Sensitive Ratiometric Fluorescence Detection of TetracyclineResidues in Food Samples Based on Eu/Zr-MOF. Food Chem.2024, 436, 137717.
(24) Qiu, J.; Dai, D.; Yao, J. Tailoring Metal−Organic Frameworks for Photocatalytic H2O2 Production. Coord. Chem. Rev. 2024, 501,215597.
(25) Kondo, Y.; Kuwahara, Y.; Mori, K.; Yamashita, H. Design of Metal-Organic Framework Catalysts for Photocatalytic HydrogenPeroxide Production. Chem 2022, 8 (11), 2924−2938.
(26) Du, X.-D.; Yi, X.-H.; Wang, P.; Zheng, W.; Deng, J.; Wang, C.-C. Robust Photocatalytic Reduction of Cr(VI) on UiO-66-NH2(Zr/Hf) Metal-Organic Framework Membrane under Sunlight Irradiation.Chem. Eng. J. 2019, 356, 393−399.
(27) Zhang, B.; Pei, Y.; Maligal-Ganesh, R. V.; Li, X.; Cruz, A.;Spurling, R. J.; Chen, M.; Yu, J.; Wu, X.; Huang, W. Influence of Snon Stability and Selectivity of Pt-Sn@UiO-66-NH2 in FurfuralHydrogenation. Ind. Eng. Chem. Res. 2020, 59 (39), 17495−17501.
(28) Wang, M.; Yang, L.; Guo, C.; Liu, X.; He, L.; Song, Y.; Zhang, Q.; Qu, X.; Zhang, H.; Zhang, Z.; Fang, S. Bimetallic Fe/Ti-BasedMetal−Organic Framework for Persulfate-Assisted Visible LightPhotocatalytic Degradation of Orange II. ChemistrySelect 2018, 3(13), 3664−3674.
(29) Meng, S.; Li, G.; Wang, P.; He, M.; Sun, X.; Li, Z. Rare EarthBased MOFs for Photo/Electrocatalysis. Materials Chemistry Frontiers. Mater. Chem. Front. 2023, 17, 806−827.
(30) Mahata, P.; Mondal, S. K.; Singha, D. K.; Majee, P.Luminescent Rare-Earth-Based MOFs as Optical Sensors. DaltonTrans. 2017, 46 (2), 301−328.
(31) Zong, Y.; Li, Z.; Wang, X.; Ma, J.; Men, Y. Synthesis and High Photocatalytic Activity of Eu-Doped ZnO Nanoparticles. Ceram. Int.2014, 40 (7), 10375−10382.
(32) Li, Y.; Wang, J.; Huang, Z.; Qian, C.; Tian, Y.; Duan, Y. An EuDoped Zr-Metal-Organic Framework for Simultaneous Detection and Removal of Antibiotic Tetracycline. J. Environ. Chem. Eng. 2021, 9(5), 106012.
(33) He, X.; Liu, Y.; Wang, Q.; Wang, T.; He, J.; Peng, A.; Qi, K.Facile fabrication of Eu-based metal−organic frameworks for highlyefficient capture of tetracycline hydrochloride from aqueous solutions.Sci. Rep. 2023, 13 (1), 11107.
(34) Choi, J. R.; Tachikawa, T.; Fujitsuka, M.; Majima, T.Europium-Based Metal-Organic Framework as a Photocatalyst forthe One-Electron Oxidation of Organic Compounds. Langmuir 2010,26 (13), 10437−10443.
(35) Xu, X. Y.; Yan, B. Eu(III) Functionalized Zr-Based MetalOrganic Framework as Excellent Fluorescent Probe for Cd2+Detection in Aqueous Environment. Sens. Actuators, B 2016, 222,347−353.
(36) Subudhi, S.; Paramanik, L.; Sultana, S.; Mansingh, S.;Mohapatra, P.; Parida, K. A Type-II Interband AlignmentHeterojunction Architecture of Cobalt Titanate Integrated UiO-66-NH2: A Visible Light Mediated Photocatalytic Approach Directedtowards Norfloxacin Degradation and Green Energy (Hydrogen)Evolution. J. Colloid Interface Sci. 2020, 568, 89−105.
(37) Tripathy, S. P.; Subudhi, S.; Ray, A.; Behera, P.; Swain, G.;Chakraborty, M.; Parida, K. MgIn2S4/UiO-66-NH2MOF-Based Heterostructure: Visible-Light-Responsive Z-Scheme-Mediated

Synergistically Enhanced Photocatalytic Performance toward Hydrogen and Oxygen Evolution. Langmuir 2023, 39 (21), 7294−7306.

(38) Li, C.; Huang, J.; Zhu, H.; Liu, L.; Feng, Y.; Hu, G.; Yu, X.Dual-Emitting Fluorescence of Eu/Zr-MOF for Ratiometric SensingFormaldehyde. Sens. Actuators, B 2017, 253, 275−282.

(39) Prakash Tripathy, S.; Dash, S.; Ray, A.; Subudhi, S.; Parida, K.Inexpensive Carbon Based Co-Catalyst Modified Zr-MOF TowardsPhotocatalytic H2O2 and H2 Production. Chem. -Asian J. 2025, 20,No. e202401115.

(40) Mosleh, S.; Rezaei, K.; Dashtian, K.; Salehi, Z. Ce/Eu RedoxCouple Functionalized HKUST-1 MOF Insight to Sono-Photodegradation of Malathion. J. Hazard. Mater. 2021, 409, 124478.

(41) Nguyen, H. T. T.; Tran, K. N. T.; Van Tan, L.; Tran, V. A.; Doan, V. D.; Lee, T.; Nguyen, T. D. Microwave-AssistedSolvothermal Synthesis of Bimetallic Metal-Organic Framework forEfficient Photodegradation of Organic Dyes. Mater. Chem. Phys. 2021,272, 125040.

(42) Subudhi, S.; Swain, G.; Tripathy, S. P.; Parida, K. UiO-66-NH2Metal-Organic Frameworks with Embedded MoS2 Nanoflakes for Visible-Light-Mediated H2and O2 Evolution. Inorg. Chem. 2020,59 (14), 9824−9837.

(43) Liu, D.; Li, M.; Li, X.; Ren, F.; Sun, P.; Zhou, L. Core-Shell Zn/ Co MOFs Derived Co3O4/CNTs as an Efficient MagneticHeterogeneous Catalyst for Persulfate Activation and OxytetracyclineDegradation. Chem. Eng. J. 2020, 387, 124008.

(44) Zheng, J.; Sun, L.; Jiao, C.; Shao, Q.; Lin, J.; Pan, D.; Naik, N.;Guo, Z. Hydrothermally Synthesized Ti/Zr Bimetallic MOFs DerivedN Self-Doped TiO2/ZrO2 Composite Catalysts with EnhancedPhotocatalytic Degradation of Methylene Blue. Colloids Surf., A 2021,623, 126629.

(45) Sonowal, K.; Kalita, S. J.; Purkayastha, S. K.; Goswami, J.;Basyach, P.; Das, R.; Borborah, A.; Guha, A. K.; Saikia, L. HighlyLuminescent Eu3+-Incorporated Zr-MOFs as Fluorescence Sensorsfor Detection of Hazardous Organic Compounds in Water and FruitSamples. ACS Omega 2024, 9 (2), 2504−2518.

(46) Haque, Z.; Thakur, G. S.; Parthasarathy, R.; Gerke, B.; Block,T.; Heletta, L.; Pöttgen, R.; Joshi, A. G.; Selvan, G. K.; Arumugam, S.;Gupta, L. C.; Ganguli, A. K. Unusual Mixed Valence of Eu in TwoMaterials-EuSr2Bi2S4F4 and Eu2SrBi2S4F4: Mössbauer and X-RayPhotoemission Spectroscopy Investigations. Inorg. Chem. 2017, 56(6), 3182−3189.

(47) Dash, S.; Tripathy, S. P.; Subudhi, S.; Behera, P.; Mishra, B. P.;Panda, J.; Parida, K. A Visible Light-Driven α-MnO2/UiO-66-NH2 SScheme Photocatalyst toward Ameliorated Oxy-TCH Degradationand H2 Evolution. Langmuir 2024, 40 (8), 4514−4530.

(48) Xu, D.; Li, X.; Liu, J.; Huang, L. Synthesis and Photocatalytic Performance of Europium-Doped Graphitic Carbon Nitride. J. RareEarths 2013, 31 (11), 1085−1091.

(49) Murugadoss, G. Synthesis and study of optical and thermal properties of multi layers coated CdS core−shell nanocomposites. J.Lumin. 2014, 146, 430−434.

(50) Acharya, L.; Biswal, L.; Mishra, B. P.; Das, S.; Dash, S.; Parida, K. A Schottky/Z-Scheme Hybrid for Augmented Photocatalytic H2and H2O2 Production. Chem. -Eur. J. 2024, 30 (46), No. e202400496.

(51) Hankin, A.; Bedoya-Lora, F. E.; Alexander, J. C.; Regoutz, A.;Kelsall, G. H. Flat Band Potential Determination: Avoiding thePitfalls. J. Mater. Chem. A 2019, 7 (45), 26162−26176.

(52) Li, H.; Wang, X.; Zhang, X.; He, M.; Zhang, J.; Liu, P.; Tang,X.; Li, C.; Wang, Y. Eu-MOF Nanorods Functionalized with LargeHeterocyclic Ionic Liquid for Photoelectrochemical Immunoassay ofα-Fetoprotein. Anal. Chim. Acta 2022, 1195, 339459.

(53) Chen, S.; Xu, X.; Gao, H.; Wang, J.; Li, A.; Zhang, X. FineTuning the Metal Oxo Cluster Composition and Phase Structure of Ni/Ti Bimetallic MOFs for Efficient CO2 Reduction. J. Phys. Chem.

C2021, 125 (17), 9200−9209.
(54) Zhang, A.; Zhang, J. Effects of Europium Doping on the Photocatalytic Behavior of BiVO4. J. Hazard. Mater. 2010, 173 (1−3), 265−272.
(55) Xiaohong, W.; Wei, Q.; Xianbo, D.; Weidong, H.; Zhaohua, J.Dopant Influence on the Photo-Catalytic Activity of TiO2 FilmsPrepared by Micro-Plasma Oxidation Method. J. Mol. Catal. A: Chem.2007, 268 (1−2), 257−263.
(56) Qiu, J.; Yao, J. Ligand Functionalization of Metal-Organic Frameworks for Photocatalytic H2O2 Production. Eur. J. Inorg. Chem.2024, 27 (10), No. e202300773.
(57) Palanivel, B.; Mani, A. Conversion of a Type-II to a Z-Scheme Heterojunction by Intercalation of a 0D Electron Mediator betweenthe Integrative NiFe2O4 /g-C3N4. Composite Nanoparticles: boostingThe Radical Production For Photo-Fenton Degradation. ACS Omega2020, 5 (31), 19747−19759.
(58) Kumar Pradhan, S.; Bariki, R.; Kumar Nayak, S.; Panda, S.; Kanungo, S.; Mishra, B. G. Low Temperature in Situ Fabrication ofNiFe2O4/Tetragonal-BiVO4/Bi2MoO6 Ternary Heterostructure: AConjugated Step-Scheme Multijunction Photocatalyst with Synergistic Charge Migration for Antibiotic Photodegradation andH2Generation. J. Colloid Interface Sci. 2024, 654, 523−538.

ISSN 1520-5045

Fault Diagnosis in Chemical Reactors with Data-Driven Methods

Pu Du, Nabil M. Abdel Jabbar, Benjamin A. Wilhite, and Costas Kravaris*

A B S T R A C T

This study investigates fault diagnosis, encompassing fault detection, isolation, and estimation, with experimental data in acontinuous stirred-tank reactor (CSTR) for the liquid-phase catalyticoxidation of 3-picoline with hydrogen peroxide. Two key faults wereexamined: coolant inlet temperature spikes (fault 1) and 3-picoline feedconcentration decreases (fault 2). Data-driven methods, including randomforest (RF) and k-nearest neighbors (KNN), successfully detected,isolated, and estimated faults under nominal conditions. However, bothdata-driven and model-based residual generators were disrupted by a shiftin the heat transfer coefficient (U). An isolation forest (IF) algorithm wasused for anomaly detection and model recalibration, restoring modelbased performance. Updated data sets enabled RF and KNN to adapteffectively, demonstrating their scalability and adaptability. Experimental results highlight the strengths of both methods, advocatingfor a combined framework for robust fault diagnosis.

1. INTRODUCTION

Fault diagnosis is a critical aspect of process safety in the chemical industry, where the reliability of operations candirectly influence productivity, economic performance, and,most importantly, safety.1,2 Chemical processes are highlycomplex and involve multiple interrelated variables, oftenoperating under extreme conditions of temperature, pressure,and chemical reactivity. Any undetected faults within thesesystems can lead to equipment malfunction, production losses,environmental hazards, and, in severe cases, catastrophicaccidents involving the loss of life. Therefore, ensuring robustand timely fault diagnosis systems is paramount to mitigaterisks and enhance the overall reliability of industrialoperations.3

Fault diagnosis systems aim to detect, isolate, and estimate faults as early as possible to enable timely corrective actions,with each objective becoming progressively more challenging.In the chemical industry, faults can arise from various sourcesincluding sensor failures, actuator malfunctions, equipmentdegradation, and process disturbances. As processes becomemore automated and large-scale, human operators often facechallenges in manually identifying abnormal conditions due tothe overwhelming amount of data generated by processsensors. Hence, automated fault diagnosis methods havegained prominence as key components of process safetyframeworks. Early and accurate diagnosis not only preventsaccidents but also optimizes maintenance schedules, reducesdowntime, and enhances process efficiency. The necessity ofrobust fault diagnosis systems in the chemical industry has propelled the development of two primary approaches: modelbased and data-driven methods.4−6

Each approach offers distinct advantages and faces its own set of challenges. Model-based fault diagnosis involvesconstructing a mathematical representation of the system tocompare real-time data with model-predicted outputs.Deviations from the expected behavior, known as residuals,are indicative of faults.7 In contrast, data-driven approachesrely on historical operational data to train machine learningmodels to detect and classify faults.8,9 While model-basedmethods leverage knowledge of the system's physics, datadriven techniques exploit patterns and trends hidden withinlarge data sets.Model-based fault diagnosis techniques have long beenfavored in chemical process control due to their strongfoundation in process physics. These methods are based onfirst principles�such as mass and energy balances�or empirical models that describe the behavior of the system.The core idea is to generate residuals, or error signals, bycomparing the system's actual measurements with predictionsfrom the model. If a fault occurs, the residuals will deviatesignificantly from zero, indicating abnormal behavior. Popularmodel-based fault diagnosis techniques include observerbased,10−13 parameter estimation,7,14 and parity spaceapproaches.15,16

Model-based approaches offer the advantage of physical insight, enabling fault detection, root cause analysis, and faultsize estimation without relying on extensive historical data.They are particularly reliable for rare or unmonitored faults butare heavily dependent on the accuracy of the system model.Developing such models for complex chemical processes ischallenging and time-consuming, requiring a deep knowledgeof process dynamics and operational variables. Additionally,real-world systems evolve over time due to factors such asequipment aging or operational changes, leading to modelmismatch and potential diagnostic errors. Adaptive modeling isoften needed to recalibrate the model, adding complexity andeffort, which limits the practical implementation of modelbased methods despite their reliability.

On the other hand, data-driven fault diagnosis methods have gained increasing popularity with the rise of machine learningand big data analytics. Data-driven approaches do not requireexplicit knowledge of the underlying system dynamics.8,17Instead, they rely on patterns, correlations, and anomaliespresent in the historical process data. Techniques such asrandom forest18,19 (RF), isolation forest20,21 (IF), supportvector machines22,23 (SVM), artificial neural networks24−26(ANN), and principal component analysis22,27,28 (PCA) arecommonly used in data-driven fault diagnosis applications.John MacGregor and Nomikos have made monumentalcontributions to process monitoring and fault detection inchemical processes, proposing a PCA-based approach usingonly data from successful batches to monitor a styrene−butadiene semibatch reactor.29 An advanced fault isolationmethod has been developed to handle both simple andcomplex faults by extracting fault signatures and comparingthem with a fault library of historical data.30 Additionally, afault-tolerant control strategy employing data-driven latentvariable models constructed from historical process data ishighlighted, emphasizing their reduced dimensionality andinterpretability.31 Recent studies, particularly in Industrial &Engineering Chemistry Research (I&ECR), have focused onintegrating machine learning (ML) and artificial intelligence (AI) with process monitoring and fault diagnosis.32 By linking fault diagnosis models with real-time digital replicas of physicalsystems, these approaches enable proactive maintenance,predictive analytics, and performance optimization.33−36The strength of data-driven methods lies in their ability tohandle complex, nonlinear systems without the need fordetailed models of the process. They are particularly wellsuited for systems in which developing an accurate model isimpractical or infeasible. Moreover, once trained, data-drivenmodels can be deployed to monitor systems in real-time anddetect a wide range of faults with minimal human intervention.These methods are also highly scalable, making themapplicable to large and complex processes with multiplesensors and data points. However, the major challengeassociated with data-driven approaches is the requirement forlarge and diverse data sets. In many cases, particularly for faultsize estimation, data-driven models often require training ondata sets that encompass a diverse range of fault scenarios ensure satisfactory performance.37,38 In the chemical industry,where processes often run under nominal operating conditionsfor extended periods, it is difficult to obtain sufficient datarepresenting the various faulty states.

Recently, combined fault diagnosis methods, which incorporate the strengths of model-based and data-driven techniques, have emerged as a promising solution to overcome the limitations of both approaches.39−41 These methods aim to integrate the physical insights offered by model-basedapproaches with the pattern-recognition capabilities of datadriven methods. For instance, model residuals can be used asinputs to a machine learning model, enabling more accurate fault classification. Alternatively, data-driven methods can beused to update model parameters in real-time, improving themodel's adaptability to changing system conditions.

Despite the potential advantages of combined approaches, their practical implementation remains limited, especially whenapplied to experimental data for achieving all three aspects offault diagnosis: detection, isolation, and estimation. Moststudies in the literature focus on simulation-based validation,where fault scenarios can be artificially generated and tested.For example, the Tennessee Eastman (TE) process is acommon testbed for data-driven and model-based methods.42−44 As for experimental study, a hybrid approach combining an extended Kalman filter (EKF) with aprobabilistic neural network classifier has been successfullyapplied for fault detection and diagnosis in fed-batch and batchreactors, providing accurate monitoring through the estimationof reactor parameters and classification of fault types.45 Arobust fault detection methodology for hybrid process systems,incorporating tools from unknown input observer theory andLyapunov stability, has been developed to reliably distinguishbetween faults, mode transitions, and uncertainties.46 A hybriddata/model-based approach combining SVM with an observeris proposed for fault detection and isolation in nonlinearchemical reactions, effectively reducing the reliance on preciseprocess models or extensive training data.23 A hybrid modelcombining first-principles and neural networks was developedfor automatic fault detection and identification, leveraging bothsimulation data and historical process information. Tested onreal data from a methanol−water distillation column, thismethod outperformed traditional first-principles models byeffectively identifying faults and demonstrating its potential forapplication in refining and petrochemical processes.47

Recently, we introduced a comprehensive fault diagnosis methodology for a CSTR chemical reaction system, leveragingmodel-based residual generators as estimators, systematic dataprocessing to mitigate noise, and predefined thresholds forfault alarms. These residual generators, designed as functionalobservers decoupled from disturbances, estimate fault sizes.Fault isolation is achieved through multiple independent residual generators.48,49 The experiment successfully demonstrated the effectiveness of fault diagnosis in a CSTR acrossvarious fault scenarios.50 During these experiments, anintriguing phenomenon caught our attention: after switchingequipment, the previous model's performance declined.Further experimentation suggested that this might be due toa change in the heat transfer coefficient. This raised importantquestions about how to detect model mismatches or parameterchanges and how we could leverage known experimental datato enhance the fault diagnosis. Addressing these issues wasessential to our work.

In this study, we examine data-driven approaches for fault diagnosis in chemical reactors, comparing them with modelbased observers. While model-based residual generators excelin robustness and accuracy, especially when the system'sdynamics are well understood, data-driven methods like RFand KNN offer promising, scalable solutions. Whereas both methods performed well under nominal conditions, systemparameter changes, like shifts in the heat transfer coefficient (U), posed challenges for both approaches. To address this, we implemented an isolation forest (IF) algorithm for anomalydetection and model recalibration. The study shows thatcombining data-driven and model-based methods can enhancefault diagnosis, with data-driven techniques becoming morerobust after training in updated system conditions.

2. BACKGROUND AND METHOD

This section introduces the reaction system and summarizes key results achieved using model-based fault diagnosistechniques. However, some challenges remain that cannot beeffectively addressed by model-based methods alone. Thislimitation motivates the exploration of a hybrid approach thatleverages the strengths of both model- and data-driventechniques. Additionally, the fundamentals of the data-drivenmethods applied in this work are briefly outlined.

2.1. Reactor (CSTR) Model and Experiment Setup.

The N-oxidation of alkylpyridine is a crucial reaction in drug synthesis and pharmaceutical applications. Studies have shownthat a continuous stirred tank reactor (CSTR) is an effectivesystem for the N-oxidation of 3-picoline using hydrogenperoxide,51 a process aligned with green chemistry principles.The reaction mechanism is illustrated in Figure 1.

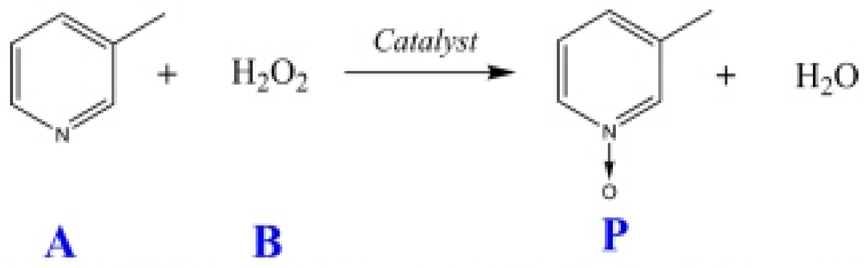

Figure 1. Reaction of catalyzed 3-picoline (A) *N*-oxidation with hydrogen peroxide (B) to produce *N*-oxidized 3-picoline (P) and water.

The CSTR setup and experimental process are schematically represented in Figure 2, with a 50 mL jacketed glass The objective is to detect, isolate, and estimate two faults inthis process (for detailed information, refer to the cited work).During the experiments, faults were introduced, and sensorreadings (TT1 for reactor temperature, TT2 for jackettemperature, and AT for 3-picoline concentration) were usedto successfully diagnose faults. This was achieved using model based residual generators derived from the functional observer applied to the system equations (eqs 1−5). Fault detection,isolation, and estimation were successfully achieved in our experiments using model-based residual generators.50

The reaction model is built with mass and energy balances, where CA is the concentration of reactant 3-picoline, CB is theconcentration of reactant hydrogen peroxide, w(t) is theunknown kinetics variation, R(CA,CB,T) is the reaction rate, Tis the reactor temperature, δt = 0.1 s as the discretization time interval, and Tj is the jacket temperature. The system dynamicsand the specifics of the residual generators are detailed asfollows:50

$$C_A(k+1) = C_A(k) + \delta_t\Big(\frac{F}{V}(C_{A,\text{in}} - C_A(k) - f_2(k)) - (1 + w(k))R(C_A(k), C_B(k), T(k))\Big) \quad (1)$$

$$C_B(k+1) = C_B(k) + \delta_t\Big(\frac{F}{V}(C_{B,\text{in}} - C_B(k)) - (1 + w(k))R(C_A(k), C_B(k), T(k))\Big) \quad (2)$$

$$T(k+1) = T(k) + \delta_t\Big(\frac{F}{V}(T_{\text{in}} - T(k)) - \frac{UA}{\rho C_p V}(T(k) - T_j(k))\Big) + \delta_t\Big(\frac{-\Delta H}{\rho C_p}(1 + w(k))R(C_A(k), C_B(k), T(k))\Big) \quad (3)$$

$$T_j(k+1) = T_j(k) + \delta_t\Big(\frac{F_j}{V_j}(T_{j,\text{in}} - T_j(k) + f_1(k)) + \frac{UA}{\rho_j C_{p,j} V_j}(T(k) - T_j(k))\Big) \quad (4)$$

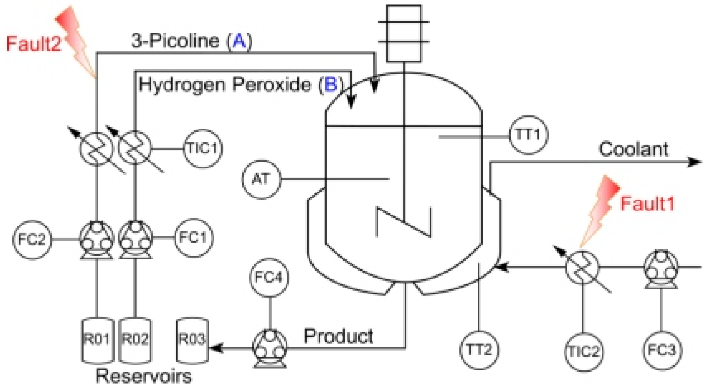

Figure 2. Schematic of experimental apparatus, indicating sensor and control locations.

$$y_1 = C_A(k) + \eta_1(k)$$
$$y_2 = T(k) + \eta_2(k)$$
$$y_3 = T_j(k) + \eta_3(k) \tag{5}$$

Residual generators were constructed for this system to implement fault diagnosis, which remain below a threshold ifthere is no fault happening and respond to faults (f1,f 2), and toprovide an estimate of these fault sizes.For fault 1, a spike in coolant feed temperature Tj,in, thefollowing functional observer was built,

$$z_1(k+1) = \alpha_1 z_1(k) - \frac{UA(1-\alpha_1)}{\rho_j C_{p,j} F_j} y_2'(k) - \left(\frac{(1-\alpha_1)^2 V_j}{\delta_t F_j} - 1 + \alpha_1 - \frac{UA(1-\alpha_1)}{\rho_j C_{p,j} F_j} \right) y_3'(k) \tag{6}$$

$$r_1(k) = z_1(k) + \frac{(1-\alpha_1) V_j}{\delta_t F_j} y_3'(k) \tag{7}$$

Whereas the detection of fault 2, inlet feed ratio of $C_{A,in}$, and the 3-picoline concentration decrease, similarly, the following functional observer was built.

$$z_2(k+1) = \alpha_2 z_2(k) + \left(\frac{(1-\alpha_2)^2 V}{\delta_t F} - 1 + \alpha_2 \right) y_1'(k) + \frac{\rho C_p}{-\Delta H} \left(\frac{(1-\alpha_2)^2 V}{\delta_t F} - 1 + \alpha_2 - \frac{UA(1-\alpha_2)}{\rho C_p F} \right) y_2'(k) + \frac{UA(1-\alpha_2)}{-\Delta H F} y_3'(k) \tag{8}$$

$$r_2(k) = z_2(k) - \frac{(1-\alpha_1) V}{\delta_t F} y_1'(k) - \frac{(1-\alpha_1) V \rho C_p}{\delta_t F(-\Delta H)} y_2'(k) \tag{9}$$

In eqs 6−9, y 1, y2, andy3represent the output measurementsin deviation form, α1 and α2 are tunable parameters thatrepresent the observer eigenvalues, r1 and r2 are the residualsthat also represent estimates of f1 and f2, respectively, underthe assumption that they are of step or ramp type. The detailsof individual parameter values are given in Table S1.50

It is important to emphasize that the residual generators are unaffected by fluctuations in the reaction kinetic rate, whichcould otherwise introduce significant errors. Moreover, the tworesidual generators are decoupled, allowing for effective faultisolation. The experimental results demonstrated successfulfault diagnosis for both faults, providing highly accurateestimates of their magnitudes.50

2.2. Random Forest (RF), K-Nearest Neighbors (KNN), and Artificial Neural Networks (ANN) for Fault Diagnosis. The random forest regressor is an ensemblelearning technique tailored for regression tasks.18 It constructsmultiple decision trees during training and averages their predictions to enhance accuracy and mitigate overfitting.Unlike individual decision trees, which are prone to highvariance and overfitting, random forest uses bagging (bootstrapaggregation) and random feature selection to build a more robust and generalized model. This approach reduces the likelihood of overfitting and improves the model's performanceon unseen data.

The random forest algorithm applies bootstrap sampling to generate multiple training subsets. Given a data set= { } D = (x , y) I I i

n 1, where xi is the input feature and yi is the target variable, the algorithm generates t bootstrap samples. Abootstrap sample Db is used to train the decision tree. Theremaining data, called the out-of-bag (OOB) sample, can beused to estimate the model's performance.Each decision tree in the forest is constructed at each node;a subset of features Fm ⊆ F is selected at random. The splittingcriterion used in regression is typically based on minimizingthe mean squared error (MSE). Once the tree is fully grown(or meets a stopping criterion, like maximum depth), it canmake predictions for new data. The prediction for a new pointx is the average of the target values y for all samples that fall into the same leaf node as y:

$$\hat{y}(x) = \frac{1}{N_{\text{leaf}}} \sum_{i \in \text{leaf}(x)} y_i \tag{10}$$

After multiple decision trees $\{T_1, T_2, \ldots, T_t\}$, the final prediction for new input x is obtained by averaging the predictions of all trees:

$$\hat{y}(x) = \frac{1}{t} \sum_{i=1}^{t} \hat{y}_i(x) \tag{11}$$

Where y (x) i is the prediction of the i-th tree.

The k-nearest neighbors (KNN) regressor is a nonparametric, instance-based learning algorithm used for regression tasks.52 Unlike statistical model-based methods,such as random forest, KNN does not require explicit trainingor model fitting. Instead, it predicts the target value byaveraging the target values of the k-nearest neighbors in thefeature space, relying solely on the stored training data.KNN uses a distance metric, typically the Euclideandistance, to identify the closest training points to a newquery point. In KNN regression, the predicted value for a givenquery point is the average of the target values of its k-nearestneighbors. The hyperparameter k determines how manyneighbors are considered in the prediction. Because KNNdoes not build a model, the computational cost of training isminimal, but predictions can be slower, especially with large data sets.

The algorithm for KNN can be explained as follows: for a given test point x, KNN calculates its distance to all trainingpoints using a predefined distance metric. The most commondistance metric used is the Euclidean distance. Once thedistances between the test point x and all training points arecomputed, the algorithm identifies the k-nearest neighbors by selecting the k points with the smallest distances. Let

Nk(x) bethe set of k-nearest neighbors of x. Then, in KNN regression,the predicted value y(x)for a new point x is computed as theaverage of the target values of its k-nearest neighbors:

$$\hat{y}(x) = \frac{1}{k} \sum_{i \in N_k(x)} y_i \quad (12)$$

Artificial neural networks (ANNs) are a class of machine learning algorithms inspired by the structure and functioningof biological neural systems.53 ANNs learn complex patterns from data through interconnected layers of nodes or "neurons." These algorithms are widely used in tasks such asclassification, regression, and generative modeling, when dealing with high-dimensional or unstructured data.

ANNs consist of an input layer, one or more hidden layers, andan output layer. The hidden layers contain neurons that applylinear transformations followed by activation functions to theinput data, allowing the network to model nonlinearrelationships. The training process involves iteratively updatingthe network parameters (weights and biases) using optimization algorithms, e.g., stochastic gradient descent (SGD), tominimize a loss function, such as mean squared error (MSE) orcross-entropy loss. Nowadays, neural networks are thebackbone of deep learning and a cornerstone of many stateof-the-art AI systems.54

The algorithm for training a neural network can be summarized as follows: given a data set of input−outputpairs (X,Y), the network predicts outputsyby applyingforward propagation through its layers. The error between thepredicted and actual outputs is quantified using a loss function,and the gradients of this loss with respect to the networkparameters are computed using backpropagation. Finally, the are updated in the direction of the negativegradient by using an optimization algorithm. This process isrepeated iteratively, until the model converges to an optimalset of parameters. The mathematical formulation for a singleneuron in a neural network is where x is the input, W is theweight vector, b is the bias, z is the linear combination, andf(z) is the activation function. The activation functionintroduces nonlinearity, enabling the network to modelcomplex patterns.

$$z = W^{T}x + b, \; a = f(z) \quad (13)$$

2.3. Isolation Forest for Anomalies Detection.

Anomaly detection is a critical task across various domains,such as industrial monitoring, fraud detection, cybersecurity,and medical diagnostics. The objective is to identify datapoints that deviate significantly from expected patterns, whichmay indicate rare but important events such as systemmalfunctions, fraudulent activities, or network intrusions.This task is challenging due to the complexity and variabilityof real-world data, where normal behavior can fluctuatesignificantly and anomalies may be subtle or occur in highdimensional spaces.Isolation forest (IF), introduced by Liu et al.,55 offers a novelapproach to anomaly detection by focusing on the concept ofisolation rather than traditional distance or density-basedmeasures. The core principle of IF is that anomalies are "fewand different", making them easier to isolate from the rest ofthe data. Instead of evaluating a point's relative position withinthe data set, IF isolates each data point by recursivelypartitioning the data set through random splits. IF is anefficient algorithm for anomaly detection, focusing on isolatingdata points by recursively splitting the data set. Anomaliesstand out because they differ significantly from normal datapoints, and as a result, they are isolated more quickly duringthe partitioning process.The IF method offers several key advantages: (I) scalability:the algorithm scales linearly with the data set size, making itideal for large-scale applications; (ii) no assumptions aboutdata distribution: unlike methods that rely on specific datadistribution assumptions (e.g., Gaussian), IF is distribution agnostic, enhancing its robustness across various domains; (iii) handling high-dimensional data: IF performs effectively onhigh-dimensional data sets, avoiding the “curse of dimensionality” that hampers many traditional approaches.

The path length h(x) represents the number of edges traversed in an isolation tree before a point x is isolated.Anomalous points, which are more distinct, tend to haveshorter path lengths. The anomaly score is based on this pathlength but normalized to fall within the range [−1, 1] where−1 indicates anomalies and 1 represents normal data points.Given a point x, its anomaly score s(x) is calculated as

$$s(x) = 2\left(\frac{E[h(x)]}{c(n)} - 0.5\right) \tag{14}$$

Where E[h(x)] is the average path length of point x across the isolation trees and c(n) is the normalization factor,representing the average path length for a normal point in adata set of size n. The IF algorithm operates as follows: data setX of size n and a number of trees t are subsampled with size ψ,forming a subsample Xψ. Then the subsample is recursivelypartitioned with a selected feature f and a split value p withinthe range of the feature, until each data point is isolated or thetree reaches a maximum depth L. For each point x, traverse theisolation tree to compute its path length h(x). Finally, calculatethe anomaly score s(x), if it is positive, it indicates a normalpoint; on the contrary, if negative, it represents an anomaly.

3. RESULTS AND DISCUSSION

The sensor data sets were collected from open-loop experiments, as previously described and consistent with our earlier study.50 To reduce noise and ensure comparability, the datasets were normalized, and a 1200-point moving average filterwas applied to the data-driven fault prediction outputs, andresidual signals were filtered using fast Fourier transform(FFT). Data-driven training and analysis were conducted on aLenovo ThinkPad P53 (Intel 9850H CPU, Nvidia QuadroRTX 5000 mobile GPU, 128 GB RAM) using Python (Scikitlearn, TensorFlow, and PyTorch) and MATLAB on SlackwareLinux. Detailed parameters for RF, KNN, and IF are providedin Table S2 and ANN and RNN are provided in Table S3.

3.1. Data-Driven Fault Diagnosis. The residual generators have demonstrated their ability to detect, isolate, andestimate faults in the CSTR process. Following theexperimental runs, the collected data prompted the questionof whether data-driven methods could also be applied for faultdiagnosis. A total of 19 data sets with sensor readings andknown fault sizes were used, with one serving as the test setand the remaining 18 as the training set. We applied methods: random forest (RF) and k-nearest neighbors (KNN). RF is a model-based statistical approach, while KNN isnonparametric, providing a representative comparison fortesting data-driven methods.

Since we already know the exact time and magnitude of the faults from the experimental data, training the data-drivenmodels does not require knowledge of the system equations-(eqs 1−5) or the model-based residual generators (eqs 6−9).Instead, the sensor readings are used to train the models solelyon the basis of the fault occurrence times and fault sizes,making this a “model-less” approach to fault diagnosis. Thedetection thresholds were determined using a Bayesianchangepoint detection mechanism56 with one data set andtested across all data sets, ensuring effective and accurate fault

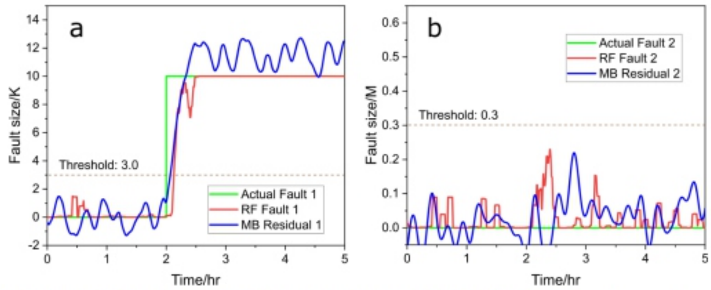

Figure 3. Predicted fault size (red) vs actual fault size (green), (a) for fault 1 and (b) for fault 2, with RF and compared to model-based (MB) residual generators (blue), under scenario a.

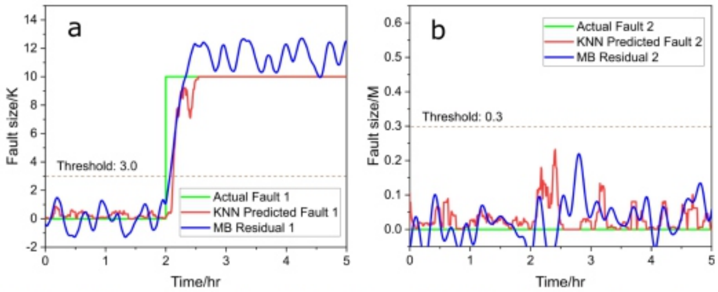

Figure 4. Predicted fault size (red) vs actual fault size (green), (a) for fault 1 and (b) for fault 2, with KNN and compared to model-based (MB) residual generators (blue), under scenario a.

detection. Additionally, the data-driven regressors accurately converged to the actual fault size, demonstrating a strong performance in fault estimation.

A comprehensive analysis was conducted as follows:
a. Only one fault is happening,

$$f_1(t) = \begin{cases} 0, & t < 2\text{ h} \\ 10, & t \geq 2\text{ h} \end{cases}, \quad f_2(t) = \begin{cases} 0, & t < 2\text{ h} \\ 0, & t \geq 2\text{ h} \end{cases}$$

With only one fault introduced into the system�fault 1, caused by a spike in coolant inlet temperature�the expectedoutcome is accurate detection and estimation of the fault size,while predictions for fault 2 remain low, as no fault associatedwith 3-picoline concentration is present.
As shown in Figure 3a, fault 1 is introduced at the 2 h mark, at which point the RF regressor (red line, eq 11) promptlydetects the fault (represented by the green line) and respondswithin 5 min, converging to the correct fault size of 10 within30 min. A threshold of 3 could be applied for fault detection,when the signals of the residual generator or RF regressorexceed this threshold, a fault is then alarmed. We alsoevaluated the performance of the moving average filter, with a1200-point window proving to be an effective choice, with R2 =0.96, and the results are provided in Table S3. Theperformance of RF is comparable to that of a model-basedresidual generator (blue line, “MB” for model-based) with aslight delay, demonstrating the efficiency of RF in faultdetection and size estimation. In Figure 3b, the signal for fault2 remains low throughout the test, confirming that no fault related to the decrease in 3-picoline concentration is present, of which the residual generator (blue line) provides a similarresult. Similarly, a threshold could be set at 0.3, and bothsignals remain below this threshold, indicating that there is nofault happening. This accurate isolation further validates therobustness of the RF model for single-fault scenarios. Theseresults highlight the ability of data-driven methods to bothdetect and isolate faults with precision comparable to modelbased residual generators, even in complex system dynamics.The same procedure was applied using the k-nearest−neighborhood (KNN) regressor, and the results are shown inFigure 4. In Figure 4a, the KNN model (red line, eq 12) swiftlyresponds to the introduced fault 1, similar to the RF results,detecting the fault promptly and converging toward the correct fault size. In

Figure 4b, the signal for fault 2 remains consistently low throughout, indicating successful fault isolation and confirming that no fault is associated with the decrease in the 3-picoline concentration. These resultsdemonstrate that the KNN regressor, like the RF model,achieves both fault isolation and size estimation effectively,reinforcing the viability of data-driven approaches in faultdiagnosis tasks. In both methods, there is a slight delay of datadriven methods compared with model-based residual generators, showing a possible quicker response in residual signals.b. Only one fault is happening,

$$f_1(t) = \begin{cases} 0, & t < 2\,\mathrm{h} \\ 0, & t \geq 2\,\mathrm{h}' \end{cases} \quad f_2(t) = \begin{cases} 0, & t < 2\,\mathrm{h} \\ 0.6, & t \geq 2\,\mathrm{h} \end{cases}$$

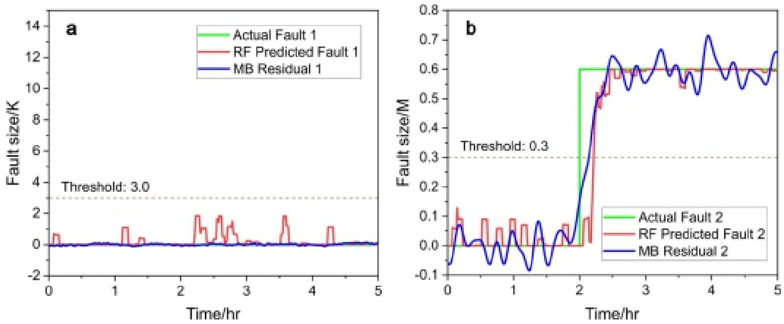

Figure 5. Predicted fault size (red) vs actual fault size (green), (a) for fault 1 and (b) for fault 2, with RF and compared to model-based (MB) residual generators (blue), under scenario b.

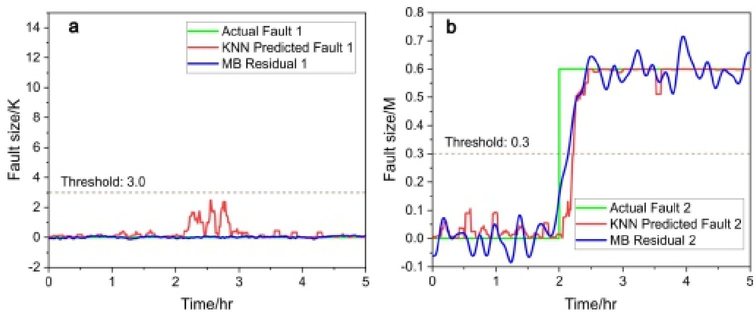

Figure 6. Predicted fault size (red) vs actual fault size (green), (a) for fault 1 and (b) for fault 2, with KNN and compared to model-based (MB) residual generators (blue), under scenario b.

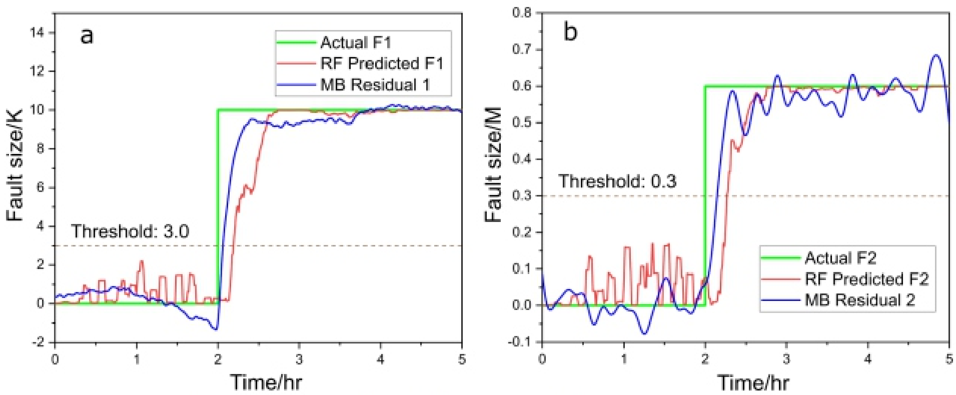

Figure 7. Predicted fault size (red) vs actual fault size (green), (a) for fault 1 and (b) for fault 2, with RF and compared to model-based (MB) residual generators (blue), under scenario c.

In the reversed scenario, where the only fault occurring in the system is fault 2�a decrease in the 3-picoline feed inletconcentration�the expectation is that the model will detectand estimate the size of fault 2, while the prediction for fault 1remains low, as no coolant inlet temperature spike is present.

In Figure 5a, the fault 1 prediction remains consistently lower than 3, indicating no fault related to the coolant inlettemperature, as expected. In Figure 5b, the model responds tofault 2 swiftly and converges to the correct fault size within 30min, showing promising results in fault detection and estimation. Similarly, when the KNN regressor is tested in

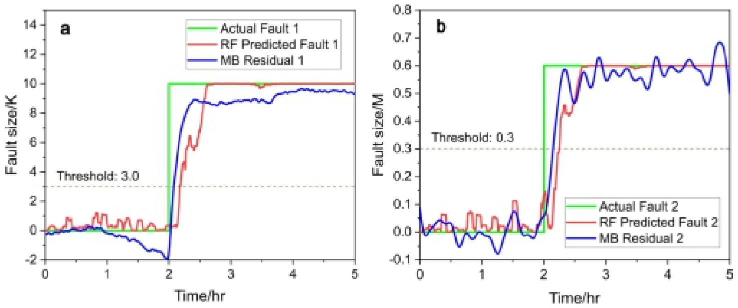

Figure 8. Predicted fault size (red) vs actual fault size (green), (a) for fault 1 and (b) for fault 2, with KNN and compared to model-based (MB) residual generators (blue), under scenario c.

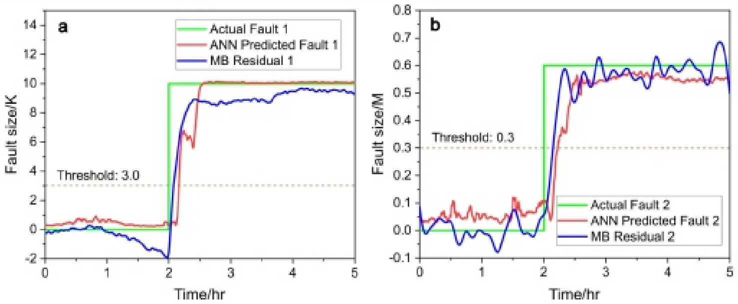

Figure 9. Predicted fault size (red) vs actual fault size (green), (a) for fault 1 and (b) for fault 2, with ANN and compared to model-based (MB) residual generators (blue), under scenario c.

this scenario: in Figure 6a, the predicted value for fault 1 stays low, though slightly higher than that of the RF model, stillconfirming no fault. In Figure 6b, the KNN model promptlydetects fault 2, accurately estimating its size with a short response time.

Despite minor discrepancies observed in both fault scenarios, the models consistently detect faults when theyoccur, although the precision of the magnitude estimationvaries. Crucially, the timing of fault detection is accurate inboth cases, with the models successfully identifying both theonset and the resolution of faults. This is especially clear in thecase of fault 2, where the predicted and actual fault sizes nearlyconverge during the period of sustained fault, demonstratingthe models' effectiveness in accurately tracking fault behaviorover time. For both RF and KNN, a slight delay is also presentcompared with residual signals.

c. Two faults are happening,

$$f_1(t) = \begin{cases} 0, & t < 2\text{ h} \\ 10, & t \geq 2\text{ h} \end{cases}, \quad f_2(t) = \begin{cases} 0, & t < 2\text{ h} \\ 0.6, & t \geq 2\text{ h} \end{cases}$$

Figures 7 and 8 present the comparison between the actual and predicted fault sizes for fault 1 and fault 2, using twodifferent machine learning models: RF and KNN, respectively.Each figure consists of two subplots: Figures 7a and 8arepresent fault 1, and Figures 7b and 8b represent fault 2. Inboth cases, the predictions are compared against the ground offault sizes, along with model-based residual signals.

The random forest model shows a very close alignment between the predicted fault size (red line) and the actual faultsize (green line). The model captures the onset of the faultaround 2 h, and the prediction remains accurate throughoutthe fault duration. As for the residual signal, there is a smalldeviation, less than 1.0 K, especially during the sustained faultevent (fault size ~10), which is acceptable. The sharp rise andstable fault size during this period suggest that random foresthandles significant faults efficiently and with high precision.Prior to the major fault event, the RF model exhibits somesmall fluctuations in the predicted fault size that occur in the time range between 0 and 1.5 h. These small

deviations do not affect the overall value as they are below the detection threshold.
The KNN also shows strong predictive performance with the predicted fault size (red line) following the actual fault size(green line) very closely during the main fault period. The riseof the fault at approximately 2 h and the sustained fault arecaptured well.
For fault 2, both models exhibit similar performance, but the random forest model shows more variability and fluctuation inits predictions. This might indicate that random forest is moreprone to overfitting to noise in cases where the fault dynamicsare more complex, but all fluctuations are well below detectionthresholds. As for the model-based residual signal (MB, theblue line), the noise level is much higher than data-driven

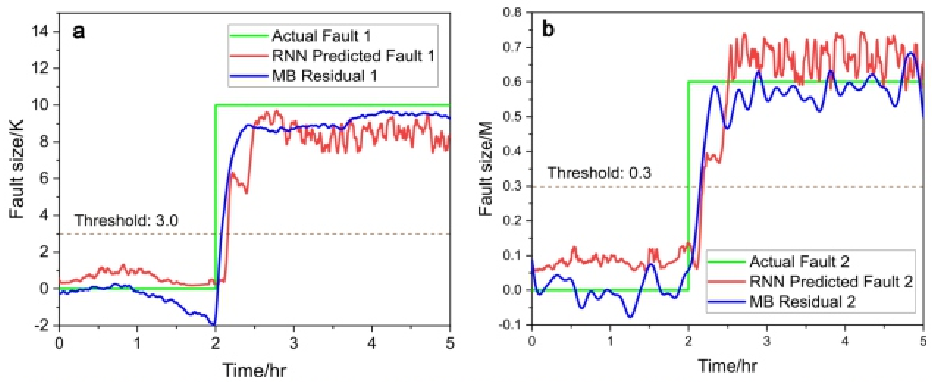

Figure 10. Predicted fault size (red) vs actual fault size (green), (a) for fault 1 and (b) for fault 2, with RNN and compared to model-based (MB) residual generators (blue), under scenario c.

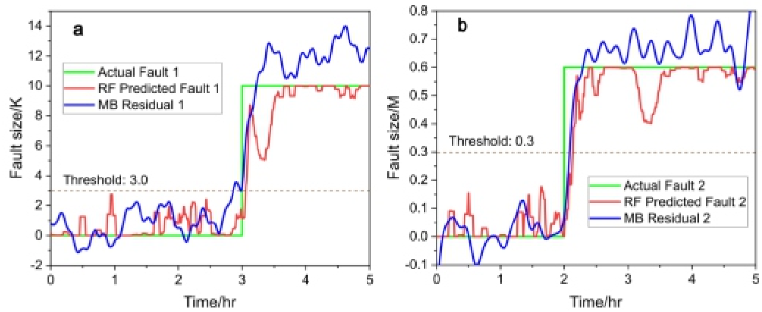

Figure 11. Predicted fault size (red) vs actual fault size (green), (a) for fault 1 and (b) for fault 2, with RF and compared to model-based (MB) residual generators (blue), under scenario d.

methods; however, it has a better prompt response to the fault happening.
Neural networks have gained popularity in recent years to their ability to model complex, nonlinear systems effectively.Building on the fault diagnosis conducted using KNN and RF,we also applied artificial neural networks (ANN) and recurrentneural networks (RNN) to explore their effectiveness. Thesemethods were chosen to leverage their capacity for capturingintricate patterns and, in the case of RNN, for addressingtemporal dependencies within the data.The fault diagnosis achieved using an ANN and an RNN isillustrated in Figures 9 and 10. In Figures 9a and 10a, the ANNand RNN successfully identify fault 1 by comparing the actualfault (green line) with the predicted fault (red line). Thethreshold of 3.0 (dotted line) is used to detect faultoccurrences. Similarly, in Figures 9b and 10b, fault 2 isdiagnosed with a threshold of 0.3, where the ANN and RNNboth capture the fault dynamics through the alignment of theactual fault (green line) and predicted fault (red demonstrates the effectiveness of neural networks in detecting and predicting fault conditions. Figure 10 plotted using RNNappears to exhibit higher noise levels in the predicted compared with Figure 9. This increased noise could be attributed to RNN's sensitivity to temporal dependencies, which may amplify variations in the data.
While the neural network demonstrates strong performance in fault diagnosis, the computational time

required is much higher compared to RF and KNN. The average timeconsumption for a single cycle of training and testing usingKNN, RF, ANN, and RNN is detailed in Table S5.Additionally, Table S6 compares the performance of thesemethods in estimating fault sizes against the actual fault values.We will present results only for KNN and RNN, as theydemonstrate satisfactory performance.d. Two faults happening at different times

$$f_1(t) = \begin{cases} 0, & t < 3\text{ h} \\ 10, & t \geq 3\text{ h}' \end{cases} \quad f_2(t) = \begin{cases} 0, & t < 2\text{ h} \\ 0.6, & t \geq 2\text{ h} \end{cases}$$

It is crucial to verify fault isolation with experimental data that fault 1 and fault 2 are happening at two different times.The RF model accurately predicts the onset and magnitudeof fault 1 in Figure 11a. The predicted fault size (red line)closely follows the actual fault size (green line), particularlyduring the critical period after 3 h, where the fault size risessharply and stabilizes around a fault size of 10. The modelconsistently captures the duration and magnitude, demonstrating a high prediction precision during the main fault event.

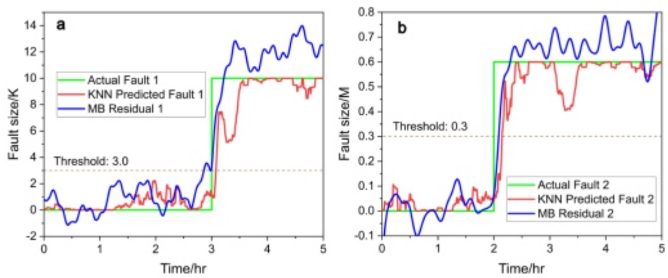

Figure 12. Predicted fault size (red) vs actual fault size (green), (a) for fault 1 and (b) for fault 2, with KNN and compared to model-based (MB) residual generators (blue), under scenario d.

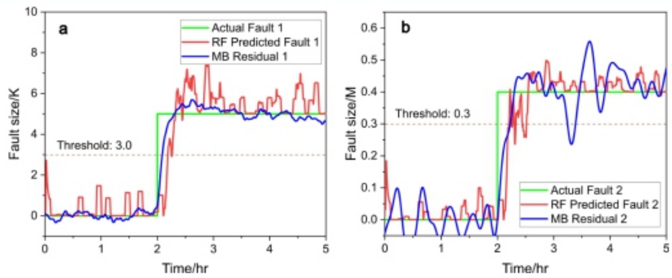

Figure 13. Predicted fault size (red) vs actual fault size (green), (a) for fault 1 and (b) for fault 2, with RF and compared to model-based (MB) residual generators (blue), under scenario e.

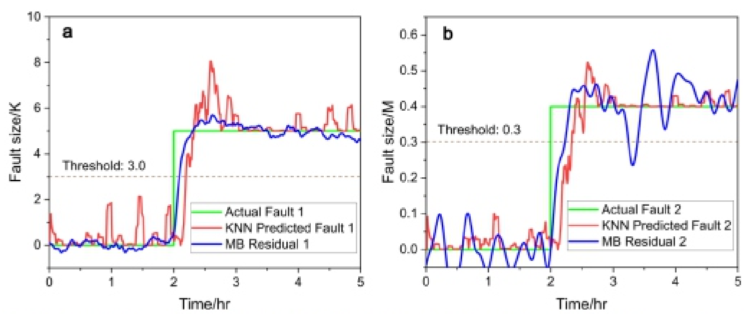

Figure 14. Predicted fault size (red) vs actual fault size (green), (a) for fault 1 and (b) for fault 2, with KNN and compared to model-based (MB) residual generators (blue) under scenario e.

The KNN model similarly demonstrates strong predictive performance for fault 1 in Figure 12a, with the predicted faultsize (red line) following the actual fault size (green line)closely. The model effectively captures the sharp rise in the fault size around 3 h, maintaining accuracy throughout thesustained fault period. As for the model-based residual signal (MB, the blue line), we observe an overshoot, giving a 1.2

Koverestimation of fault size, which is within the experimental tolerance.

For fault 2, in Figure 11b, the predicted random forest model fault size (red line) captures the general trend of thefault, which begins around 2 h and persists until the end of thetest. After the fault reaches its maximum (fault size 0.6), therandom forest model stabilizes and follows the actual fault size(green line) more closely. In Figure 12b, the KNN modeloffers slightly smoother predictions for fault 2. While thepredicted fault size (red line) does fluctuate in the early faultperiod (around 3 h), the overall estimation is sound.

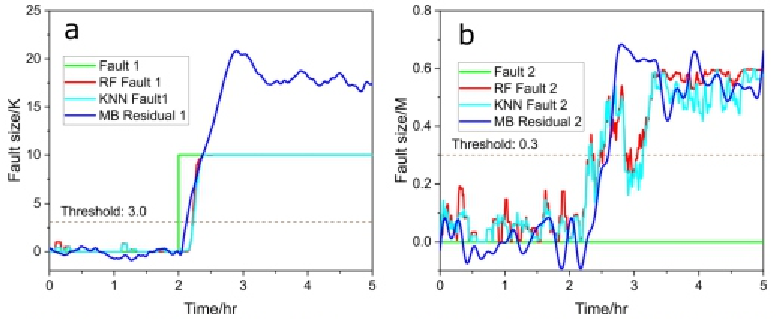

Figure 15. Predicted fault size vs actual fault size with residual generators, RF (red) and KNN (cyan), (a) for fault 1 and (b) for fault 2, and compared to model-based residual generators (blue).

These results exhibit successful fault isolation; the noise level is not too high to invalidate fault detection, and especially theestimation for both fault sizes is remarkably good. The slowerresponse compared with residual generators is not unforeseeable, as model-based methods have the edge in the system dynamics.

e. Two smaller faults are happening

$$f_1(t) = \begin{cases} 0, & t < 2\,\text{h} \\ 5, & t \geq 2\,\text{h} \end{cases}, \quad f_2(t) = \begin{cases} 0, & t < 2\,\text{h} \\ 0.4, & t \geq 2\,\text{h} \end{cases}$$

Figures 13 and 14 demonstrate the performance of fault prediction models RF and KNN for a smaller fault scenario,respectively. Each figure consists of two subplots: a representsfault 1 and b represents fault 2, where the faults are smaller inmagnitude compared to previous scenarios.

In this smaller fault scenario, the random forest model shows relatively good performance in Figure 13a. The predicted faultsize (red line) aligns with the actual fault size (green line),particularly after the fault onset around 2 h. However,compared to the larger fault scenario, the random forestmodel introduces more variability in its predictions. The predicted fault size fluctuates around the actual fault size,especially after 2.5 h, where the model tends to overestimatethe fault magnitude. The KNN model provides more stablepredictions for fault 1 under the smaller fault scenario in Figure14a after 3 h. The predicted fault size (red line) follows theactual fault size (green line) closely, with fewer deviationscompared with the random forest model. There is a minoroverestimation of the fault size around 2.5 h, but overall, themodel tracks the actual fault size more consistently. Theresidual signal shows superb performance with both accuracyand responsiveness.

For fault 2, the random forest model (Figure 13b) and the KNN model (Figure 14b) exhibit a slight overestimate at thebeginning of the fault occurrence , and the KNN model showsa larger overshoot at around 2.5 h. Overall, the KNN model'sability to provide smoother predictions with fewer oscillationsmakes it better suited for capturing the smaller faults in fault 2,as it appears less sensitive to noise or minor deviations in thedata especially after 3 h.

Estimating smaller faults is generally more challenging due to the lower signal-to-noise ratio, a difficulty also withmodel-based observers, as discussed in our previous study.50The results demonstrate that data-driven methods (RF andKNN) are capable of diagnosing these minor faults effectively.

In conclusion, both models are effective at detecting smaller faults. Model performance: both random forest (RF) and knearest neighbors (KNN) demonstrated strong performance indetecting and isolating faults as well as estimating their sizes.The circular iteration ensured robustness and consistencyacross the data set. However, in all the cases, model-basedresidual signals show better responsiveness and faster faultdetection. Accuracy: the average accuracy across all tests washigh, with minimal variance between data sets. This indicatesthe effectiveness of both RF and KNN across differentoperational conditions. Fault Isolation: both methods successfully isolated the faults in the system, identifying the affectedcomponents without false positives or significant misclassifications. Fault size estimation: the size estimation of faults waswithin acceptable error margins, showing that data-drivenmethods, when properly trained, can provide reliable faultmagnitude estimates without relying on model-based equations.

3.2. Isolation Forest for Anomalies Detection. A major limitation of the model-based approach is that not all processescan be easily modeled, and even with a validated model,operational parameter changes may still occur. Similarly, datadriven methods cannot reliably diagnose faults without priorknowledge of faulty data sets or at least similar conditions fortraining. For example, during experimentation, it was observedthat after reassembling the equipment the previously effectivemodel-based residual generators showed reduced performance,while data-driven methods produced false detections. Thissetup considered a scenario in which only a single fault waspresent in the process, as described below.

$$f_1(t) = \begin{cases} 0, & t < 2\text{ h} \\ 10, & t \geq 2\text{ h}' \end{cases} \quad f_2(t) = \begin{cases} 0, & t < 2\text{ h} \\ 0, & t \geq 2\text{ h} \end{cases}$$

The model-based residual signals are shown as blue lines. For fault 1 in Figure 15a, the model-based residual signalspikes above 20 before stabilizing around 17, which is over60% higher than the actual fault size, indicating a clearoverestimation. In Figure 15b, despite no fault being presentfor fault 2, the residual signal incorrectly estimates around 0.5,as a false positive. For the data-driven methods, RF (red lines)and KNN (cyan lines), the performance for fault 1 in Figure15a is notably strong, accurately detecting and estimating thefault size at 10. However, both methods also produced falsepositives for fault 2 in Figure 15b. All methods failed under the system parameter change, which is expected. Data-driven methods struggled due to the lack of similar scenarios in thetraining sets, and the model-based observer failed because theparameter change caused a mismatch in the system model,invalidating the residual signals.

This was traced back to a change in the heat transfer coefficient with additional experiments. It is crucial to detectchanges in the heat transfer coefficient (U) before any faultsare introduced into the system. Early detection allows fortimely adjustments to the model parameters, preventingpotential losses due to detection delays when actual faultsoccur. Therefore, the goal is to detect shifts in U during thenonfault steady-state operation, enabling proactive model adjustments before faults impact system performance.

In data-driven methods, detecting changes in the heat transfer coefficient (U) is equivalent to identifying anomalousdata sets compared to a set of nominal runs. Therefore, it isnatural to apply an anomaly detection algorithm, with Isolationforest (IF) being an ideal choice due to its simplicity and lowcomputational resource requirements. The isolation forest (IF)parameter settings include 200 estimators, a contaminationlevel of 0.2, and a maximum sample size of 256. Further detailson all parameter settings are provided in Table S2. The sensordata sets, collected before any faults were introduced into thesystem and with a known U = 18 W/(m2·K) (calculated usinga heat transfer area of 0.08 m2), are used to train the IF model.After training, several data sets with potentially altered Uvalues are tested against the model, and anomaly scores arecalculated according to eq 14.The results are summarized in Figure 16, where four datasets were randomly selected for testing: two with old U = 18

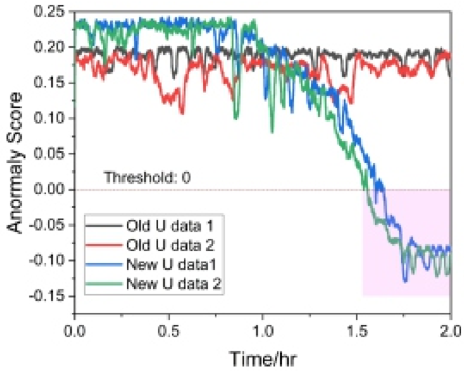

Figure 16. Isolation forest anomaly score for process *U* change.

W/(m2·K) and two with new U. In the figure, the two data setswith U = 18 show consistently positive anomaly scores,indicating that the sensor readings align with the training set.In contrast, the two data sets with altered U values show agradual detection of anomalies by the IF model, with anomalyscores dropping sharply into the negative range and stabilizingaround −0.1, as marked by the pink area in Figure 16. Thissuccessful anomaly detection confirms a change in U within these two data sets.

Once an anomaly is detected, the next step is to adjust the model parameter (U) to ensure that the residual generatorscontinue to function optimally for fault diagnosis. There arenumerous regressors available in the data-driven toolbox forestimation tasks. However, a key drawback of data-driven methods is that models must be trained with data sets corresponding to various known U values. In practice, the Uvalues may not always be known a priori, which can result inunreliable output estimates. To address this, we refer back tothe system model described in eqs 1−5.

Assuming the system is in a steady state and no faults are present, we can derive an equation from eqs 1 and 3, resultingin eq 15. Additionally, by considering eq 4 alone, we canestablish eq 16. Both of these equations provide estimates ofthe U value, offering a more reliable approach than purely datadriven methods.

$$U_1 = \frac{F}{VA(T(k) - T_j(k))}(T_{\text{in}} - T(k)) + \frac{-\Delta HF}{(T(k) - T_j(k))}(C_{A,\text{in}} - C_A(k)) \tag{15}$$

$$U_2 = -\frac{F\rho_j C_{pj}}{(T(k) - T_j(k))}(T_{j,\text{in}} - T_j(k)) \tag{16}$$

Direct calculation using eq 16, as shown in Figure 17a, incorporates a moving average filter with a window size of6000 points. However, the results are suboptimal due to thehigh noise levels. Not all data sets can be reliably calculatedusing eqs 15 and 16 because the divisor involves temperaturemeasurements, which are subject to sensor noise. As noted ineq 5, floating-point division can lead to significant errors whenthe divisor is small.

The mean values of the calculated lines in Figure 17a are 17.6 and 19.07, which are close to the actual value of 18 W/(m2·K). However, the high noise level makes direct calculationimpractical for all data sets. This issue arises because thereactor jacket's thickness is only around 0.2 mm, resulting in alarge heat transfer coefficient. Consequently, the temperaturedifference between T − Tj is small and is exacerbated evenmore, as the measurement noises (eq 5) of temperature have avariance over 0.6, which can lead to significant errors in thecalculation due to the small magnitude of the temperature difference.

A more effective approach is to frame the problem as an optimization task. By rearranging eqs 15 and 16, we derive theresiduals as follows:

$$\text{Residual}_1 = F\rho C_p(T_{in} - T) + -\Delta HF(C_{A,in} - C_A) - U_1 A(T - T_j) \quad (17)$$

$$\text{Residual}_2 = -F_j\rho_j C_{p,j}(T_{in} - T) - U_2 A(T - T_j) \quad (18)$$

The objective function to be minimized is the sum of the squared residuals:

$$\text{Objective} = \sum \text{Residual}_1(i)^2 + \sum \text{Residual}_2(i)^2 \quad (19)$$

under the condition with the lower bound [U1 U2] = [0 0]. The optimization problem is solved using the global trustregion reflective algorithm, and the results are plotted in Figure17b. The calculated curves exhibit much smoother behavior.The nominal runs, old U data 1 (black line) and old U data 2(red line), fluctuate between 15 and 20, indicating stable butslightly lower U estimates over the actual value of 18. Theoverall trend for these nominal conditions remains relatively constant.

In contrast, the changed conditions, new U data 1 (green line) and new U data 2 (blue line), show fluctuations around

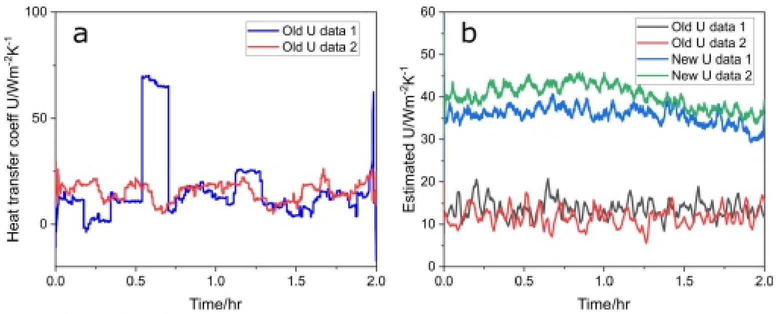

Figure 17. Direct calculation of U values for two nominal runs (a) and optimization estimates (b).

40 W/(m2·K), representing significantly higher U valuescompared to the nominal runs. This stark difference in Uvalues between the old U and new U conditions reflects achange in the heat transfer coefficient. The mean values ofFigure 17b, calculated U, are summarized in Table 1.

Table 1. Calculated U Values from Optimization

Parameter	Old U data 1	Old U data 2	New U data 1	New U data 2
U/W/(m^{2}K)	16.57	17.74	35.6	33.1

Using this method, following data triage, the experimental data revealed two distinct categories of U values: one centeredaround 18 W/(m2·K) (average 17.8, standard deviation 1.12)and another centered around 40 W/(m2·K) (average 38.9,

standard deviation 3.1), demonstrating good stability. After isolation forest (IF) anomaly detection, if a data set is flaggedas negative, the U value is recalculated to update the modelbased residual generators for fault diagnosis.The results are depicted in Figure 18, showing the faultdiagnosis for both fault 1 and fault 2 using parameter-updatedmodel-based residual generators. In Figure 18a on the left, theblue line represents the updated residual signal, which slightlyoverestimates the fault size after the 2 h mark, stabilizingaround 11.5, within acceptable experimental tolerance. The redline shows the previous residual signal, as seen in Figure 15a,which deviates significantly from actual fault 1 (green line). InFigure 18b on the right, the results for fault 2 detection are shown, with no actual fault present (as indicated by the green line staying flat at zero). The updated residual signal (blueline), although showing some fluctuations, does not exceed thefault detection threshold. This updated signal performs muchbetter than the previous residual signal in Figure 15b, indicatedby the red line.The procedure is outlined in the flowchart presented in Figure 19. Initially, sensor readings are analyzed using theisolation forest (IF) algorithm for anomaly detection. If no anomalies are found, the system proceeds with the modelbased residual generators using the default U value. However,if the anomaly scores drop below zero, indicating a potentialissue, then an optimization algorithm is triggered to recalibratethe U value. This updated U value is then used to adjust theresidual generators, allowing the model-based fault diagnosis tocontinue accurately under the new conditions.To apply a data-driven method, a backup model-based residual generator must be used for fault diagnosis in the newparameter-changed scenario until sufficient data sets with thenew parameter and fault conditions are collected. Once thesedata sets are validated against actual faults, they areincorporated into the data-driven RF and KNN training sets,labeled with the corresponding U value. This process updatesthe training sets, enabling data-driven methods to adapt to thenew conditions.To evaluate the efficacy of this approach, seven data setswith U = 40 W/(m2·K) were used. Figure 20 presents the faultdiagnosis results with RF and KNN. The same data set fromFigure 13 is used as the testing set, and six new data sets

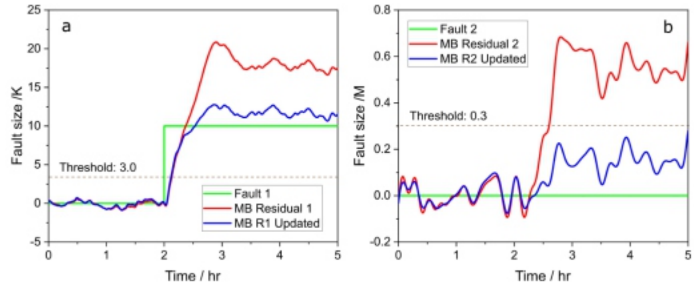

Figure 18. Model-based residual signal responses after parameter update (blue) and before update (red) compared with actual fault size (green).

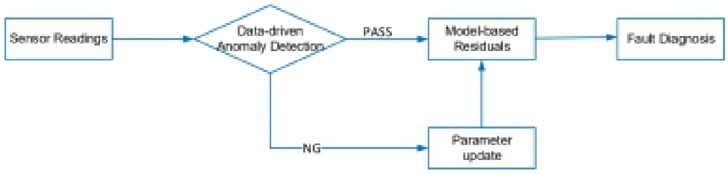

Figure 19. Flowchart of parameter update for model-based fault diagnosis.

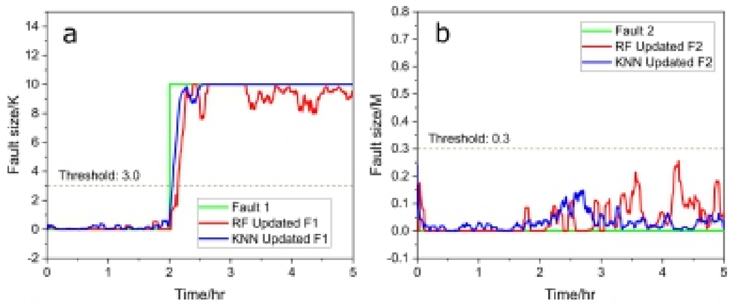

Figure 20. Predicted fault size vs actual fault size (green) with RF (red) and KNN (blue), (a) for fault 1 and (b) for fault 2 after training sets updated.

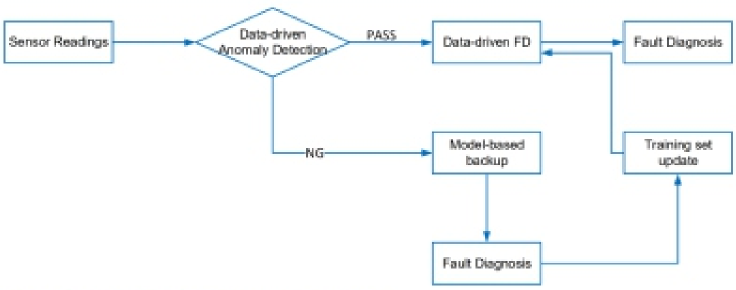

Figure 21. Flowchart of training set update for data-driven fault diagnosis.

marked with U = 40 were incorporated into the data-driven training set. This process allowed for data-driven approaches totrain and gain new knowledge about the system, thusenhancing fault diagnosis.
The result is shown in Figure 20, presenting the fault diagnosis results for both fault 1 and fault 2 using trainingupdated RF and KNN. In Figure 20a on the left, the red lineshows the RF model's prediction, which closely follows theactual fault size but fluctuates slightly after the initial detection,oscillating just below the true fault magnitude. The blue line,representing the KNN prediction, also aligns well with theactual fault, responding quickly and providing accurateestimates with fewer fluctuations compared with the RFprediction. In Figure 20b on the right, the results for fault 2detection are displayed, where no actual fault is present (asindicated by the green line remaining flat at zero). Both the RF(red line) and KNN (blue line) predictions show minorfluctuations hovering slightly above zero. Nevertheless, these signals remain below the threshold of 0.3, indicating that there is no fault.As more training scenarios are gathered, it has beendemonstrated that data-driven methods can also effectivelyperform fault diagnosis, matching the reliability of model-basedapproaches. Overall, the data-driven approaches (RF andKNN) demonstrate strong performance for fault 1, accuratelydetecting and estimating the fault size. In the case of fault 2,despite some fluctuations, there are no false positives andreliable fault isolation.This procedure is illustrated in Figure 21. Sensor readingsare first fed into the anomaly detection process using theisolation forest (IF). If no anomaly is detected, the systemapplies the data-driven fault diagnosis as outlined in Section3.1. However, if an anomaly is detected, a backup model-basedfault diagnosis, as shown in Figure 19, is initiated. Oncesufficient new data with different fault scenarios are collected,the data-driven fault diagnosis model is retrained with the

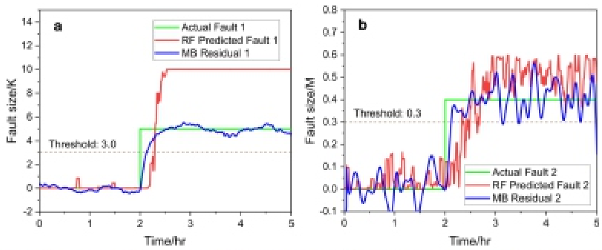

Figure 22. Predicted fault size vs actual fault size (green), (a) for fault 1 and (b) for fault 2 with RF (Red) and model-based residual generator (blue).

updated training set to enhance its fault diagnosis capabilities under the new conditions.
3.3. Challenges in Data-Driven Fault Diagnosis. Datadriven methods have shown great promise in fault diagnosis due to their ability to model complex systems using historicaldata. However, their effectiveness is highly dependent on thequality and diversity of the training data. Without a diversedata set that includes faulty scenarios across a wide range ofoperational conditions, these models often fail to generalize,leading to poor performance in real-world applications, asshown in Figure 15. When properly trained with comprehensive data that captures all potential fault types andoperating conditions, data-driven models excel in faultdetection and diagnosis, offering accurate solutions, as shownin Figure 20. The key lies in ensuring that the training datacover all critical scenarios.The question arises whether data are required for all faultsizes. To explore this, a test was conducted using a training setwith only larger fault sizes (fault 1 at 10 and fault 2 at 0.6),while the testing set comprised smaller faults (fault 1 at 5 andfault 2 at 0.4). Figure 22 illustrates the fault diagnosis resultsfor both fault 1 and fault 2, comparing the actual fault values,predicted fault values, and residual signals. This test providesinsight into how well the models generalize to smaller faultsizes when they are trained only on larger faults.In Figure 22b, fault 2 is introduced at the 2 h mark, with thegreen line indicating the actual fault size of 0.6. Prior to this,the noise in both the predicted fault signal (red line) and theresidual signal (blue line) stays well below the threshold of 0.3,indicating no false positives before the fault occurs. After 2 h,both the predicted fault signal and the residual signal increase,with the red line overestimating the actual fault

size of 0.4,while the blue residual signal fluctuates but stays close to theexpected value of 0.4. Similar results were achieved usingKNN; additionally, ANN and RNN were applied, yielding comparable results (not included in the article).

This phenomenon highlights the importance of having diverse training scenarios for accurate fault diagnosis, arequirement that may be difficult to achieve in real industrialsettings. The question of what constitutes the minimal trainingset catches our attention. Further studies are needed to addressthis.

4. CONCLUSION

In this study, the effectiveness of data-driven methods such as RF and KNN for fault diagnosis in a CSTR chemical reactorsystem is evaluated compared to model-based residualgenerators. The focus is on detecting, isolating, and estimatingthe size of two key faults: fault 1, a coolant inlet temperaturespike, and fault 2, a decrease in the 3-picoline feedconcentration. Both RF and KNN demonstrated strongperformance under nominal conditions, accurately identifyingfaults and estimating their sizes. However, both data-drivenand model-based approaches faced difficulties after a change inthe heat transfer coefficient (U), a process condition change,which led to misaligned predictions and false positives. Toaddress this, an IF algorithm is employed for anomalydetection, allowing system model recalibration and restoringthe accuracy of the model-based residual generators. For datadriven methods, the inclusion of new data sets with updatedparameters in the training successfully restored their performance.

Overall, while model-based methods remain reliable due to their deep understanding of system dynamics, data-drivenapproaches offer scalability and efficacy without the need fordetailed system models. The integration of both methods into a combined framework offers an optimal solution.

A challenge with data-driven methods is their reliance on diverse training data sets; without sufficient variety, faultdiagnosis accuracy diminishes, as seen in overestimations whentrained only on larger fault sizes. Future work will focus onenhancing the robustness of data-driven methods, particularlyby optimizing training sets with comprehensive fault scenariosand improving their ability to handle system parameterchanges to achieve fault diagnosis accuracy comparable tomodel-based approaches. And we will develop and test newmodels to enhance sensitivity and accuracy in detecting smallerfaults. The sensitivity analysis of heat transfer efficiency will beconducted when sufficient data covering a broader range of Uvalues becomes available. To further enhance the applicabilityof our approach, future work will explore strategies forreducing prediction delays, such as optimizing modelarchitectures for efficiency or implementing online learningtechniques to enable real-time performance. We will alsointegrate data-driven and model-based methods throughadaptive model adjustment, where data-driven techniquesdynamically refine model parameters, and physics-guidedlearning, which implants physical constraints into neural networks. Additionally, transfer learning using model-based simulations will be explored to improve data-driven models inscenarios with limited real-world fault data.

■ ASSOCIATED CONTENT

***sı Supporting Information**

The Supporting Information is available free of charge at https://pubs.acs.org/doi/10.1021/acs.iecr.4c04042.Design parameters of CSTR experiment in Table S1.Parameters for all data-driven methods in Table S2 andTable S4. Moving average filtering performance in termsof determination coefficient in Table S3. Average timeconsumption for 1 cycle of training and testing in TableS5 and the performance across scenario a to e in TableS6 (PDF)

■ AUTHOR INFORMATION

Corresponding Author

Costas Kravaris − Artie McFerrin Department of Chemical Engineering, Texas A&M University, College Station, Texas77843, United States of America; orcid.org/0000-0003-0951-9493; Email: kravaris@tamu.edu

Authors

Pu Du − Artie McFerrin Department of Chemical Engineering, Texas A&M University, College Station, Texas 77843,United States of America

Nabil M. Abdel Jabbar − Chemical and Biological Engineering Department, American University of Sharjah, Sharjah 26666, United Arab Emirates

Benjamin A. Wilhite − Artie McFerrin Department of Chemical Engineering, Texas A&M University, CollegeStation, Texas 77843, United States of America;orcid.org/0000-0003-2595-2094Complete contact information is available at:https://pubs.acs.org/10.1021/acs.iecr.4c04042

Notes

The authors declare no competing financial interest.

■ ACKNOWLEDGMENTS

Financial support from the National Science Foundation through the grant CBET-2133810 is thankfully acknowledged.The second author, Nabil M. Abdel Jabbar, acknowledges thesupport of the American University of Sharjah for his sabbatical leave at Texas A&M University during Spring 2024.

■ REFERENCES

(1) Isermann, R. Fault-Diagnosis Applications: model-Based Condition Monitoring: actuators, Drives, Machinery, Plants, Sensors, and FaultTolerant Systems; Springer Science & Business Media, 2011.

(2) Mhaskar, P.; Liu, J.; Christofides, P. D. Fault-Tolerant Process Control: methods and Applications; Springer Science & Business Media, 2012.

(3) Dash, S.; Venkatasubramanian, V. Challenges in the Industrial Applications of Fault Diagnostic Systems. Comput. Chem. Eng. 2000,24 (2), 785−791.

(4) Venkatasubramanian, V.; Rengaswamy, R.; Yin, K.; Kavuri, S. N. A Review of Process Fault Detection and Diagnosis: Part I:Quantitative Model-Based Methods. Comput. Chem. Eng. 2003, 27(3), 293−311.

(5) Tidriri, K.; Chatti, N.; Verron, S.; Tiplica, T. Bridging DataDriven and Model-Based Approaches for Process Fault Diagnosis and Health Monitoring: A Review of Researches and Future Challenges. Annu. Rev. Control 2016, 42, 63−81.

(6) Mansouri, M.; Harkat, M.-F.; Nounou, H. N.; Nounou, M. N. Data-Driven and Model-Based Methods for Fault Detection andDiagnosis; Elsevier, 2020.

(7) Gao, Z.; Cecati, C.; Ding, S. X. A Survey of Fault Diagnosis and Fault-Tolerant Techniques�Part I: Fault Diagnosis with ModelBased and Signal-Based Approaches. IEEE Trans. Ind. Electron. 2015,62 (6), 3757−3767.

(8) Qin, S. J. Survey on Data-Driven Industrial Process Monitoring and Diagnosis. Ann. Rev. Control 2012, 36 (2), 220−234.

(9) Dai, X.; Gao, Z. From Model, Signal to Knowledge: A DataDriven Perspective of Fault Detection and Diagnosis. IEEE Trans. Ind. Inform. 2013, 9 (4), 2226−2238.

(10) Ding, S. X. Model-Based Fault Diagnosis Techniques: design Schemes, Algorithms, and Tools; Springer Science & Business Media,2008.

(11) Isermann, R. Model-Based Fault-Detection and Diagnosis −Status and Applications. Ann. Rev. Control 2005, 29 (1), 71−85.

(12) Frank, P. M. Fault Diagnosis in Dynamic Systems via State Estimation-a Survey. In System Fault Diagnostics, Reliability andRelated Knowledge-Based Approaches; Springer, 1986; pp 35−98.

(13) Sotomayor, O. A. Z.; Odloak, D. Observer-Based Fault Diagnosis in Chemical Plants. Chem. Eng. J. 2005, 112 (1), 93−108.

(14) Isermann, R. Fault Diagnosis of Machines via Parameter Estimation and Knowledge Processing�Tutorial Paper. Automatica1993, 29 (4), 815−835.

(15) Patton, R. J.; Chen, J. A Review of Parity Space Approaches to Fault Diagnosis. IFAC Proc. Vol. 1991, 24 (6), 65−81.

(16) Gertler, J. Fault Detection and Isolation Using Parity Relations. Control Eng. Pract. 1997, 5 (5), 653−661.

(17) Ding, S. X. Data-Driven Design of Fault Diagnosis and FaultTolerant Control Systems; Springer, 2014.

(18) Breiman, L. Random Forests. Mach. Learn. 2001, 45 (1), 5−32.

(19) Yang, B.-S.; Di, X.; Han, T. Random Forests Classifier for Machine Fault Diagnosis. J. Mech Sci. Technol. 2008, 22 (9), 1716−1725.

(20) Wang, H.; Jiang, W.; Deng, X.; Geng, J. A New Method for Fault Detection of Aero-Engine Based on Isolation Forest. Measurement 2021, 185, 110064.

(21) Liu, Y.; Li, Z.; Chen, H. Artificial Intelligence-Based Fault Detection and Diagnosis: Towards Application in a Chemical Process.2023 CAA Symposium On Fault Detection, Supervision And Safety ForTechnical Processes (SAFEPROCESS); IEEE, 2023; pp 1−6.

(22) Chiang, L. H.; Kotanchek, M. E.; Kordon, A. K. Fault Diagnosis Based on Fisher Discriminant Analysis and Support Vector Machines.Comput. Chem. Eng. 2004, 28 (8), 1389−1401 .

(23) Sheibat-Othman, N.; Laouti, N.; Valour, J.-P.; Othman, S. Support Vector Machines Combined to Observers for Fault Diagnosisin Chemical Reactors. Can. J. Chem. Eng. 2014, 92 (4), 685−695.

(24) Watanabe, K.; Matsuura, I.; Abe, M.; Kubota, M.; Himmelblau, D. M. Incipient Fault Diagnosis of Chemical Processes via ArtificialNeural Networks. AichE J. 1989, 35 (11), 1803−1812.

(25) Wu, H.; Zhao, J. Deep Convolutional Neural Network Model Based Chemical Process Fault Diagnosis. Comput. Chem. Eng. 2018,115, 185−197.

(26) Aidan, A.; Abdel-Jabbar, N.; Ibrahim, T. H.; Nenov, V.; Mjalli, F. Neural Network Modeling and Optimization of SchedulingBackwash for Membrane Bioreactor. Clean Techn Environ. Policy2008, 10 (4), 389−395.

(27) Dong, D.; McAvoy, T. J. Nonlinear Principal Component Analysis�Based on Principal Curves and Neural Networks. Comput.Chem. Eng. 1996, 20 (1), 65−78.

(28) Jiang, Q.; Yan, X.; Zhao, W. Fault Detection and Diagnosis in Chemical Processes Using Sensitive Principal Component Analysis.Ind. Eng. Chem. Res. 2013, 52 (4), 1635−1644.

(29) Nomikos, P.; MacGregor, J. F. Monitoring Batch Processes Using Multiway Principal Component Analysis. AichE J. 1994, 40 (8),1361−1375.

(30) Yoon, S.; MacGregor, J. F. Fault Diagnosis with Multivariate Statistical Models Part I: Using Steady State Fault Signatures. J.Process Control 2001, 11 (4), 387−400.

(31) MacGregor, J.; Cinar, A. Monitoring, fault diagnosis, faulttolerant control and optimization: Data driven methods. Comput. Chem. Eng. 2012, 47, 111−120.

(32) Baldea, M.; Broadbelt, L. J.; Ierapetritou, M. G.; Li, C.; Luo, Z.-H.; Ma, X.; Morbidelli, M.;

Patwardhan, A. W.; Scurto, A. M.; Walton, K. S.; et al. 2023 in Retrospective: Trends in Chemical Engineering.Ind. Eng. Chem. Res. 2024, 63 (41), 17419−17429.
(33) Ma, Y.; Shi, H.; Tan, S.; Tao, Y.; Song, B. Double Branch Rebalanced Network for Class Imbalance Learning in Process FaultDiagnosis. Ind. Eng. Chem. Res. 2023, 62 (2), 1057−1072.
(34) Wen, H.; Amin, M. T.; Khan, F.; Ahmed, S.; Imtiaz, S.; Pistikopoulos, E. Assessment of Situation Awareness Conflict Riskbetween Human and AI in Process System Operation. Ind. Eng. Chem.Res. 2023, 62 (9), 4028−4038.
(35) Wu, D.; Bi, X.; Zhao, J. ProTopormer: Toward Understandable Fault Diagnosis Combining Process Topology for Chemical Processes. Ind. Eng. Chem. Res. 2023, 62 (21), 8350−8361.
(36) Balsora, H. K.; S, K.; Joshi, J. B.; Sharma, A.; Chakinala, A. G. Artificial Neural Network-Based Models for the Prediction of BiomassPyrolysis Products from Preliminary Analysis. Ind. Eng. Chem. Res.2023, 62 (36), 14311−14319.
(37) Wang, Q.; Taal, C.; Fink, O. Integrating Expert Knowledge With Domain Adaptation for Unsupervised Fault Diagnosis. IEEETrans. Instrum. Meas. 2022, 71, 1−12.
(38) Lundgren, A.; Jung, D. Data-Driven Fault Diagnosis Analysis and Open-Set Classification of Time-Series Data. Control Eng. Pract.2022, 121, 105006.
(39) Yin, M.; Li, J.; Shi, Y.; Qi, C.; Li, H. Fusing Logic Rule-Based Hybrid Variable Graph Neural Network Approaches to FaultDiagnosis of Industrial Processes. Expert Syst. Appl. 2024, 238,121753.
(40) Sharma, N.; Liu, Y. A. A Hybrid Science-Guided Learning Approach for Modeling Chemical Processes: A Review.AichE J. 2022, 68 (5), No. e17609.
(41) Jing, Y.; Ge, X.; Liu, B. Toward Understandable SemiSupervised Learning Fault Diagnosis of Chemical Processes Based on Long Short-Term Memory Ladder Autoencoder (LSTM-LAE) andSelf-Attention (SA). Comput. Chem. Eng 2024, 189, 108817.
(42) Amin, M. T.; Imtiaz, S.; Khan, F. Process System Fault Detection and Diagnosis Using a Hybrid Technique. Chem. Eng. Sci.2018, 189, 191−211.
(43) Monroy, I.; Benitez, R.; Escudero, G.; Graells, M. A SemiSupervised Approach to Fault Diagnosis for Chemical Processes. Comput. Chem. Eng. 2010, 34 (5), 631−642.
(44) Yin, S.; Ding, S. X.; Haghani, A.; Hao, H.; Zhang, P. A Comparison Study of Basic Data-Driven Fault Diagnosis and ProcessMonitoring Methods on the Benchmark Tennessee Eastman Process.J. Process Control. 2012, 22 (9), 1567−1581.
(45) Benkouider, A.; Kessas, R.; Yahiaoui, A.; Buvat, J.; Guella, S. A Hybrid Approach to Faults Detection and Diagnosis in Batch andSemi-Batch Reactors by Using EKF and Neural Network Classifier. J.Loss Prev. Process Ind. 2012, 25 (4), 694−702.
(46) Hu, Y.; El-Farra, N. H. Robust Fault Detection and Monitoring of Hybrid Process Systems with Uncertain Mode Transitions. AichE J.2011, 57 (10), 2783−2794.
(47) Picabea, J.; Maestri, M.; Cassanello, M.; Horowitz, G. Hybrid Model for Fault Detection and Diagnosis in an Industrial DistillationColumn. Chem. Prod. Process Model. 2021, 16 (3), 169−180.
(48) Venkateswaran, S.; Sheriff, M. Z.; Wilhite, B.; Kravaris, C.
Design of Functional Observers for Fault Detection and Isolation in Nonlinear Systems in the Presence of Noises. J. Process Control 2021,108, 68−85.
(49) Venkateswaran, S.; Kravaris, C. Disturbance Decoupled Functional Observers for Fault Estimation in Nonlinear Systems. In2024 American Control Conference (ACC); IEEE, 2024, pp. 1518−1524.
(50) Du, P.; Wilhite, B.; Kravaris, C. Model-Based Fault Diagnosis for Safety-Critical Chemical Reactors: An Experimental Study. AichEJ. 2024, 70, e18565.
(51) Cui, X.; Mannan, M. S.; Wilhite, B. A. Towards Efficient and Inherently Safer Continuous Reactor

Alternatives to Batch-Wise Processing of Fine Chemicals: CSTR Nonlinear Dynamics Analysis ofAlkylpyridines N-Oxidation. Chem. Eng. Sci. 2015, 137, 487−503.
(52) Keller, J. M.; Gray, M. R.; Givens, J. A. A Fuzzy K-Nearest Neighbor Algorithm. IEEE Trans. Syst. Man. Cybern. 1985, SMC-15(4), 580−585.
(53) Rosenblatt, F. The Perceptron: A Probabilistic Model for Information Storage and Organization in the Brain. Psychol. Rev.1958, 65 (6), 386−408.
(54) Vaswani, A. Attention Is All You Need. arXiv. 2017.
(55) Liu, F. T.; Ting, K. M.; Zhou, Z.-H. Isolation Forest. 2008 Eighth IEEE International Conference On Data Mining, 2008; pp 413−422.
(56) Fearnhead, P. Exact and Efficient Bayesian Inference for Multiple Changepoint Problems. Stat. Comput. 2006, 16 (2), 203−213.

ISSN 1520-5045

Celebrating the Birth Centenary of Quantum Mechanics: A Historical Perspective

Venkat Venkatasubramanian*

ABSTRACT

In July 1925, Werner Heisenberg submitted a paper to Zeitschrift f uӗr Physik entitled 'On quantum-theoreticalreinterpretation of kinematic and mechanical relationships', thusgiving birth to quantum mechanics. In the following year, buildingon de Broglie's wave-particle duality, Erwin Schrӧdinger developedwave mechanics, and soon, Max Born provided a probabilisticinterpretation of the wave function. The theory was furtherenriched by the exclusion principle of Wolfgang Pauli and theuncertainty principle of Heisenberg, which ultimately led to thedevelopment of relativistic quantum mechanics by Dirac. TheCopenhagen Interpretation created a probabilistic framework forunderstanding the theory. Over the past century, quantummechanics has paved the way for advances in quantum fieldtheory, computing, and modern technologies. This historical narrative provides insights into the complex discovery process that led to the development of quantum mechanics, which can potentially guide novel breakthroughs amid challenging conceptual struggles,as seen in the field of artificial intelligence today.

1. WHY IS THE HISTORY OF QUANTUM MECHANICS IMPORTANT?

This year, we mark a historic occasion: the centenary of the birth of quantum mechanics. A hundred years ago, the field ofquantum mechanics emerged through the pioneering efforts ofprimarily Werner Heisenberg, Erwin Schrӧdinger, and MaxBorn.1 Their groundbreaking contributions unraveled themysteries of the atomic world, transforming our understandingof reality itself. Quantum mechanics stands as one of humanity'smost profound intellectual achievements. Its founding principles�quantization, wave-particle duality, probability, uncertainty, and superposition� dramatically redefined our understanding of the universe. Jagdish Mehra, the authoritativechronicler of the history of quantum theory, declared:1,2"The birth of quantum mechanics presents us with one ofthe most remarkable episodes in the history of science; it isas rich, complex, dramatic, and touching as any in thehistory of human thought."Quantum mechanics, with its further development asquantum field theory, is a magnificently beautiful theory,perhaps second only in its beauty to the general theory ofrelativity. But quantum mechanics is far more surprising thangeneral relativity in its strangeness with concepts such asquantum entanglement – "spooky action-at-a-distance," as Einstein put it-, that whisper yet-to-be-revealed deeper secrets of reality that seem almost mystical.

In the July 1925 paper,3 Heisenberg introduced matrix mechanics, marking the first comprehensive formulation ofquantum theory that focused on observable quantities such asenergy and spectral transitions. Between November 1925 andJanuary 1926, Erwin Schrӧdinger developed wave presenting the now-famous Schrӧdinger equation, an alternative, yet equivalent, description of quantum systems.Soon, Max Born provided the probabilistic interpretation of thewave function, reshaping our notion of determinism andcausality in physics.

These milestones were part of an extraordinary period of intellectual explosion, during which luminaries such as NielsBohr, Paul Dirac, and Wolfgang Pauli contributed to theframework that continues to underpin modern physics.1,2 Thiscentennial is an opportunity to reflect on the profound humancapacity for imagination and discovery. It is also an opportunityto marvel at "the unreasonable effectiveness of mathematics inthe natural sciences," as Eugene Wigner wondered!4

This year, let us take a moment to appreciate and enjoy this crowning achievement of the human mind, which reveals themagnificent beauty of the hidden order of the cosmos. Thispaper is written with this objective in mind. Another importantreason for studying the early history of quantum mechanics isthat it is one of the rare occasions when a considerable wealth offirst-hand accounts of momentous discoveries is available.1Fortunately, many of the original architects of quantum theorylived long lives and documented their discoveries in detail inpapers, autobiographies, and interviews. These accounts offervaluable insights into the discovery process that can help guidenovel discoveries during periods of profound conceptualdifficulties and confusion, such as the current state of artificialintelligence.

Therefore, I will quote the original writings of the main protagonists wherever appropriate, as I am convinced that theirown expressions lend authenticity and clarity to the very murkyprocesses behind great conceptual discoveries. My hope is togive the reader a sense of what is involved in achieving majorconceptual breakthroughs. As Max Planck said:"In the history ofscience, a new concept never springs up in its complete and finalform, as in the ancient Greek myth, Pallas Athene sprang upfrom the head of Zeus." Heisenberg further elaborated:5"The history of physics is not only a sequence ofexperimental discoveries and observations, followed bytheir mathematical description; it is also a history ofconcepts. For an understanding of the phenomena, the firstcondition is the introduction of adequate concepts.Only with the help of correct concepts can we really knowwhat has been observed. When we enter a new field, veryoften, new concepts are needed. As a rule, new concepts comeup in a rather unclear and undeveloped form. Later, theyare modified, sometimes they are almost completelyabandoned and are replaced by some better concepts,which then, finally, are clear and well-defined."

In the remainder of this Commentary, I provide a historical perspective that highlights key breakthroughs. This perspectiveis meant for those unfamiliar with quantum mechanics or itshistorical development. It is not aimed at experts. The objectiveof this paper is not to teach readers quantum mechanics but onlyto expose them to the central ideas, their historical evolution,and the conceptual struggles, with a moderate amount ofmathematics to illustrate these points. Given the scope of thisperspective and its constraints, I will not discuss themathematical details, referring the readers to more comprehensive sources.1,6−10 Furthermore, this is a personalperspective that reflects what I consider important andinteresting developments. However, I believe that mostquantum experts agree with the observations made in this paper.

2. TWO CLOUDS IN THE HORIZON: THE "1900-MOMENT"

At the dawn of the 20th century, on April 27, 1900, Lord Kelvin delivered an important lecture at the Royal Institution inLondon,11 summarizing the status of physics with the title"Nineteenth-Century Clouds Over the Dynamical Theory ofHeat and Light." The "clouds" that bothered him were the twotroublesome experiments that did not agree with the theoreticalpredictions: (i) the null result of the Michelson-Morleyexperiment, which could not detect the motion of the Earththrough ether, and (ii) the ultraviolet catastrophe of blackbody radiation. Lord Kelvin correctly recognized the gravity of the situation and appreciated the profound uncertainty in the fundamentals of classical physics.As we know, these two "clouds" revolutionized physics, indeed all science, over the following three decades.12

The first "cloud" led to the birth of the theory of relativity, completelyupending our understanding of space, time, gravity, and thecosmos itself. The second gave us quantum mechanics, openingthe secret door to an almost"magical"realm that we did not evenknow existed all around us all of the time. In fact, quantumtheory was born soon in the same year, 1900, when Max Planckpresented his quantum hypothesis at a meeting of the GermanPhysical Society on December 14th, initiating the dispersal of the second cloud.13

This scientific drama unfolded like a well-written suspense thriller full of plot twists, turns, and surprising conceptual leaps,except that it was written in the language of mathematics,namely, linear algebra, differential equations, and probabilitytheory, echoing Galileo's declaration:14"Philosophy is written in this grand book, I mean theuniverse, which stands continually open to our gaze, but itcannot be understood unless one first learns to comprehendthe language in which it is written. It is written in thelanguage of mathematics."In the annals of history, certain periods stand out as inflectionpoints, times when scientific, technological, or social changesdrastically altered the trajectory of our civilization. That momentin 1900, when Kelvin announced that all was not well in physics,was such a tipping point. The innovations that followed, both theory and in practical applications, continue to transform oursocieties and economies profoundly. There is no other thirtyyear period in history where our understanding of the universewas so dramatically upended as it was during 1900−1930.

3. ACT I: THE BIRTH OF QUANTUM THEORY (1900−1913)

Between 1900 and 1930, physicists were compelled to abandon classical mechanics in favor of quantum mechanics because theformer could not predict or explain the atomic structure,spectrallines, and dual nature of matter and radiation as both waves andparticles. This drama of frenetic intellectual activity occurred infour surprising breakthroughs. In the following sections, Iprovide an overview of these key advances.

3.1. Max Planck and Quantum Theory (1900). As noted, the roots of quantum mechanics can be traced to the "cloud"thatLord Kelvin worried about in the context of blackbody radiation.A blackbody is an idealized object that absorbs and emitselectromagnetic radiation at all frequencies. Classical physicspredicted the intensity of this radiation using the Rayleigh-Jeanslaw:

$$I(\lambda, T) = \frac{2ck_BT}{\lambda^4} \tag{1}$$

where I(λ, T) is the radiation intensity, c is the speed of light, kB is Boltzmann's constant, T is the temperature, and λ is thewavelength of the radiation. This equation worked well at longwavelengths but diverged to infinity at short wavelengths, asshown in Figure 1, known as the ultraviolet catastrophe, a termcoined by Paul Ehrenfest in 1911.

Max Planck (Figure 2) got interested in this problem and, after a six-year struggle, introduced a revolutionary hypothesis:energy is not emitted continuously but in discrete Planck accomplished this in two critical steps, presented at the

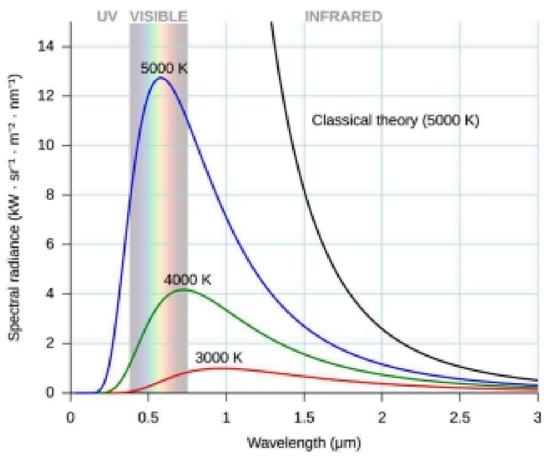

Figure 1. Ultraviolet catastrophe in classical Rayleigh-Jeans law. Reproduced with permission from ref 15. Copyright 2010 Darth Kule.

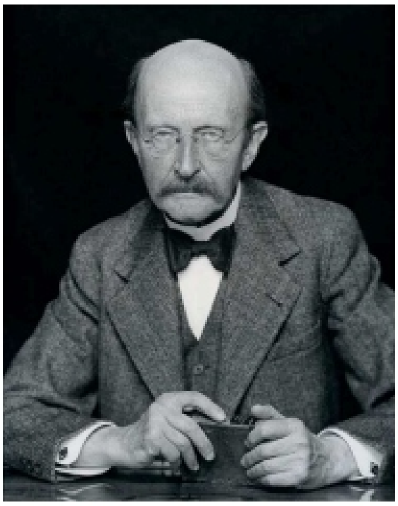

Figure 2. Max Planck. Reproduced with permission from ref 18. Copyright 1938 Hugo Erfurth.

German Physical Society meetings: (i) Discovering the correct radiation formula (on October 19, 1900) and (ii) Providing itsconceptual justification via the quantum hypothesis (onDecember 14, 1900).Let us hear about the first step from Planck himself from hisscientific autobiography:17"In fact, my previous studies of the Second Law ofThermodynamics came to stand me in good stead now,for at the very outset I hit upon the idea of correlating notthe temperature but the entropy of the oscillator with itsenergy. It was an odd jest of fate that a circumstance whichon former occasions I had found unpleasant, namely, thelack of interest of my colleagues in the direction taken by myinvestigations, now turned out to be an outright boon. Whilea host of outstanding physicists worked on the problem ofspectral energy distribution, from both the experimental andtheoretical aspects, every one of them directed his effortssolely toward exhibiting the dependence of the intensity ofradiation on the temperature On the other hand, I suspected that the fundamental connection lies in the dependence of entropy upon energy. Asthe significance of the concept of entropy had not yet come tobe fully appreciated, nobody paid any attention to themethod adopted by me, and I could work out mycalculations completely at my leisure, with absolutethoroughness, without fear of interference or competition ...In this way, a new radiation formula was obtained, and Isubmitted it for examination to the Berlin Physical Society,at the meeting on October 19, 1900."Although Rudolf Clausius introduced the concept of entropyin 1864, it remained undervalued by the scientific community,surprisingly, for nearly three decades. This highlights thesignificant amount of time required for revolutionary to gain widespread acceptance. Reflecting on this, Planck later remarked rather sardonically:17"A new scientific truth does not triumph by convincing itsopponents and making them see the light, but rather becauseits opponents eventually die out, and a new generation growsup that is familiar with it."Planck's new radiation law is given by

$$I(\lambda, T) = \frac{2hc^2}{\lambda^5}\frac{1}{e^{hc/\lambda k_B T} - 1} \qquad (2)$$

(h is Planck's constant) correctly described experimental data at all wavelengths and resolved the ultraviolet catastrophe.However, Planck was unsatisfied with the clever guessworkthat led to its discovery. He wanted to know its significance, and so he proceeded with the second step:17"But even if the absolutely precise validity of the radiationformula is taken for granted, so long as it had merely thestanding of a law disclosed by a lucky intuition, it could notbe expected to possess more than a formal significance. Forthis reason, on the very day that I formulated this law, Ibegan to devote myself to the task of investing it with a truephysical meaning. This quest automatically led me to studythe interrelation of entropy and probability�in other words, to pursue the line of thought inaugurated byBoltzmann.Since the entropy S is an additive magnitude but theprobability W is a multiplicative one, I simply postulatedthat S = k · log W, where k is a universal constant; and Iinvestigated whether the formula for W, which is obtainedwhen S is replaced by its value corresponding to the aboveradiation law, could be interpreted as a measure ofprobability ... It is, understandably, often called Boltzmann'sconstant. However, this calls for the comment that Boltzmann never introduced this constant, nor, to the best of my knowledge, did he ever think of investigating itsnumerical value."Interestingly, the famous equation S = k log W, which isinscribed on Boltzmann's tomb in Vienna, was not stated in thisform by Boltzmann. It was Planck who expressed the Boltzmannresult in this now familiar form.16Applying Boltzmann's reasoning about entropy from his 1877paper19 to blackbody radiation, Planck was led to the concept ofdiscrete packets of energy, which he termed quanta.13,20 He was,however, uncomfortable with this idea as he was aware that hewas violating the continuity principle,21 a fundamental principlethat dates back to Leibnitz, who famously said:22 "Natura nonfacit saltus" (Latin for "nature does not make jumps"). This principle also serves as the foundation for differential and integral calculus.Planck alerts us to this crucial feature of his theory in hisDecember 14, 1900, paper:13"If E [the total energy] is considered to be a continuousdivisible quantity, this distribution is possible in infinitelymany ways. We consider, however � this is the mostessential point of the whole calculation � E to be composedof a well defined number of equal parts [of magnitude ϵ]and use thereto the constant of nature h = 6.55 × 10−27 ergsec [setting ϵ = hν]." About his break with classical physics tradition and his embracing of Boltzmann's "atomistic" ideas, which he had beencritical of for many years, Planck would later recall:"Briefly summarized, what I did can be described as simplyan act of desperation. By nature, I am peacefully inclinedand reject all doubtful adventures. But by then I had beenwrestling unsuccessfully for six years (since 1894) with theproblem of equilibrium between radiation and matter, and Iknew that this problem was of fundamental importance tophysics; I also knew the formula that expresses the energydistribution in normal spectra. A theoretical interpretationtherefore had to be found at any cost, no matter how high.It was clear to me that classical physics could offer nosolution to this problem and would have meant that all ofthe energy would eventually transfer from matter intoradiation. In order to prevent this, a new constant isrequired to ensure that energy does not disintegrate. But theonly way to recognize how this can be done is to start from adefinite point of view. This approach was opened to me bymaintaining the laws of thermodynamics. The two laws, itseems to me, must be upheld under all circumstances. Forthe rest, I was ready to sacrifice every one of my previousconvictions about physical laws."Although historians continue to debate how much Planckrealized the significance of his quantum hypothesis,13,20,21 ErwinPlanck later recalled what his father told him soon after hisdiscovery:20"Either what I have found out now is complete nonsense orit might be one of the greatest discoveries in physics sinceNewton."

Planck proposed that the energy of a radiation mode isquantized and proportional to its frequency:

$$E = nh\nu \qquad n = 1, 2, 3, \ldots \tag{3}$$

where h is Planck's constant and ν is the frequency of the radiation. This assumption prevented infinite energy at shortwavelengths and correctly described blackbody radiation. Usingenergy quantization, Planck derived the formula presented above, now expressed in terms of frequency ν:

$$I(\nu, T) = \frac{2h\nu^3}{c^2}\frac{1}{e^{h\nu/k_BT} - 1} \tag{4}$$

Max Planck was awarded the 1918 Physics Nobel Prize for his discovery. Although Planck gave birth to quantum theory, heremained a reluctant revolutionary for a long time, viewingquantization only as a "mathematical trick" rather than as afundamental law of nature. After all, he was very much a part ofthe old guard and therefore was hesitant to abandon the "sacred"principle of continuity. It was only much later that he camearound to accepting the new reality.

3.2. Albert Einstein and the Photoelectric Effect (1905).

On the other hand, the Young Turk who followed Planck next in this exciting drama was a rebellious iconoclast who was rearing to upend the very foundations of physics, notjust radiation theory. Enter Albert Einstein (Figure 3), a 26-year

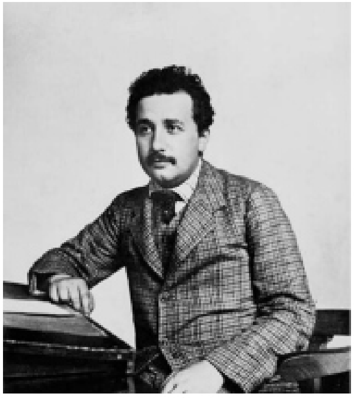

Figure 3. Albert Einstein. Reproduced with permission from ref 23. Copyright 1905 Lucien Chavan.

old unknown clerk at the Swiss Patent Office in Bern. While Planck saw quantization as just a "mathematical trick", not afeature of physical nature, Einstein took it more seriously as afundamental property of nature. He was open to such radicalrethinking as he was, at the same time, busy overthrowing theNewtonian concepts of space and time in his new theory ofspecial relativity, which dispersed the first "cloud" that LordKelvin worried about.

In his Annus Mirabilis, 1905, Einstein extended Planck's idea and proposed that light itself consists of quantized particlescalled photons, each carrying energy E = hν, to solve a puzzlingresult in the photoelectric effect, where light incident on a metalsurface ejects electrons. The classical wave theory of lightpredicted that increasing the light intensity should increase theelectron energy. However, experiments showed that noelectrons are emitted below a threshold frequency, regardlessof intensity. They further showed that the electron energydepends on the frequency, not the intensity. The higher lightintensity increased the number of emitted electrons, but nottheir individual energy.Einstein's theory treats the photoelectric effect as a one-toone interaction between a photon and an electron. The energybalance equation is

$$h\nu = W + E_k \quad (5)$$

where hν is the energy of the incoming photon, W (or work function) is the minimum energy required to free an electronfrom the metal, and Ek is the maximum kinetic energy of theemitted electron. This equation explained all of the experimentalresults. Reflecting on his groundbreaking papers from 1905,which included his first two on relativity, he regarded only thelight-quanta paper as genuinely revolutionary. Einstein wasawarded the Nobel Prize in Physics in 1921 for this discovery. Itis interesting to note that the prize was not for his work onrelativity.From the perspective of the evolution of quantum theory,Einstein's theory confirmed the particle nature of light,supporting the idea that light exhibits both wave and particleproperties, i.e., wave-particle duality. This paved the way for theacts that followed next.

3.3.Niels Bohr and theHydrogen Atom (1913). In 1897, J. J. Thomson at Cambridge discovered the electron in cathoderay tube experiments. Ernest Rutherford, who had trained underThomson, showed in his gold foil experiment at Manchester in1911 that the atom is mostly an empty space with a tiny, dense,positively charged nucleus with orbiting electrons. However,classical electrodynamics predicted that electrons should spiralinto the nucleus due to radiation loss. Furthermore, the atomicspectra of hydrogen showed discrete spectral lines, contradictingclassical physics, which predicted a continuous spectrum.In 1911, Niels Bohr (Figure 4) arrived in England to study atomic structure under Thomson first and with Rutherford later

Figure 4. Niels Bohr. Reproduced with permission from ref 24. Copyright 1922 AB Lagrelius & Westphal.

in Manchester. In 1913, in a series of three papers, Bohr proposed an atomic model that resolved the contradictions.While Einstein extended Planck's quantum hypothesis tophotons, Bohr further extended it to electrons by introducingquantized orbits for electrons. Bohr's atomic model introducedthree key quantum postulates:25

(i) Electrons move in fixed circular orbits around the nucleus,where their angular momentum is quantized:

$$L = n\hbar = n\frac{h}{2\pi}, \quad n = 1, 2, 3, ... \tag{6}$$

where L is the electron's angular momentum, $\hbar = h/2\pi$ is the reduced Planck constant, and n is the principal quantum numberspecifying the allowed orbits. This assumption preventedelectrons from spiraling into the nucleus, ensuring atomicstability.

(ii) The total energy of an electron in orbit is also quantized and given by

$$E_n = -\frac{13.6\text{eV}}{n^2} \tag{7}$$

where En is the energy of an electron in orbit n, and −13.6 eV is the ground-state energy of hydrogen (energy levels are negative,meaning that electrons are bound to the nucleus). Thisquantization explains why the atoms do not radiate continuously.

(iii) Electrons can transition between orbits, i.e., performquantum jumps, by absorbing or emitting a photon of energy:

$$E_{\text{photon}} = h\nu = E_i - E_f \tag{8}$$

where ν is the frequency of emitted/absorbed light and Ei and Ef are the initial and final energy levels. This correctly explainedhydrogen's spectral lines, known as the Balmer series, given by

$$\frac{1}{\lambda} = R_H\left(\frac{1}{n_f^{\,2}} - \frac{1}{n_i^{\,2}}\right) \tag{9}$$

where RH is the Rydberg constant.

Thus, the Bohr model successfully explained the atomic stability and correctly predicted hydrogen spectral lines.26 Mostimportantly, Bohr had conceptually generalized Planck's"mathematical trick" and made quantization a fundamentalfeature of nature. Bohr was awarded the Nobel Prize in Physicsin 1922. With this, the first act ends, and the stage is set for evenmore surprising twists and turns.

4. ACT II: DE BROGLIE AND WAVE-PARTICLE DUALITY (1923−1924)

About ten years after Bohr, the next crucial conceptual breakthrough came in the form of further generalization of thewave-particle duality of light. In 1923, Prince Louis de Broglie(Figure 5) introduced the shocking concept of matter waves,

Figure 5. Louis de Broglie. Reproduced with permission from ref 29.

which impressed Einstein so much that he remarked:27 "He has lifted a corner of the great veil." Put simply, de Broglie askedhimself: If light, which was thought of as a wave, can exhibitparticle-like behavior (as photons), why cannot particles likeelectrons exhibit wave-like behavior? He defended this idea inhis Ph.D. thesis on 25 November 1924, in Paris.28 In this thesis,he proposed wave-particle duality for matter, suggesting that"matter waves" obey the equation

$$\lambda = \frac{h}{p} \tag{10}$$

where λ is the de Broglie wavelength and p is momentum. In 1927, Davisson and Germer, and independently Thomson andReid, confirmed this idea in electron diffraction experiments. deBroglie received his Nobel Prize in Physics in 1929, a mere fiveyears after his Ph.D. defense. Davisson and Thomson received theirs in 1937.

One question physicists and historians have puzzled over for many years is why de Broglie, who discovered matter waves, didnot proceed to discover Schrӧdinger's wave equation. Althoughwe cannot be certain, experts have identified several reasons afterconducting careful studies. Here, I quote Olivier Darrigol:27"A first element of the answer is that, notwithstanding withhis grand analogy between dynamics and optics, he (deBroglie) was shy in adventuring beyond the approximationof geometrical optics. He focused on retrieving results of thereceived quantum theory, such as the Bohr−Sommerfeldconditions, and he underplayed the more disturbingconsequences of his concept of matter waves.

Another possible obstacle to his developing a wave theory of matter was his conviction that both light and matter had adual nature, implying the synchronous motion of waves andparticles. This duality focused on the interplay betweenwaves and particles rather than on the search for a newwave equation.

Third and most importantly, de Broglie believed that the analogy between light and matter implied the electromagnetic nature of his matter waves. Consequently, he alsobelieved that matter waves obeyed the d'Alembertianequation of electromagnetism. Direct evidence of thisconviction is found in a note of 1925 in which he describesthe intrinsic oscillation of an electron in its rest frame as thestationary superposition of the retarded and advancedsolutions of the d'Alembertian equation.The same heuristic principle, the analogy between matterand light, led de Broglie to the matter waves and preventedhim from seeking a specific equation for these waves!"

Therein lies a very important lesson in the use of analogies to discover new conceptual breakthroughs. One should not take ittoo literally or expect an exact analogy of the new phenomenonin every detail. Although de Broglie was correct in reasoning thatthe wave-particle duality of light implied a similar duality forelectrons (matter, in general), he took this analogy too far toreason that matter waves would also be electromagnetic innature. This is where the analogy broke down. Fortunately,Schrӧdinger did not make this mistake!

5. ACT III: THE BIRTH OF QUANTUM MECHANICS (1925−1927)

Finally, we arrive at the main event, the birth of quantum mechanics. The key characters are Werner Heisenberg, ErwinSchrӧdinger, Max Born, Paul Dirac, and Wolfgang Pauli. Even adecade after the Bohr atom, atomic phenomena have remainedlargely unexplained, with many disturbing fundamentalquestions. There was no coherent mathematical theory yet,only a collection of seemingly ad hoc rules of quantum behavior.The transition from classical mechanics to quantum mechanicsremained an elusive goal before 1925.

5.1. Heisenberg and Born: Matrix Mechanics. The first major breakthrough in resolving this impasse was initiated by23-year-old Heisenberg (Figure 6) in his historic 1925 papernoted earlier,3 marking the birth of quantum mechanics.Heisenberg's innovative idea, guided by Bohr's CorrespondencePrinciple, was to retain classical mechanics equations but replacethe classical position coordinate with a quantum-theoreticalquantity. The new position quantity contains information aboutthe measurable line spectrum of an atom rather than theunobservable orbital of the electron. He devised a specialkinematical rule for multiplying position quantities. Mehra givesa vivid description of this momentous discovery:

Figure 6. Werner Heisenberg. Reproduced with permission from ref 31
Copyright 1933 German Federal Archives.

"With the coming of spring in 1925, Heisenberg had developed a case of severe hay fever, which would just notleave him, and he decided to take a week or ten days off inJune 1925 at the rocky island of Helgoland in the NorthSea. At Helgoland, not only did he cure his hay fever butwiped the nose clean of the chronic colds of erstwhileproblems of atomic mechanics ...At Helgoland, Heisenberg divided his time in taking longwalks, reading Goethe's West-Ostlicher Divan, and seekingto give his vague ideas on quantum mechanics a moredefinite shape. There he solved two problems ...The example of the anharmonic oscillator showed him thata dynamical problem in quantum theory could be solvedwith the help of his scheme.

As he (Heisenberg) recalled:30 'It was almost three o'clock in the morning before the final result of my computations laybefore me. The energy principle had held for all of the terms,and I could no longer doubt the mathematical consistencyand coherence of the kind of quantum mechanics to whichmy calculations pointed. At first, I was deeply alarmed. had the feeling that, through the surface of atomic phenomena, I was looking at a strangely beautiful interiorand felt almost giddy at the thought that I now had to probethis wealth of mathematical structures nature had sogenerously spread out before me. I was far too excited tosleep, and so, as a new day dawned, I made a trip to thesouthern tip of the island, where I had been longing to climba rock jutting out into the sea. I now did so without toomuch trouble, and waited for the sun to rise.'"After he returned from Helgoland, Heisenberg gave his paperto Max Born (Figure 7) in early July for his opinion. Heisenbergwas working as Born's research assistant at the University ofGöttingen at that time. Born had been keenly aware of thedifficulties in quantum theory for some time as he wrote:32 "Itbecomes increasingly probable that not only new assumptionswill be needed in the sense of physical hypotheses, but that theentire system of concepts of physics must be rebuilt from theground up." So, when he saw Heisenberg's new mathematical

Figure 7. Max Born. Reproduced with permission from ref 33. Copyright 1954 German Federal Archives.

formulation of kinematics of quantum systems, Born immediately recognized its importance, as he recalls:2 "I began to ponder about his symbolic multiplication andwas soon involved in it. I thought the whole day and couldhardly sleep at night ... In the morning I suddenly saw thelight: Heisenberg's symbolic multiplication was nothing butthe matrix calculus, well-known to me since my student daysfrom the lectures of Rosanes in Breslau."A few days later, on July 19, 1925, Born traveled fromGöttingen to Hanover to attend a meeting of the GermanPhysical Society, where he informed Wolfgang Pauli about thematrices. Pauli was critical:2"Yes, I know that you are fond of a tedious and complicatedformalism. You are only going to spoil Heisenberg's physicalideas by your futile mathematics."To a modern physicist, it is astonishing that Heisenberg didnot know about matrices when he made his great discovery, as headmits:5"At that time I must confess I did not know what a matrixwas and did not know the rules of matrix multiplication."As Fedak and Prentis describe,34 it was Born who recognizedthat the next step was to formalize Heisenberg's theory using thelanguage of matrices, which he did with his student PascualJordan35 after Pauli turned him down.2 This was followed byanother paper by Born, Heisenberg, and Jordan.36 It was alsoBorn who coined the name Quantum Mechanics for the newfield.34,37 Born expressed Heisenberg's results in a more elegantform using the matrix notation. If Q and P are the position andmomentum matrices, they satisfy

$$[P, Q] = PQ - QP = (h/2\pi i)I \qquad (11)$$

where I isthe identity matrix, and the quantity [P,Q]is known as the commutator. It is important to note that using matrices is notjust a matter of mathematical elegance. What Heisenberg haddiscovered inadvertently was one of the fundamental aspects ofquantum reality: its dynamic variables are represented byoperators (and hence matrices), unlike classical variables, whichare represented by scalars. This critical feature was independently recognized by Paul Dirac around the same time38 (more on this below). These papers introduced a novelapproach to atomic Hamiltonian mechanics using non commutative quantum methods. This marked the beginning of a new phase in theoretical physics, characterized by the use ofHermitian matrices, commutators, and eigenvalue problems askey mathematical tools in atomic theory.

This noncommutativity of position and momentum matrices led to a major breakthrough two years later, in 1927, whileHeisenberg was visiting the Niels Bohr Institute in Copenhagen.He describes what happened one late evening as he took a strollthrough Faelledparken, the lovely park behind the institute:30

"It must have been one evening after midnight when Isuddenly remembered my conversation with Einstein and particularly his statement, 'It is the theory which decideswhat we can observe.' I was immediately convinced that thekey to the gate that had been closed for so long must besought right here. I decided to go on a nocturnal walkthrough Faelled Park and to think further about the matter.We had always said so glibly that the path of the electron inthe cloud chamber could be observed. But perhaps what wereally observed was something much less. Perhaps we merelysaw a series of discrete and ill-defined spots through whichthe electron had passed. In fact, all we do see in the cloudchamber are individual water droplets, which must certainlybe much larger than the electron. The right question shouldtherefore be: Can quantum mechanics represent the fact thatan electron finds itself approximately in a given place andthat it moves approximately with a given velocity, and canwe make these approximations so close that they do not cause experimental difficulties?

A brief calculation after my return to the Institute showed that one could indeed represent such situations mathematically and that the approximations are governed by whatwould later be called the uncertainty principle of quantummechanics: the product of the uncertainties in the measuredvalues of the position and momentum (i.e., the product ofmass and velocity) cannot be smaller than Planck'sconstant. This formulation, I felt, established the muchneeded bridge between cloud chamber observations and themathematics of quantum mechanics. True, it had still to beproved that any experiment whatsoever was bound to set upsituations satisfying the uncertainty principle, but this struckme as plausible a priori since the processes involved in theexperiment or the observation had necessarily to satisfy thelaws of quantum mechanics. On this presupposition,experiments are unlikely to produce situations that do accord with quantum mechanics. 'It is the theory which
decides what we can observe.' I resolved to prove this bycalculations based on simple experiments during the nextfew days."The uncertainty principle states that there is an intrinsic limitto how precisely we can simultaneously measure the position qand the momentum p of a particle. Heisenberg derived the following inequality:

$$\Delta q \cdot \Delta p \geq \frac{\hbar}{2} \tag{12}$$

where Δq is the standard deviation of position and Δp is the standard deviation of momentum. If we try to measure aparticle's position very precisely (Δq small), the uncertainty inmomentum Δp increases. Conversely, if we measure themomentum precisely, the uncertainty in the position grows.This principle is not due to measurement errors but rather aninherent property of quantum systems.

Given this history of the uncertainty principle and its close association with the Niels Bohr Institute, I found it so fitting, in alighter vein, to see this cartoon (Figure 8) displayed on a door ofthe Institute during my visit in August of 2022.

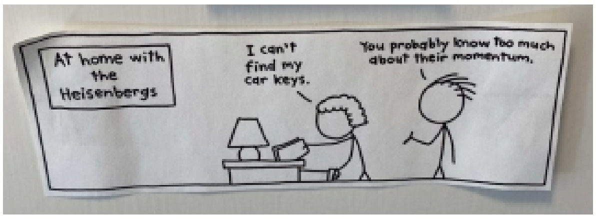

Figure 8. Cartoon on a wall of the Niels Bohr Institute. Photo by the author in 2022. Artist unknown.

There are serious implications captured by this fundamental property of nature. (i) Observer's interference: the very act measurement disturbs the system. (ii) Wave-particle duality: position and momentum cannot be simultaneously well-defined.(iii) Limits of classical concepts: the classical idea of a trajectorydoes not hold in the quantum realm.

Heisenberg would later speak in sheer awe of the startling simplicity and beauty of the new theory:30“If nature leads us to mathematical forms of great simplicityand beauty � by forms, I am referring to coherent systemsof hypotheses, axioms, etc. � to forms that no one haspreviously encountered, we cannot help thinking that theyare ‘true,’ that they reveal a genuine feature of nature ... Youmust have felt this too: the almost frightening simplicity andwholeness of the relationships which nature suddenlyspreads out before us and for which none of us was in theleast prepared.”Heisenberg was awarded the 1932 Nobel Prize in Physics.Given Born and Jordan’s pivotal role in the discovery ofquantum mechanics, it is natural to wonder why they were leftout. In 1933, Heisenberg wrote Born saying:39“The fact that I am to receive the Nobel Prize alone, forwork done in Göttingen in collaboration�you, Jordan, andI�this fact depresses me, and I hardly know what to writeto you. I am, o f course, glad that our common now appreciated and I enjoy the recollection of the beautiful time of collaboration. I also believe that all good physicistsknow how great was your and Jordan’s contribution to thestructure of quantum mechanics�and this remainsunchanged by a wrong decision from outside. Yet I myselfcan do nothing but thank you again for all the finecollaboration and feel a little ashamed.”Fortunately, Born was awarded the Nobel Prize in Physics in1954 for his fundamental research in quantum mechanics,especially for his statistical interpretation of the wave function (as discussed below). Engraved on Max Born’s tombstone in Göttingen is a one-line epitaph: pq − qp = h/2πi.

5.2. Schrödinger’s Wave Mechanics (1926). 1925 was already an amazing year, but the quantum mechanics revolutionwas not yet finished for the year. Following a line of attack that isdifferent from the matrix mechanics formalism, ErwinSchrödinger (Figure 9) was developing something veryinteresting. Inspired by de Broglie’s matter waves, he introducedwave mechanics, and the fundamental equation governingquantum evolution, the Schrödinger equation:

Figure 9. Erwin Schrödinger. Reproduced with permission from ref 40. Copyright 1930 Nobel Foundation.

$$i\hbar \frac{\partial}{\partial t}\psi = \hat{H}\psi \tag{13}$$

where $\hat{H}$ is the Hamiltonian operator and ψ is the wave function. The time-independent version,

$$-\frac{\hbar^2}{2m}\nabla^2\psi + V\psi = E\psi \tag{14}$$

explains energy quantization and atomic structure. Schrödinger showed that wave mechanics is mathematically equivalent tomatrix mechanics.

Just as he proposed the matrix formalism to clarify Heisenberg's quantum mechanics, Max Born once again steppedup and clarified the meaning of the wave function in wavemechanics in 1926.41 Born interpreted the wave function ψ(x, t)as a probability amplitude. The probability of finding a particle at position x is given by:

$$P(x) = |\psi(x)|^2 \qquad (15)$$

This marked a fundamental conceptual shift from a deterministic perspective of the universe in classical mechanicsto a probabilistic view of quantum mechanics. It is indeed quiteremarkable that such a fundamental interpretation thatcompletely revolutionized our view of the universe wasmentioned in a mere footnote of Born's 1926 paper.41 In fact,there is a fascinating backstory to this. In a paper written on theoccasion of the birth centenary of Born in 1982, Abraham Paisobserved:42

"Then, Born declares: 'ϕmn (i.e. the wavefunction, ψ(x)) determines the probability for the scattering of the electronfrom the z-direction into the direction [θ, ϕ].' At best, this statement is vague. Born added a footnote inproof to his evidently hastily written paper: 'A more preciseconsideration shows that the probability is proportional tothe square of ϕmn.' He should have said 'absolute square.' But he clearly had got the point, and so the correctexpression for the transition probability concept enteredphysics via a footnote.

I shall return shortly to the significant fact that originally associated probability with ϕmn rather than with |ϕmn|2. As I learned from recent private discussions, Dirachad the very same idea at that time. So did Wigner, whotold me that some sort of probability interpretation was thenon the minds of several people, and that he, too, had thoughtof identifying ϕmn or |ϕmn| with a probability. When Born'spaper came out and |ϕmn|2 turned out to be the relevantquantity, 'I was at first taken aback but soon realized thatBorn was right,' Wigner said." It is absolutely incredible and deeply instructive that such afundamental feature of quantum mechanics, namely, itsprobabilistic nature, was initially guessed wrong even by giantslike Born, Dirac, and Wigner, and was subsequently corrected ina footnote only during the proof stage of the manuscript. Again,this teaches us valuable lessons about the nature of the discoveryprocess, particularly fundamental concepts.

Over the years, many have wondered why Schrödinger, of alltheoretical physicists, took up de Broglie's ideas and developedthem into wave mechanics.43 We briefly saw above why deBroglie himself did not do it. Raman and Forman provide aninteresting account43 that de Broglie was not taken seriously bythe quantum establishment:

"Thus in Copenhagen and in Gottingen, where atomicphysics was pursued in the Copenhagen spirit, de Brogliewould certainly have had the reputation of a renegade, if notexactly a crank, who stuck obstinately to his own illconceived theories ... Thus among the central Europeanphysicists deeply involved in the problems of theoreticalspectroscopy, and this was indeed the great majority of thoseseriously concerned with the quantum theory, de Brogliemust have had a very bad reputation." On the other hand, Schrödinger had no such biases against deBroglie and so took his work seriously. There is a well-knownanecdote due to Dirac44 that the first wave equation Schrödingerguessed later became known as the relativistic Klein-Gordonequation. When this equation, applied to the hydrogen atom, didnot yield the familiar results, Schrödinger abandoned thisequation, searched again for a better candidate, and discoveredthe famous Schrödinger equation.Felix Bloch, the 1952 Nobel laureate in Physics, who was astudent at ETH-Zurich at that time, provides additional details45on the events when Schrödinger participated in their physicscolloquium run by Peter Debye (Nobel Prize in Chemistry,1936). Bloch recalls Schrödinger's seminar in early 1925:

“Once at the end of a colloquium I heard Debye saying something like: ‘Schrӧdinger, you are not working right nowon very important problems anyway. Why don’t you tell ussome time about that thesis of de Broglie, which seems tohave attracted some attention.’So, in one of the next colloquia, Schrӧdinger gave a beautifully clear account of how de Broglie associated awave with a particle and how he could obtain thequantization rules of Niels Bohr and Sommerfeld bydemanding that an integer number of waves should be fittedalong a stationary orbit. When he had finished, Debyecasually remarked that he thought that this way of talkingwas rather childish. As a student of Sommerfeld he hadlearned that, to deal properly with waves, one had to have awave equation ... Just a few weeks later he (Schrӧdinger)gave another talk in the colloquium which he started bysaying: ‘My colleague Debye suggested that one should havea wave equation; well, I have found one!’”Prompted by Debye, Schrӧdinger discovered his equation in about three months, between November 1925 and
January 1926, and published a series of four papers on wavemechanics entitled Quantization as an eigenvalue Problem.46−48It is understandable that the members of the “CopenhagenEstablishment” did not discover the wave equation, as they did not take de Broglie seriously. But I have often wondered why Einstein or Debye did not discover the wave equationthemselves. I believe that while Einstein understood theimportance of de Broglie’s matter wave concept, he was toopreoccupied with his search for the unified field theory, which heworked on for the rest of his life. As for Debye, it appears that hehad some regrets, as narrated again by Bloch:45“Many years later, I reminded Debye of his remark aboutthe wave equation; interestingly enough he claimed that hehad forgotten about it, and I am not quite sure whether thiswas not the subconscious suppression of his regret that hehad not done it himself. In any event, he turned to me with abroad smile and said: ‘Well, wasn’t I right?’” ”
Initially, Heisenberg’s matrix mechanics and Schrӧdinger’s wave mechanics appeared to be very different from each other,and an acrimonious debate ensued over which one was correct.In a footnote to a 1926 paper, Schrӧdinger wrote: “I wasdiscouraged, if not repelled, by what appeared to me ratherdifficult method of transcendental algebra, defying any visualization.” Meanwhile, Heisenberg complained to Pauli: “Themore I think about the physical part of Schrӧdinger theory, themore detestable I find it.” Fortunately, the debate wasresolved in1926. Schrӧdinger, along with Carl Eckert, working independently, demonstrated that the two new mechanics, althoughsuperficially very different, were mathematically equivalent toeach other.Schrӧdinger was awarded the Nobel Prize in Physics in 1933,which he shared with Paul Dirac, discussed next, for theircontributions to quantum mechanics.5.3. Commutator and the Poisson Brackets: Dirac’sDiscovery (1928−1930). Right before the paper by Born,Heisenberg, and Jordan was published in January 1926, anotherpaper outlining the whole framework of quantum mechanics waspublished in the Proceedings of the Royal Society by Paul Dirac(Figure 10), then a research student of R. H. Fowler’s inCambridge. Reflecting on Heisenberg’s paper, Dirac recalled:49

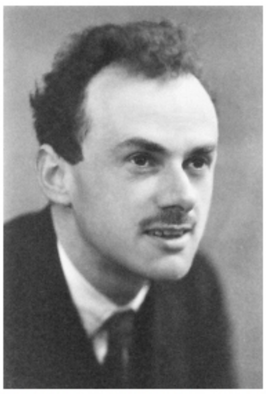

Figure 10. Paul Dirac. Reproduced with permission from ref 50. Copyright 1933 Nobel Foundation.

"During a long walk on a Sunday it occurred to me that the commutator might be the analogue of the Poisson bracket,but I did not know very well then what a Poisson bracketwas. I had just read a bit about it and forgotten most ofwhat I had read. I wanted to check up on this idea, but Icould not do so because I did not have any book at homethat gave Poisson brackets, and all the libraries were closed.So I had just to wait impatiently until Monday morningwhen the libraries were open to check on what Poissonbracket really was. Then I found that they would fit, but Ihad one impatient night of waiting."By recognizing the link between these two brackets, Diraceffectively clarified the connection between Heisenberg'svariables and classical variables, giving the formulation a moreclassical appearance. Meanwhile, it neatly highlighted the precisepoint where the reformulation diverged from the classicaltheory.Dirac was one of the most brilliant theoretical physicists of thetwentieth century, making profound contributions to quantummechanics, quantum field theory, and relativistic quantummechanics. His work introduced the Dirac equation, predictedthe existence of antimatter, and laid the mathematicalfoundation for quantum electrodynamics (QED). Dirac sharedhis Nobel in 1933 with Schrödinger.

5.4. Pauli Exclusion Principle (1925). As I wrap up this period of frenetic activity, I would be remiss if I did not mentionthe contributions of Wolfgang Pauli (Figure 11), particularly hisexclusion principle. Pauli made fundamental contributions toquantum mechanics and quantum field theory, significantlyshaping modern physics. His most famous work includes thePauli exclusion principle, his contributions to spin theory, thetheory of quantum electrodynamics (QED), and the predictionof the neutrino.In 1925, Pauli formulated the exclusion principle, stating that no two identical fermions can occupy the same quantum statesimultaneously. Mathematically, this means that for a system oftwo electrons, the wave function Ψ must be antisymmetric underparticle exchange: $\Psi(1, 2) = -\Psi(2, 1)$. This ensures that if twoelectrons were in the same quantum state, then the wavefunction would be zero, prohibiting such configurations.

Figure 11. Wolfgang Pauli. Reproduced with permission from ref 51. Copyright 1945 Nobel Foundation.

The Pauli exclusion principle explains: (i) electron shell structure of atoms, (ii) periodic table organization and whydifferent elements have distinct chemical properties, and (iii)stability of matter, as it prevents electrons from collapsing intothe lowest energy state. For his contributions to the development of quantum mechanics, Pauli was awarded the Nobel Prizein Physics in 1945.

6. ACT IV: THE COPENHAGEN INTERPRETATION (1927−1930)

Starting with Heisenberg's matrix mechanics in 1925 and concluding with Dirac's relativistic quantum theory in 1930, in ashort span of five years, a coherent mathematical formalism ofquantum mechanics emerged. However, its conceptualimplications seriously bothered several leading physicists,including those who contributed to its development, such asEinstein, Schrödinger, and others. Objecting to the probabilisticfoundations of quantum mechanics, Einstein was perhaps themost vocal, famously saying:52 "God does not play dice with theuniverse." On quantum entanglement,52 he called it "spookyaction at a distance." Schrödinger devised the famousSchrödinger's cat paradoxto highlight the interpretational issuesof quantum mechanics.

Despite such objections, physicists converged around a set of principles advocated by Bohr and Heisenberg in 1927, known asthe Copenhagen Interpretation, which has remained the mostwidely accepted view of quantum mechanics for a century. Thekey tenets of this view are: (i) Nature at the quantum level isintrinsically probabilistic, and the square of the wave function$|\psi(x, t)|$
2 gives the probability of finding a particle at (x, t). (ii) A quantum system exists in a superposition until measured, atwhich point it collapses into a definite state. (iii) The act ofmeasurement affects the system. (iv) Key quantities such asenergy, momentum, spin, etc. are quantized.There are some fundamental concerns with thisinterpretationof quantum mechanics, particularly with respect to the wavefunction collapse, which we shall not go into.53−56 The fact thatthe predictions of quantum mechanics have been fantasticallyaccurate, as verified by countless experiments over the decades,although its conceptual foundations are somewhat murky,prompted N. David Mermin, the physics professor who taught me quantum mechanics at Cornell, to summarize the Copenhagen Interpretation as "Shut up and calculate!" Thisquote is often misattributed to Richard Feynman.

7. IMPACT OF QUANTUM MECHANICS IN CHEMICAL ENGINEERING

Although the objective of this paper is not on the application of quantum mechanics, I would like to briefly mention its profoundimpact on chemical engineering and materialsscience.58,59 Fromreaction kinetics to materials design, quantum mechanicsprovides the fundamental principles that govern atomicinteractions, electronic structure, chemical bonding, computational chemistry, catalysis, nanotechnology, and quantumcomputing, among other areas. Quantum mechanics providesinsights into (i) molecular interactions and reaction mechanisms, (ii) electronic structures governing chemical and materialproperties, and (iii) energy levels that define molecular andsolid-state behaviors. Using such information, chemicalengineers optimize catalysts, polymers, drug molecules, andnanomaterials, improving efficiency and sustainability.For example, the Schrödinger equation is routinely used todetermine molecular structures and properties, such as bondlengths and angles, reaction energy barriers for kinetic analysis,and molecular orbitals and charge distributions. The DensityFunctional Theory is widely used to design catalysts, semiconductors, polymers, and nanomaterials. Quantum dots are yetanother application for designing nanoscale semiconductorswith tunable electronic properties used in LED displays andphotovoltaics. Quantum confinement is utilized, for example, inthe design of graphene-based sensors and supercapacitors forenergy storage. As quantum technology advances, chemicalengineering and materials science will continue to leverage itsprinciples for sustainable industrial processes, advanced materials, and novel pharmaceuticals, driving innovation in the21st century.

8. IS AI AT A "1900-MOMENT"?

From its origins in abstract thought to its applications in materials science and quantum computing, quantum mechanicsis a testament to the power of the human intellect to unlock nature's most closely guarded secrets. Quantum mechanicsrevolutionized physics by fundamentally altering our understanding of nature on the atomic scale. As Bohr remarked: "Ifquantum mechanics has not profoundly shocked you, youhaven't understood it yet."The key conceptual breakthroughs, summarized in Table 1,reveal an interesting finding. It appears that even the pioneersmissed the next conceptualstep. For example, Planck consideredhis quantum hypothesis merely a "mathematical trick," not afundamental law of nature, and, therefore, missed theconnection with the photoelectric effect. Einstein understoodthis connection, but surprisingly, he did not realize its implications for other kinds of matter when he applied thehypothesis to photons. It was Bohr who connected it to electrons and their atomic orbitals, yet he, too, failed to grasp itsgenerality. de Broglie was the one who perceived the universalnature of the wave-particle duality. However, his excessivereliance on electromagnetic wave analogies prevented him fromdiscovering the wave equation, a feat accomplished bySchrödinger. Again, Schrödinger did not quite understand conceptual significance of the wave function, which Born later

Table 1. Key Developments in Quantum Mechanics (1900–1930)

Year	Development
1900	Following Boltzmann's reasoning, Planck proposes his quantum hypothesis: Energy is quantized in discrete packets (quanta, $E = h\nu$).
1905	Einstein's photoelectric effect: Light behaves as particles (photons) with energy ($E = h\nu$).
1913	Bohr's atomic model: Electrons exist in quantized orbits, explaining hydrogen spectra.
1924	de Broglie's wave-particle duality: Matter exhibits both wave-like and particle-like properties.
1925	Heisenberg's matrix mechanics: The first mathematical formulation of quantum mechanics.
1925	Pauli Exclusion Principle: No two identical fermions (e.g., electrons) can occupy the same quantum state simultaneously, explaining the structure of electron shells in atoms.
1926	Schrödinger's wave equation: Describes quantum states using wave functions.
1926	Born's probabilistic interpretation: The absolute square of the wave function represents probability amplitudes, introducing the statistical nature of quantum mechanics.
1927	Heisenberg's uncertainty principle: Position and momentum cannot be precisely known simultaneously.
1927	The Copenhagen Interpretation: Quantum mechanics is fundamentally probabilistic. The wave function collapses upon measurement, and complementarity dictates that quantum objects exhibit either particle or wave-like behavior depending on observation.
1927	Confirmation of wave-particle duality in electron diffraction experiments by Davisson-Germer and Thomson-Reid.
1928	Dirac's relativistic quantum theory: Introduced the Dirac equation and predicted antimatter.
1930	Dirac's quantum field theory: Established the foundation of quantum electrodynamics (QED).

interpreted probabilistically. Dirac accomplished the next conceptual step.This analysis teaches us how hard conceptual discoveries are.As Heisenberg remarked: "As a rule, new concepts come up in arather unclear and undeveloped form." This sequence of missedopportunities reminds us of how, in the technology space, IBMmissed Microsoft (i.e., creating a software giant), Microsoftmissed Apple (i.e., Apple products), Apple missed Google missed Facebook, and all of them missed OpenAI. Allwere gigantic missed opportunities. I wonder what else liesahead that we are missing now!

The early history of quantum mechanics illustrates how messy the discovery process really is. The textbooks and courses oftengloss over this aspect, presenting the final equations as if theywere reached clearly, smoothly, and logically. This is rarely thecase. They are often discovered through clever guesswork. Eventhe most beautiful Einstein field equations of gravity werediscovered in this manner.60 I am reminded of a remark by HenriPoincare:61 "Guessing before proving! Need I remind you that itis so that all important discoveries have been made?"

Our analysis also reveals that the key challenges were conceptual rather than mathematical. Planck's revolutionaryquantum hypothesis is mathematically trivial: $\epsilon = h\nu$. Einstein'sNobel-winning equation is so simple that a high school student can understand: $h\nu = W + E_k$. Even Heisenberg-Born's matrixformulation or Schrödinger's equation is not tricky mathematically. Mathematical sophistication first emerged through Dirac'srelativistic quantum mechanics and later in quantum fieldtheory. Furthermore, the mathematical tools were alreadyavailable and ready to be applied once the conceptual difficultieswere resolved. For example, matrices, probability theory, andpartial differential equations�the main tools of quantum mechanics�have been around for a long time. Similarly, for the theory of relativity. The mathematics of special theory is just elementary high school algebra, but the conceptual breakthroughs about space and time were colossal. The general theoryrequired more sophisticated mathematics, to be sure, but it wasreadily available, thanks to Riemann.60The only instance in the history of physics where themathematical framework was also lacking, along with the needfor a conceptual breakthrough, was the discovery of the theory ofgravitation. In addition to the conceptual breakthrough ofuniversal gravitation, Newton also had to develop themathematical tool needed, namely, the calculus. However, thisis the only exception that I am aware of.This analysis suggests another valuable lesson for the presenttime. Like the 1900s clouds, I believe we have a large cloud nowon the horizon: the lack of a theory for deep neural networks large language models. By theory, I mean fundamental organizing principles that can predict important system-wideproperties, such as the structure and behavior of LLMs, fromtoken-level properties.62,63 To be sure, significant progress hasbeen made in the last three decades in neural network training,including the development of the backpropagation algorithm,various regularization techniques, reinforcement learning, andtransformer architecture, among others. However, these aremerely recipes for training; they do not provide a comprehensivetheory of deep neural networks or large language models(LLMs). This is the central conceptual challenge facing AI today.

In 1972, physics Nobel laureate Philip Anderson published an influential paper entitled "More is Different".64 He observed:"The behavior of large and complex aggregates ofelementary particles, it turns out, is not to be understoodin terms of a simple extrapolation of the properties of a fewparticles. Instead, at each level of complexity, entirely newproperties appear, and the understanding of the newbehaviors requires research that we think is as fundamentalin its nature as any other ... At each stage, entirely new laws,concepts, and generalizations are necessary, requiringinspiration and creativity to just as great a degree as inthe previous one. Psychology is not applied biology, nor biology applied chemistry."

In this sense, invoking another physics analogy, Newtonianmechanics and $F = ma$ can explain the dynamics of a fewparticles. However, when we have Avogadro's number (6.02×10^{23}) of molecules dynamically interacting in a gas, the collectivebehavior cannot be explained by applying Newton's law 10^{23}times! To be sure, $F = ma$ is going on at the molecular level, butmuch more happens at the system level that cannot beunderstood by Newton's Second Law alone.To explain macroscopic phenomena, we need entirely newconcepts, such as temperature, free energy, entropy, andchemical potential, to predict and explain the behavior ofagas. These concepts are absent at the individual particle level in Newtonian mechanics. We require an entirely new conceptual and mathematical framework, known as statistical mechanics, toaddress this new physics. It turns out that we need the SecondLaw of Thermodynamics and not the Second Law of Newton.This dichotomy between classical and statistical mechanics islike the proverbial "seeing trees but not the forest". The $F = ma$perspective is "seeing the trees," and $S = k \ln W$ is "seeing theforest."Likewise, large language models are not mere stochasticautocomplete engines. They have new emergent capabilitiesthatrequire creating a new conceptual framework similar to the transformation from Newtonian to statistical mechanics or from classical to quantum mechanics. The LLMs may not havedeveloped a human-like understanding of their domain, but they seem to have acquired a different kind of understanding andintelligence. Although it is difficult to say without anyuncertainty that AI is at a "1900-moment," the signs are compelling. For millennia, we have taken for granted themeanings of words such as "understanding" and "intelligence"without much introspection. With the advent of LLMs, we arecompelled to reevaluate our understanding of such concepts.LLMs raise profound philosophical questions about consciousness, free will, and the nature of creativity and intelligence,conceptual questions with which we are only beginning tograpple.

So, what would a mathematical theory of LLMs look like? As noted, I believe mathematical tools are already available: linearalgebra, probability theory, statistical mechanics, game theory,graph theory, group theory, and topology. The challenge lies indiscovering new concepts necessary for this problem. Asdiscussed, quantum theory was born from the analysis of theenergy distribution in blackbody radiation. Classical physicsbased theories could not explain this distribution, whichcompelled Planck to propose a quantum hypothesis. Similarly,in well-trained deep neural networks, the connection weights aredistributed lognormally. Neither the Hopfield nor theBoltzmann Machine model, which were recognized with the2024 Nobel Prize in Physics, can predict or explain thelognormal outcome. Recently, a new conceptual framework,63called statistical teleodynamics, which combines game theory andstatistical mechanics, has been proposed to predict this outcomeas a first step toward a mathematical theory of LLMs. Borrowingfrom physics, the Hopfield and Boltzmann machine modelsemploy energy minimization, where as the new framework useseffective-utility maximization from economics as its organizing principle.

The ultimate theory of LLMs can potentially upend our views of cognition and sentience, much like the "1900-moment" did inphysics a century ago. Thus, as Planck and Heisenberg remarkedabout how new concepts are born amid profound confusion,understanding the historical evolution of the quantummechanical concepts could be helpful in a similar situation tothat we face in artificial intelligence.

■ AUTHOR INFORMATION

Corresponding Author

Venkat Venkatasubramanian – Complex Resilient Intelligent Systems Laboratory Department of Chemical Engineering,Columbia University, New York, New York 10027, UnitedStates; orcid.org/0000-0002-4923-0582;Email: venkat@columbia.eduComplete contact information is available at:https://pubs.acs.org/10.1021/acs.iecr.5c00942

Notes

The author declares no competing financial interest.

■ ACKNOWLEDGMENTS

The genesis of this paper goes back to my visit to the Niels Bohr Institute in Copenhagen in August 2022, when I was invited topresent a seminar in their famous Seminar Room A. During myvisit, they kindly provided me with the office that was onceHeisenberg's about a century ago. I would like to thank my hosts,Poul Henrik Damgaard and Karel Proesmans, for their warm hospitality. I am also grateful to Michael Baldea and Jhoan ToroMendoza for inviting me to write this Commentary. I also thankRana Biswas, Krishnan Kumaran, V. Govind Manian, BenO'Shaughnessy, Ramamurti Shankar, Naz Taskiran, Alex Urban,and four anonymous reviewers for their helpful comments.

■ *REFERENCES*

(1) Mehra, J. The Historical Development ofQuantum Theory; SpringerVerlag: New York, 2001; Vol. 1−6.
(2) Mehra, J. The Birth of Quantum Mechanics; CERN: Geneva, 1976;Werner Heisenberg memorial lecture at the CERN colloquium, 30 Mar.1976.
(3) Heisenberg, W. Uber quantentheoretische Umdeutung kinematischer und mechanischer Beziehungen. Zeitschrift fuِr Physik 1925,33, 879−893.
(4) Wigner, E. The Unreasonable Effectiveness of Mathematics in the Natural Sciences. Communications in Pure and Applied Mathematics1960, 13, 1.
(5) Heisenberg, W. Development of Concepts in the History of Quantum Theory. American Journal of Physics 1975, 43, 389−394.
(6) Shankar, R. Principles of Quantum Mechanics, 2nd ed.; Springer:New York, 1994.
(7) Greene, B. The Elegant Universe: Superstrings, Hidden Dimensions, and the Quest for the Ultimate Theory, 25th ed.; W. W. Norton &Company: New York, 2024.
(8) Rovelli, C. Reality Is Not What It Seems: The Journey to Quantum Gravity; Riverhead Books: New York, 2017.
(9) Wilczek, F. A Beautiful Question: Finding Nature's Deep Design; Penguin Press: New York, 2015.
(10) Carroll, S. Quanta and Fields: The Biggest Ideas in the Universe;Dutton: New York, 2023.
(11) Kelvin, L. W. T. Nineteenth Century Clouds over the Dynamical Theory of Heat and Light. The London, Edinburgh, and DublinPhilosophical Magazine and Journal of Science 1901, 2, 1−40.
(12) Gamow, G. 30 Years That Shook Physics: The Story of Theory; Dover Publications: New York, 1966.
(13) Nauenberg, M. Max Planck and the Birth of the Quantum Hypothesis. American Journal of Physics 2016, 84, 879−882.
(14) Popkin, R. H. The Philosophy of the 16th and 17th Centuries; Simon and Schuster: New York, 1966.
(15) Blackbody radiation. https://en.wikipedia.org/wiki/Blackbody_radiation, Accessed on 10 April 2025.
(16) Planck, M. Ueber das Gesetz der Energieverteilung im Normalspectrum. Annalen der Physik 1901, 309, 553−563.
(17) Planck, M. Scientific Autobiography and Other Papers; Philosophical Library: New York, 1968; Paperback edition, August 1,1968.
(18) Erfurth, H. Max Planck Exhibit. 1938; https://www.dhm.de/ lemo/bestand/objekt/max-planck, Accessed on 10 April 2025.
(19) Sharp, K.; Matschinsky, F. Translation of Ludwig Boltzmann'sPaper "On the Relationship between the Second FundamentalTheorem of the Mechanical Theory of Heat and Probability Calculations Regarding the Conditions for Thermal Equilibrium".Entropy 2015, 17, 1971−2009. (a) Originally published in Originallypublished in Sitzungberichte der Kaiserlichen Akademie derWissenschaften. Mathematisch-Naturwissenschaftliche ClasseSitzungberichte der Kaiserlichen Akademie der Wissenschaften. MathematischNaturwissenschaftliche Classe; Abt. II, LXXVI 1877, pp 373−435 (Wien.Ber. 1877, 76, 373−435). Reprinted in , Vol. II, reprint 42, pp 164−223,Barth, Leipzig, 1909.
(20) Hermann, A. The Genesis of Quantum Theory; MIT Press:Cambridge, MA, 1971.
(21) Gearhart, C. A. Planck, the Quantum, and the Historians. Physics Perspectives 2002, 4, 170−215.
(22) Stanford Encyclopedia of Philosophy, Continuity. n.d.; https://plato.stanford.edu/entries/continuity/, Accessed: 2025-02-22.
(23) Chavan, L. Albert Einstein in Swiss Patent Office. 1905; https://

www.lbi.org/griffinger/record/213882, Accessed on 10 April 2025.
(24) Nobel-Foundation Niels Bohr - Biographical. 1922; https://www.nobelprize.org/prizes/physics/1922/bohr/biographical/, Accessed on 10 April 2025.
(25) Bohr, N. On the Constitution of Atoms and Molecules. Philos. Mag. 1913, 26, 1−25.
(26) Ford, K. W. Niels Bohr's First 1913 Paper: Still Relevant, Still Exciting, Still Puzzling. The Physics Teacher 2018, 56, 500−502.
(27) Darrigol, O. In Erwin Schrödinger - 50 Years After (ESI Lectures in Mathematics and Physics); Reiter, W. L., Yngvason, J., Eds.; EuropeanMathematical Society, 2013.
(28) de Broglie, L. Recherches sur la theorie´ des quanta. Annales de Physique (10e serie)´ 1925, III, 10, Doctoral thesis defended in Paris, November 25, 1924.322128
(29) Who's Who in the History of Quantum Mechanics. 1929; http://www.physics.umd.edu/courses/Phys420/Spring2002/Parra_Spring2002/HTMPages/whoswho.htm, Accessed on 10 April 2025.
(30) Heisenberg, W. Physics and Beyond: Encounters and Conversations; Harper & Row: New York, 1971.
(31) Bundesarchiv Bild183-R57262, Werner Heisenberg.jpg. 1933;https://en.wikipedia.org/wiki/File:Bundesarchiv_Bild183-R57262,_Werner_Heisenberg.jpg, Accessed on 10 April 2025.
(32) Born, M. Quantentheorie und Störungsrechnung. Naturwissenschaften 1923, 11, 537−542.
(33) Nobel-Foundation Max Born - Biographical. 1954; https://www.nobelprize.org/prizes/physics/1954/born/biographical/, Accessed on10 April 2025.
(34) Fedak, W. A.; Prentis, J. J. The 1925 Born and Jordan Paper 'On Quantum Mechanics. American Journal of Physics 2009, 77, 128−139.
(35) Born, M.; Jordan, P. Zur Quantenmechanik. Zeitschrift für Physik 1925, 34, 858−888.
(36) Born, M.; Heisenberg, W.; Jordan, P. Zur Quantenmechanik II.Zeitschrift für Physik 1926, 35, 557−615.
(37) Born, M. Über Quantenmechanik. Zeitschrift für Physik 1924, 26,379−395.
(38) Dirac, P. A. M. The Fundamental Equations of Quantum Mechanics. Proceedings of the Royal Society of London, Series A 1925, 109(752), 642−653.
(39) Born, M. My Life: Recollections of a Nobel Laureate; Taylor & Francis: New York, 1978.
(40) Nobel-Foundation Erwin Schro¨dinger - Biographical. 2023;http://nobelprize.org/nobel_prizes/physics/laureates/1933/schrodinger-bio.html, Accessed on 10 April 2025.
(41) Born, M. Zur Quantenmechanik der Stoßvorgange.¨Zeitschrift für Physik 1926, 37, 863−867.
(42) Pais, A. Max Born and the Statistical Interpretation of Quantum Mechanics. Address to the Annual Meeting of the Optical Society ofAmerica, 1982; On the occasion of the centenary of Born's birth,October 21.
(43) Raman, V. V.; Forman, P. Why Was It Schrödinger Who Developed de Broglie's Ideas? Historical Studies in the Physical Sciences1969, 1, 291−314.
(44) Scott, W. T. Erwin Schrödinger: An Introduction to His Writings; University of Massachusetts Press: Amherst, MA, 1967.
(45) Bloch, F. Heisenberg and the Early Days of Quantum Mechanics.Physics Today 1976, 29, 23.
(46) Schrödinger, E. Quantisierung als Eigenwertproblem, Erste Mitteilung. Annalen der Physik 1926, 384, 361−376.
(47) Mehra, J. The Golden Age of Theoretical Physics, Vol. 2; World Scientific: Singapore, 2001.
(48) Kragh, H. Erwin Schrödinger and the Wave Equation: The Crucial Phase. Centaurus 1982, 26,

154.
(49) Mehra, J. In Aspects of Quantum Theory; Salam, A., Wigner, E. P.,Eds.; Cambridge University Press: Cambridge, 1972.
(50) Nobel-Foundation The Nobel Prize in Physics 1933. 1933; https://www.nobelprize.org/prizes/physics/1933/summary/, Accessed on 10April 2025.
(51) Nobel-Foundation Wolfgang Pauli - Biographical. 1945; http://nobelprize.org/nobel_prizes/physics/laureates/1945/pauli-bio.html,Accessed on 10 April 2025.
(52) Born, M.; Einstein, A. In The Born-Einstein Letters; Born, H., Ed.;Walker and Company: New York, 1971.
(53) Briggs, G. A. D.; Butterfield, J. N.; Zeilinger, A. The Oxford Questions on the foundations of quantum physics. Proceedings of theRoyal Society A: Mathematical, Physical and Engineering Sciences 2013,469, 20130299.
(54) Skibba, R. Quantum-theory wars. Nature 2018, 555, 582.
(55) Carroll, S. What Does Quantum Theory Really Mean? Nature 2025.
(56) Camilleri, K. The revolutionary dawn of quantum mechanics.Nature 2025, 637 (8045), 269−271.
(57) Mermin, N. D. Could Feynman Have Said This? Physics Today 2004, 57, 10−11.
(58) Kroemer, H. Quantum Mechanics for Engineering: Materials Science and Applied Physics; Pearson, 2019.
(59) Stefanucci, G. Quantum Mechanics for Material Science: An Introduction; Springer, 2024.
(60) Janssen, M.; Renn, J. How Einstein Found His Field Equations:Sources and Interpretation; Springer Nature Switzerland AG, 2022.
(61) Poincaré, H. The Value of Science; The Science Press: New York,NY, 1907; Translated by George Bruce Halsted.
(62) Venkatasubramanian, V. Do large language models "understand" their knowledge? AIChE J. 2025, 71, e18661.
(63) Venkatasubramanian, V.; Sanjeevrajan, N.; Khandekar, M.;Sivaram, A.; Szczepanski, C. Jaynes Machine: The Universal Microstructure in Deep Neural Networks. Comput. Chem. Eng. 2025, 192,108908.
(64) Anderson, P. W. More is different. Science 1972, 177, 393−396.

Instructions for Authors

Essentials for Publishing in this Journal

1 Submitted articles should not have been previously published or be currently under consideration for publication elsewhere.

2 Conference papers may only be submitted if the paper has been completely re-written (taken to mean more than 50%) and the author has cleared any necessary permission with the copyright owner if it has been previously copyrighted.

3 All our articles are refereed through a double-blind process.

4 All authors must declare they have read and agreed to the content of the submitted article and must sign a declaration correspond to the originality of the article.

Submission Process

All articles for this journal must be submitted using our online submissions system. http://enrichedpub.com/ . Please use the Submit Your Article link in the Author Service area.

Manuscript Guidelines

The instructions to authors about the article preparation for publication in the Manuscripts are submitted online, through the e-Ur (Electronic editing) system, developed by **Enriched Publications Pvt. Ltd**. The article should contain the abstract with keywords, introduction, body, conclusion, references and the summary in English language (without heading and subheading enumeration). The article length should not exceed 16 pages of A4 paper format.

Title

The title should be informative. It is in both Journal's and author's best interest to use terms suitable. For indexing and word search. If there are no such terms in the title, the author is strongly advised to add a subtitle. The title should be given in English as well. The titles precede the abstract and the summary in an appropriate language.

Letterhead Title

The letterhead title is given at a top of each page for easier identification of article copies in an Electronic form in particular. It contains the author's surname and first name initial .article title, journal title and collation (year, volume, and issue, first and last page). The journal and article titles can be given in a shortened form.

Author's Name

Full name(s) of author(s) should be used. It is advisable to give the middle initial. Names are given in their original form.

Contact Details

The postal address or the e-mail address of the author (usually of the first one if there are more Authors) is given in the footnote at the bottom of the first page.

Type of Articles

Classification of articles is a duty of the editorial staff and is of special importance. Referees and the members of the editorial staff, or section editors, can propose a category, but the editor-in-chief has the sole responsibility for their classification. Journal articles are classified as follows:

Scientific articles:

1. Original scientific paper (giving the previously unpublished results of the author's own research based on management methods).
2. Survey paper (giving an original, detailed and critical view of a research problem or an area to which the author has made a contribution visible through his self-citation);
3. Short or preliminary communication (original management paper of full format but of a smaller extent or of a preliminary character);
4. Scientific critique or forum (discussion on a particular scientific topic, based exclusively on management argumentation) and commentaries. Exceptionally, in particular areas, a scientific paper in the Journal can be in a form of a monograph or a critical edition of scientific data (historical, archival, lexicographic, bibliographic, data survey, etc.) which were unknown or hardly accessible for scientific research.

Professional articles:

1. Professional paper (contribution offering experience useful for improvement of professional practice but not necessarily based on scientific methods);
2. Informative contribution (editorial, commentary, etc.);
3. Review (of a book, software, case study, scientific event, etc.)

Language

The article should be in English. The grammar and style of the article should be of good quality. The systematized text should be without abbreviations (except standard ones). All measurements must be in SI units. The sequence of formulae is denoted in Arabic numerals in parentheses on the right-hand side.

Abstract and Summary

An abstract is a concise informative presentation of the article content for fast and accurate Evaluation of its relevance. It is both in the Editorial Office's and the author's best interest for an abstract to contain terms often used for indexing and article search. The abstract describes the purpose of the study and the methods, outlines the findings and state the conclusions. A 100- to 250-Word abstract should be placed between the title and the keywords with the body text to follow. Besides an abstract are advised to have a summary in English, at the end of the article, after the Reference list. The summary should be structured and long up to 1/10 of the article length (it is more extensive than the abstract).

Keywords

Keywords are terms or phrases showing adequately the article content for indexing and search purposes. They should be allocated heaving in mind widely accepted international sources (index, dictionary or thesaurus), such as the Web of Science keyword list for science in general. The higher their usage frequency is the better. Up to 10 keywords immediately follow the abstract and the summary, in respective languages.

Acknowledgements

The name and the number of the project or programmed within which the article was realized is given in a separate note at the bottom of the first page together with the name of the institution which financially supported the project or programmed.

Tables and Illustrations

All the captions should be in the original language as well as in English, together with the texts in illustrations if possible. Tables are typed in the same style as the text and are denoted by numerals at the top. Photographs and drawings, placed appropriately in the text, should be clear, precise and suitable for reproduction. Drawings should be created in Word or Corel.

Citation in the Text

Citation in the text must be uniform. When citing references in the text, use the reference number set in square brackets from the Reference list at the end of the article.

Footnotes

Footnotes are given at the bottom of the page with the text they refer to. They can contain less relevant details, additional explanations or used sources (e.g. scientific material, manuals). They cannot replace the cited literature.
The article should be accompanied with a cover letter with the information about the author(s): surname, middle initial, first name, and citizen personal number, rank, title, e-mail address, and affiliation address, home address including municipality, phone number in the office and at home (or a mobile phone number). The cover letter should state the type of the article and tell which illustrations are original and which are not.

Note